

NANOSCALE ARCHITECTURE OF F-BAR PROTEINS AND THE  
SCHIZOSACCHAROMYCES POMBE CONTRACTILE RING

By

Nathan Andrew McDonald

Dissertation

Submitted to the Faculty of the  
Graduate School of Vanderbilt University  
in partial fulfillment of the requirements for

the degree of

DOCTOR OF PHILOSOPHY

in

Cell and Developmental Biology

August 11, 2017

Nashville, TN

Approved:

Kathleen L. Gould, Ph.D.

Ian G. Macara, Ph.D.

Anne K. Kenworthy, Ph.D.

Melanie D. Ohi, Ph.D.

John D. York, Ph.D.

## ACKNOWLEDGEMENTS

First and foremost, I thank my mentor Kathy Gould. Her ideas and insights have been instrumental in guiding all of my research, though she has always given me the freedom to pursue my own ideas and approaches. I am particularly grateful for her constant push to develop writing and presentation skills to effectively communicate my science. Her advice and guidance over the past years have allowed me to accomplish more than I thought possible and has trained me to be the best scientist I can be.

I am also grateful to the many collaborators I have had the fortune to work with during my graduate career. I thank Melanie Ohi, her student Scott Collier, and postdoc Yoshi Takizawa for their instruction on electron microscopy and work on the Imp2 oligomer structure. Rong Li and her student Sarah Smith provided critical equipment and support for FRET experiments. I thank Craig Vander Kooi for his work on the Imp2 crystal structure and Cdc15 structural modeling, as well as his training on protein purification and crystallization. I thank Bryan Millis and the CISR core for training on the STORM microscope and help troubleshooting super resolution imaging experiments. I am grateful to my thesis committee for constructive feedback on my graduate work. I would also like to thank the American Heart Association for providing financial support for 2 years of my research.

During my time in the Gould lab I have met and worked with many wonderful people that have made the experience enjoyable. First, I am grateful to my “Team 2012” colleagues Alaina Willet and Zac Elmore for their support and enlightening discussion, both scientific and otherwise. I am grateful to Liping Ren and Anna Feoktistova for sharing their deep expertise on yeast and biochemical experiments. I would like to

especially acknowledge my F-BAR compatriot Anna Feoktistova. Our time sharing a lab bay was hectic and crowded, but wonderful! Finally, I thank all the other scientists, students, and postdocs for creating the excellent and enjoyable atmosphere that exists in the Gould lab.

I am grateful to my parents and sister for their continual love and support; they are the ultimate role models. Finally, I am endlessly grateful to my wife Abigail Lind for her unwavering love and support, both scientifically and personally.

## TABLE OF CONTENTS

	Page
ACKNOWLEDGEMENTS .....	ii
LIST OF TABLES .....	vii
LIST OF FIGURES .....	viii
Chapters	
I. INTRODUCTION .....	1
Introduction to cytokinesis .....	1
<i>Schizosaccharomyces pombe</i> as a model organism to study cytokinesis.....	5
The F-BAR family of proteins link membranes to actin cytoskeletal rearrangements. 12	
Membrane binding.....	14
Oligomerization and membrane bending .....	16
Scaffolding to signal to the actin cytoskeleton.....	17
Cdc15 and Imp2 F-BAR proteins are scaffolds within the contractile ring.....	22
Summary .....	25
II. OLIGOMERIZATION BUT NOT MEMBRANE BENDING UNDERLIES THE FUNCTION OF CERTAIN F-BAR PROTEINS IN CELL MOTILITY AND CYTOKINESIS .....	26
Introduction .....	26
Results .....	29
The Cdc15 F-BAR domain binds membranes and is essential for function .....	29
Cdc15 represents a novel class of F-BARs that do not bend or tubulate membranes.....	30
The Cdc15 F-BAR oligomerizes in a tip-to-tip manner .....	39
Structural basis for Cdc15's F-BAR domain oligomerization and membrane binding .....	42
Cdc15 oligomerization defects impair cytokinesis.....	46
Discussion .....	53
Diverse modes of F-BAR oligomerization.....	53
Cdc15 oligomerizes to robustly scaffold a network of cytokinesis proteins.....	55
A significant fraction of F-BARs do not deform membranes .....	57
III. THE TUBULATION ACTIVITY OF THE FISSION YEAST F-BAR PROTEIN IMP2 IS DISPENSIBLE FOR ITS FUNCTION IN CYTOKINESIS .....	58
Introduction .....	58
Results .....	61
The Imp2 F-BAR is critical for CR constriction and disassembly.....	61



Structure of the Imp2 F-BAR domain .....	65
Structural basis for Imp2 membrane binding .....	66
The Imp2 F-BAR tubulates membranes by forming higher order structures .....	73
Imp2 F-BAR helical oligomerization supports membrane tubulation .....	75
The Imp2 F-BAR domain's cytokinetic function does not require tubulation or oligomerization .....	79
Discussion .....	82
Diverse modes of F-BAR oligomerization drive tubulation .....	82
Is F-BAR domain oligomerization and tubulation important in vivo?.....	84
Function of F-BAR proteins in cytokinesis .....	85
<b>IV. NANOSCALE ARCHITECTURE OF THE SCHIZOSACCHAROMYCES POMBE CONTRACTILE RING .....</b>	<b>87</b>
Introduction .....	87
Results .....	90
fPALM strategy for determining the spatial organization of contractile ring components .....	90
Spatial distribution of structural contractile ring components.....	94
Spatial distribution of signaling contractile ring components.....	99
Distinct layers around F-BAR protein scaffolds .....	102
Lateral clustering capability of contractile ring scaffolds .....	106
Discussion .....	109
Structural layers within the contractile ring .....	110
Signaling within the contractile ring .....	112
Protein clusters in the contractile ring .....	113
Building the ring bottom up.....	115
<b>V. CONCLUSIONS AND FUTURE DIRECTIONS.....</b>	<b>116</b>
Chapter summaries .....	116
F-BAR domain membrane binding and bending .....	118
Regulation of F-BAR protein function.....	122
Phosphorylation of Cdc15 controls a conformational change.....	122
Refining the structure of the contractile ring .....	126
Conclusions .....	127
Appendix	
<b>A. MATERIALS AND METHODS.....</b>	<b>128</b>
Yeast methods .....	128
Microscopy methods .....	129
Fluorescence resonance energy transfer (FRET).....	129
Fluorescence recovery after photobleaching (FRAP) .....	130
Fluorescent photoactivation localization microscopy (fPALM) .....	130

Super-resolution analysis .....	131
Protein purification and crystallization .....	132
Liposome assays.....	133
Cell Culture .....	135
Electron microscopy methods .....	135
Analytical ultracentrifugation .....	136
Circular dichroism.....	136
Structural modeling.....	137
<b>REFERENCES .....</b>	<b>138</b>

## LIST OF TABLES

Table	Page
1-1. Components of the <i>S. pombe</i> contractile ring .....	8
2-1. Human F-BAR protein tubulation .....	34

## LIST OF FIGURES

Figure	Page
1-1. Overview of cytokinesis .....	4
1-2. The <i>S. pombe</i> cell cycle and cytokinesis .....	6
1-3. <i>S. pombe</i> contractile ring constriction and septation .....	11
1-4. F-BAR proteins and binding partners .....	13
1-5. Cdc15 and Imp2 are critical contractile ring scaffolds. ....	24
2-1. The Cdc15 F-BAR domain binds membranes and is essential for function.....	31
2-2. The Cdc15 F-BAR domain binds but does not bend or tubulate membranes .....	33
2-3. A significant fraction of human F-BAR domains do not bend membranes .....	35
2-4. Cdc15 and 6 human F-BARs do not tubulate membranes under a variety of conditions.....	36
2-5. A significant fraction of human F-BAR domains do not tubulate membranes in vivo .....	37
2-6. Cdc15 and other F-BAR domains are folded and functional.....	38
2-7. The Cdc15 F-BAR domain organizes into tip-to-tip oligomers .....	40
2-8. Non-tubulating human F-BAR domains show evidence for oligomerization in solution.....	41
2-9. Structural basis for Cdc15 F-BAR domain oligomerization and membrane binding .....	43
2-10. F-BAR domain oligomerization and membrane binding.....	44
2-11. Oligomerization is critical for a stable Cdc15 scaffold at the division site and robust cytokinesis.....	47
2-12. Oligomerization is critical for Cdc15 function in cytokinesis.....	48
2-13. Oligomerization is critical for Fer and RhoGAP4 function.....	52

3-1.	The Imp2 F-BAR domain is important for cytokinesis .....	63
3-2.	The Imp2 F-BAR domain is important for cytokinesis; supplement.....	64
3-3.	Structure of the Imp2 F-BAR domain .....	65
3-4.	The Imp2 F-BAR domain binds biological membranes.....	67
3-5.	Mechanism of Imp2 F-BAR domain membrane binding .....	69
3-6.	Membrane binding is an essential function of the Imp2 F-BAR domain .....	71
3-7.	Imp2 membrane binding mutants .....	72
3-8.	The Imp2 F-BAR domain tubulates membranes through helical oligomerization	74
3-9.	Imp2 oligomerization is essential for tubulation but dispensable for cytokinesis.	77
3-10.	Imp2 F-BAR domain dimer-dimer mutant properties .....	78
3-11.	Non-tubulating F-BAR domains can complement Imp2 F-BAR domain function .....	81
3-12.	Both F-BAR fusions are present at the contractile ring.....	82
4-1.	fPALM strategy to localize contractile ring proteins with nanometer resolution relative to the plasma membrane .....	91
4-2.	The mCling-ATTO674N plasma membrane marker accurately identifies the plasma membrane edge.....	93
4-3.	Nanoscale organization of contractile ring structural components.....	94
4-4.	Vertical width parameters ( $\sigma_{\text{vert}}$ ) and localization values for strains in 5-3.....	95
4-5.	Endogenous mMaple3 tags on structural components do not perturb normal growth and division.....	96
4-6.	Nanoscale organization of contractile ring signaling components .....	100
4-7.	Vertical width parameters ( $\sigma_{\text{vert}}$ ) and localization values for strains in 5-6.....	101
4-8.	Endogenous mMaple3 tags on signaling components do not perturb normal growth and division.....	102
4-9.	FRET confirms distinct layers around F-BAR proteins in the contractile ring ...	104

4-10. Intermolecular FRET experiments.....105

4-11. Lateral organization of components in the contractile ring .....108

4-12. Schematic model of the *S. pombe* contractile ring molecular architecture.....109

5-1. Cdc15 undergoes a spatially and temporally regulated conformational change in cytokinesis .....121

5-2. Cdc15 undergoes a spatially and temporally regulated conformational change in cytokinesis .....124

5-3. Cdc15's conformational change is regulated by phosphorylation .....125

## CHAPTER I

### INTRODUCTION

#### **Introduction to cytokinesis**

Cytokinesis is the final step in the cell division cycle when one cell is physically divided into two. As cells grow and divide, it is essential that cytokinesis is properly spatially and temporally regulated with other steps in the cell cycle, particularly the duplication and segregation of the genetic material. If cytokinesis is mistimed or misplaced, the genetic material can be fragmented or unequally segregated with deleterious results on growth and development. Indeed in animals, aneuploidy resulting from missegregation of chromosomes is one route to tumorigenesis (Fujiwara *et al.*, 2005; Ganem *et al.*, 2009). Furthermore, if cytokinesis fails completely, polyploid cells with double the normal genetic content are formed and subsequently die in most cases (Fujiwara *et al.*, 2005). A detailed understanding of cytokinesis and cell division is essential to understand how these processes go awry in human disease.

Cytokinesis in all cells can be divided into four major steps: selection of a division site, formation of a division apparatus, closure of the apparatus, and final abscission and splitting of the daughter cells (Figure 1-1). Cells from different kingdoms of life utilize different molecules and various strategies to perform each of these steps, though many mechanisms are widely conserved.

First, a dividing cell must determine the site of division in order to properly separate equal copies of the genetic material to each daughter cell. Bacteria accomplish this by negatively regulating the formation of a division apparatus near cell tips and DNA. In *Escherichia coli*, inhibitory Min proteins oscillate between either cell tip, over

time leaving the center of the cell as the only region that does not inhibit assembly of the division apparatus (Lutkenhaus *et al.*, 2012). After nucleoid segregation to opposite poles, certain DNA binding proteins like SImA also inhibit division apparatus establishment, permitting formation only in the center of the cell (Haeusser and Margolin, 2016). Eukaryotic cells utilize a variety of similar mechanisms to position their division site. In the fission yeast *Schizosaccharomyces pombe*, the division site is partially selected through inhibitory signals from the cell tips, chiefly the Pom1 kinase (Huang *et al.*, 2007). The nucleus, which is maintained in the cell middle by microtubules, also provides a positive signal to select the division site by exporting the cytokinetic scaffold Mid1 at the cell middle immediately prior to mitosis (Paoletti and Chang, 2000; Daga and Chang, 2005). Alternatively, in the budding yeast *Saccharomyces cerevisiae*, the division site is determined by the location of the new daughter bud, which grows immediately proximal to the previous division site (Casamayor and Snyder, 2002). In plants, the division site is initially established by a pre-prophase band of microtubules that surround the central nucleus (Smith, 2001). In contrast to the above cell types, animal cells determine their division site late in mitosis; the position of the anaphase mitotic spindle controls the location of the division site. Activated (GTP-bound) RhoA emanates from mitotic spindle midzone to the medial cortex, where it is alone sufficient to activate the downstream formation and constriction of the division apparatus (Green *et al.*, 2012; Wagner and Glotzer, 2016).

After selecting the site for division, cells construct a division apparatus. Bacteria construct a proto-ring that is composed of FtsZ, a distant tubulin homolog, along with many binding partners (Haeusser and Margolin, 2016). In plants, the division apparatus



takes the form of the phragmoplast, a structure composed of microtubules, microfilaments, F-actin, and endoplasmic reticulum (ER) membranes that forms between segregated chromosomes (Smith, 2001). In fungi and animal cells, the division apparatus is termed the contractile ring. The contractile ring is composed of antiparallel, intertwined F-actin filaments created by formin molecules. Myosin-II motors provide tension and eventually force for constriction, while many additional protein components ensure structural integrity and link the actomyosin ring to the plasma membrane (Green *et al.*, 2012).

After the division apparatus is constructed, it must close to divide a cell's contents. In bacteria, the proto-ring matures into a "divisome" and constricts, possibly through force generated by FtsZ filaments (Szwedziak *et al.*, 2014) and peptidoglycan cell wall formation (Haeusser and Margolin, 2016). In plants, new membrane is delivered to the phragmoplast scaffold, concomitant with new cell wall synthesis, extending the division apparatus toward the cell cortex (Smith, 2001). In fungi and animal cells, the contractile ring constricts using the force of myosin-II motors pulling on actin filaments (Mishra *et al.*, 2013; Cheffings *et al.*, 2016). In fungi, a cell wall septum is also synthesized behind the contractile ring, which provides substantial constrictive force (Willet, McDonald and Gould, 2015). In all cells, considerable delivery of new membrane and cell wall material to the division apparatus is necessary to complete constriction (Albertson *et al.*, 2005).

Lastly, abscission occurs to completely separate daughter cells. This process is not well understood in bacteria; FtsZ leaves the division site before complete constriction of the divisome, implying additional factors are involved in the last steps of abscission

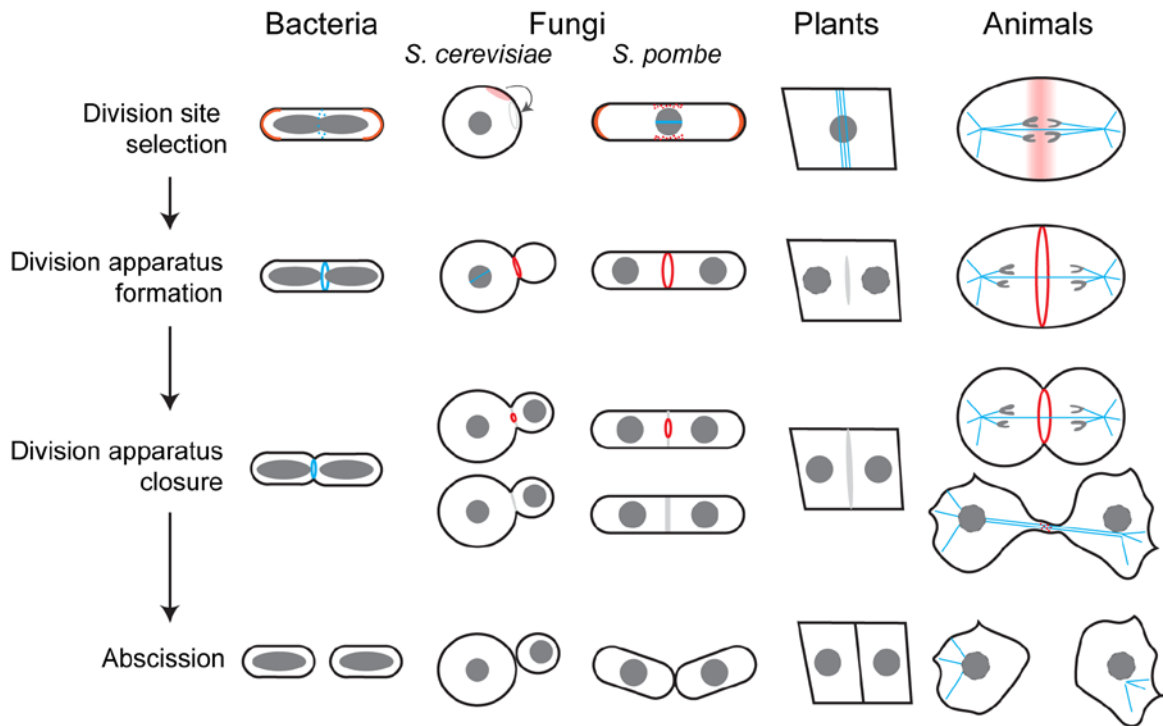


**Figure 1-1. Overview of cytokinesis.** Cytokinesis in all organisms can be divided into four stages (left). In bacteria, the division site is selected in the cell middle through negative signals from the tips (orange). A ring of FtsZ (blue), a distant tubulin homolog, is formed which matures into a divisome that constricts to divide the cell. In *S. cerevisiae*, the division site is determined by the bud site. Signals from the previous bud site (light red) position the subsequent bud site directly proximal. During mitosis, an actomyosin ring (red) is formed between mother and daughter buds that constricts concomitant with septum formation (grey). The septum is digested after constriction to release the two cells. In *S. pombe*, the division site is selected through negative signals from the tips (orange) and positive signals from the nucleus (dark grey). An actomyosin ring (red) forms and constricts along with septum formation (grey). Enzymatic digestion of the septum releases the divided cells. In plants, the division site is established in the center of the cell by a pre-prophase band of microtubules (blue). The phragmoplast (grey), a scaffold composed of microtubules, microfilaments, and membranes, forms between segregated chromosomes. This structure matures and scaffolds the construction of new cell wall material that divides the daughter cells after fusing with the outer cortex. In animal cells, positive signals from the spindle midzone (light red) specify the division site, where an actomyosin ring (red) forms and constricts. The constricted ring condenses into the midbody, which requires vesicle trafficking and ESCRT components to split the intracellular bridge.

(Haeusser and Margolin, 2016). In plants, the phragmoplast matures and extends to fuse with the plasma membrane and outer cell wall, completing division. In fungi, enzymatic digestion of inner septum material occurs to release the two daughter cells completely. In animal cells, the contractile ring constricts down to a dense structure termed the midbody, which persists for some time before complete division. Vesicle trafficking to the midbody, as well as action of ESCRT proteins is required to complete abscission and resolve the intracellular bridge (Green *et al.*, 2012).

### ***Schizosaccharomyces pombe* as a model organism to study cytokinesis**

*Schizosaccharomyces pombe* has emerged as an excellent model system to investigate eukaryotic cytokinesis. Experimentally, *S. pombe* allows facile investigation of cytokinesis due to its genetic tractability and simple biochemical manipulation. Importantly for comparison to higher eukaryotes, *S. pombe* divide in a similar manner to animal cells - symmetrically with the formation and constriction of an actomyosin contractile ring (Marks and Hyams, 1985). Furthermore, the *S. pombe* cell cycle is well characterized biochemically and physiologically (Nurse *et al.*, 1976). *S. pombe* follow a canonical eukaryotic cell cycle (Figure 1-2): a short G1 gap phase takes place while still attached to a sister cell, followed by an S DNA replication phase, a long G2 growth phase, and a mitotic M phase. The rod-shaped cells grow exclusively from both ends during interphase G1-S-G2 stages (Mitchison and Nurse, 1985). Upon mitotic entry, growth is halted, and chromosomes are organized with a bipolar microtubule spindle and segregated to opposite sides of the cell. Unlike some other eukaryotic cells, *S. pombe*

undergo a closed mitosis with a nuclear envelope that remains intact (Güttinger *et al.*, 2009).

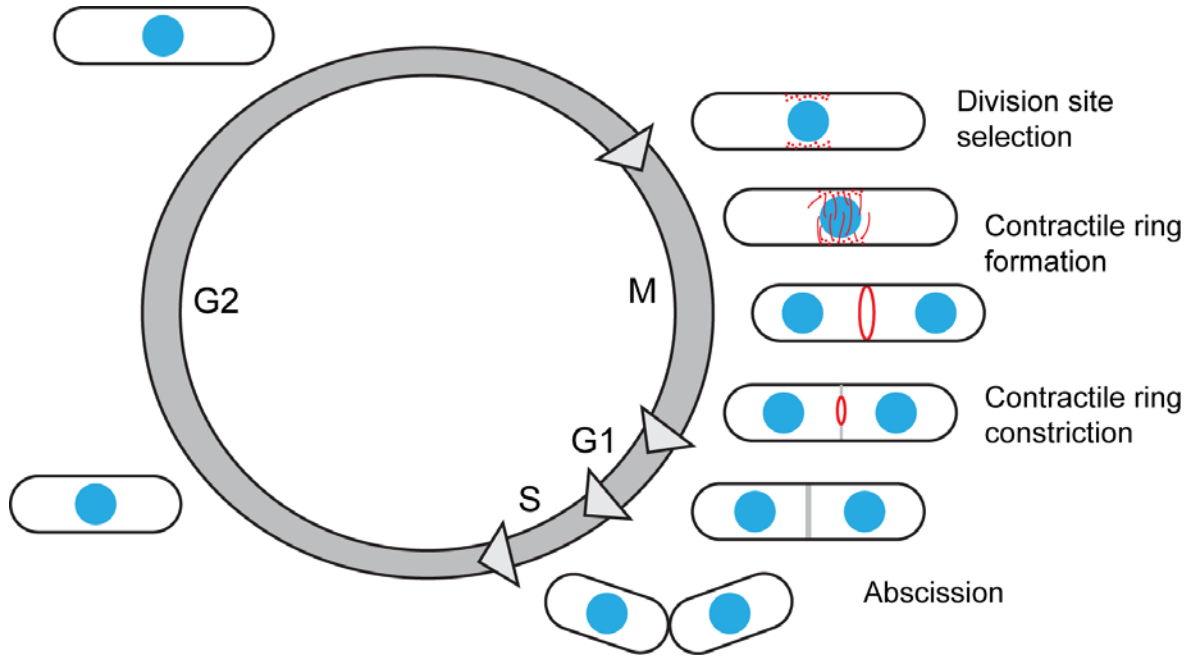


**Figure 1-2. The *S. pombe* cell cycle and cytokinesis.** The fission yeast *S. pombe* follows a canonical eukaryotic cell cycle. During log phase growth, a short G1 gap phase and an S DNA replication phase occur while still connected through a septum to a previous sister cell. The majority of cell growth occurs during a long G2 phase. Once cells reach a desired length, M phase occurs and the duplicated genetic material is segregated to opposite sides of the cell. Cytokinesis in *S. pombe* is accomplished using an actin and myosin based contractile ring (red), which forms at the center of the cell and constricts along with septum formation. Daughter cells are separated after partial enzymatic digestion of the septum.

Forward and reverse genetic experiments in *S. pombe* have generated an extensive and nearly exhaustive “parts list” of components that are required for cytokinesis or localize to the contractile ring (see Table 1-1 for components localizing to the ring). Formation of the contractile ring by these proteins begins from a broad band of precursor “nodes”, membrane-tethered protein foci in the medial region of the cell. Precursor nodes initiate ring formation through the anillin-like protein Mid1 (Wu *et al.*, 2006). Mid1 is phosphorylated by Plk1 and released from the nucleus to form nodes immediately prior to mitosis (Bahler *et al.*, 1998). After entry into mitosis, Mid1 aids in recruiting multiple essential components to precursor nodes, including IQGAP Rng2, myosin-II Myo2 and light chains Cdc4 and Rlc1, F-BAR protein Cdc15, and formin Cdc12 (Wu *et al.*, 2006; Laporte *et al.*, 2011). Though Mid1 normally initiates ring formation in a stereotypic and ordered fashion (Wu *et al.*, 2003), the ring can form in the complete absence of Mid1 and precursor nodes. Contractile rings in *mid1* $\Delta$  cells form off-center, but constrict and divide the cell efficiently (Sohrmann *et al.*, 1996). Additional components such as Rng2, Myo2, and Cdc12 can initiate ring formation in the absence of Mid1, indicating robustness and plasticity in the initial ring formation process (Tao *et al.*, 2014).

Once precursor nodes are assembled, F-actin is nucleated and elongated by the formin Cdc12 and the nodes coalesce into a ring. Ring formation from precursor nodes is well described by a “search-capture-pull-release” mathematical model, wherein formin elongates F-actin from individual nodes and myosin motors in adjacent nodes capture and pull on these filaments, occasionally releasing filaments to avoid ring collapse. In this manner, nodes are pulled together and coalesce into a contiguous ring structure. Once a complete ring is formed, multiple additional components are recruited to the division

<b>Gene</b>	<b>Protein</b>	<b>Gene</b>	<b>Protein</b>
<i>act1</i>	Actin	<i>cyk3</i>	Nebulin-family cytokinesis protein
<i>myo2</i>	Essential type-II myosin	<i>rga7</i>	F-BAR and GTPase activating protein
<i>rlc1</i>	Myosin regulatory light chain	<i>for3</i>	Formin
<i>cdc4</i>	Myosin essential light chain	<i>rho1/2</i>	Rho GTPase
<i>cdc8</i>	Tropomyosin	<i>mid2</i>	Anillin
<i>mid1</i>	Anillin	<i>blt1</i>	Precursor node protein
<i>cdc12</i>	Essential formin	<i>gef2</i>	Rho GTPase exchange factor
<i>cdc15</i>	Essential F-BAR scaffold	<i>nod1</i>	Gef2 binding partner
<i>rng2</i>	Essential IQGAP scaffold	<i>rad24</i>	14-3-3 protein
<i>myp2</i>	Type-II myosin	<i>dma1</i>	E3 ubiquitin ligase
<i>imp2</i>	F-BAR scaffold	<i>clp1</i>	Cdc14 phosphatase
<i>adf1</i>	Actin depolymerization factor cofilin	<i>orb2</i>	PAK-related kinase
<i>ain1</i>	Actin crosslinker $\alpha$ -actinin	<i>sid2</i>	Septation initiation network kinase
<i>fim1</i>	Actin crosslinker fimbrin	<i>pck1</i>	Protein kinase C
<i>twf1</i>	Twinfilin	<i>rga2</i>	Rho GTPase exchange factor
<i>acp1</i>	Actin capping protein	<i>ppb1</i>	Calcineurin phosphatase
<i>rgf3</i>	Rho GTPase exchange factor	<i>pom1</i>	DYRK family polarity kinase
<i>pxl1</i>	Paxillin	<i>paa1, par1, par2</i>	PP2A phosphatase
<i>spa2</i>	Polarity factor	<i>kin1</i>	MARK family kinase
<i>fic1</i>	C2 domain polarity factor	<i>pom2</i>	DYRK family kinase
<i>spn1/2/3/4</i>	Septins	<i>mto1</i>	Microtubule organizer
<i>rng3</i>	UCS domain Myo2 activator	<i>mto2</i>	Microtubule organizer
<i>myo51</i>	Type-V myosin	<i>chs2</i>	Chitin synthase homolog
<i>rng8/9</i>	Myo51 regulator	<i>gef3</i>	Rho GTPase exchange factor

**Table 1-1. Components of the *S. pombe* contractile ring.** Components that localize to the fully-formed, but unconstricted, contractile ring in *S. pombe*.

site including actin crosslinkers, additional myosin motors, and multiple proteins that contribute to ring stability.

Once the contractile ring is formed and chromosomes are segregated, the ring constricts in a myosin-dependent manner (Mishra *et al.*, 2013; Stachowiak *et al.*, 2014). As the ring constricts, protein components including F-actin are slowly removed to maintain a constant concentration as ring diameter decreases (Wu and Pollard, 2005), with the exception of myosin-II Myo2 which concentrates during ring constriction (Wu *et al.*, 2003). Ring components are also dynamic and continually turn over during ring formation and constriction (Cheffings *et al.*, 2016). To sustain this turnover, F-actin is continually nucleated and elongated during the constriction process by formin (Pelham and Chang, 2002).

As a cell-walled organism, cytokinesis in *S. pombe* also requires the synthesis of a new cell wall between daughter cells (Willet, McDonald and Gould, 2015). A tri-layer division septum, composed of an inner primary septum flanked by secondary septa, is deposited behind the constricting actomyosin ring to maintain a contiguous cell wall (Figure 1-3). The *S. pombe* primary septum is predominantly composed of linear  $\beta(1,3)$ glucans, while the secondary septum contains  $\alpha(1,3)$ glucans, branched  $\beta(1,3)$ glucans, linear  $\beta(1,3)$ glucans, and galactomannans (Humbel *et al.*, 2001). At least three essential glucan synthases form the primary and secondary septa; catalytic subunits of these complexes are Bgs1, Bgs4, and Ags1. Bgs1 forms linear  $\beta(1,3)$ glucans and is essential for primary septum formation. Bgs4 forms branched  $\beta(1,3)$ glucans, while Ags1 forms  $\alpha(1,3)$ glucans.  $\alpha$ -glucans are required to anchor the primary septum to the cell wall (Cortés *et al.*, 2012). Branched  $\beta$ -glucans, on the other hand, are an essential component

of the secondary septa. Cells lacking branched  $\beta$ -glucans never form a secondary septum, and only formed a twisted and unsupported primary septum (Muñoz *et al.*, 2013). If cells attempt to separate without a secondary septum, over-degradation of cell wall material occurs, resulting in lysis. Therefore, linear  $\beta$ -glucans, branched  $\beta$ -glucans, and  $\alpha$ -glucans formed by Bgs1, Bgs4, and Ags1, are all essential, cooperating to build the division septum.

Septum formation is also critical to complete cytokinesis in the center of the cell. Certain mutations compromising Bgs1 (*cps1-191*) lead to cell cycle arrest and the maintenance of contractile rings without constriction (Liu *et al.*, 1999, 2000). Additionally, compromising this glucan synthase's activity permits rings to slide and unravel (Muñoz *et al.*, 2013; Arasada and Pollard, 2014). This has also been evident in spheroplast studies; when cell walls were removed by digestion and prevented from re-forming, rings slid from the cell middle (Stachowiak *et al.*, 2014). However, when digesting enzymes were removed from spheroplasts, contractile rings formed and pinched the cell without sliding (Mishra *et al.*, 2013). Formation of the septum, therefore, is capable of “locking” the contractile ring in place (Figure 1-3).

In addition to preventing ring sliding, measurements of the forces necessary for cell division indicate septum formation contributes the predominant constriction force of cytokinesis. The contractile ring and septum must overcome turgor pressure, which in *S. pombe* cells is ~1 MPa (Proctor *et al.*, 2012). Calculations of the maximum force myosin motors in the contractile ring can exert (~15 nN, 10 kPa) indicate these forces are not sufficient. Synthesis of extracellular glucans may be able to exert a “ratchet” force as glucan synthases add subunits to glucan chains, which push against the plasma



membrane, similar to models proposed for actin at the leading edge of animal cells (Mogilner and Oster, 2003; Proctor *et al.*, 2012).

After septum formation, glucanases Agn1 and Egn1 are secreted to break down the inner primary septum which splits the daughter cells (Figure 1-3). Degradation of the primary septum in combination with outward turgor pressure facilitates separation and rounding of each daughter cell's new end (Cortés *et al.*, 2012).

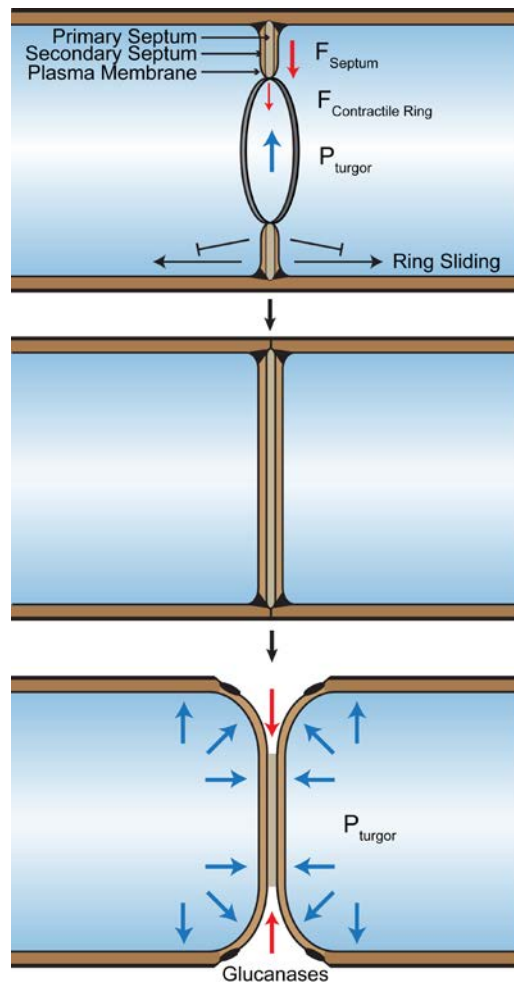






**Figure 1-3. *S. pombe* contractile ring constriction and septation.** The *S. pombe* contractile ring constricts in a myosin-dependent manner ( $F_{\text{contractile ring}}$ ) in the center of the cell. Simultaneously, a tri-layer septum is formed behind the ring. The formation of the septum “locks” the ring in place and resists sliding of the ring. Construction of the septum contributes force to constrict the ring ( $F_{\text{septum}}$ ), which is opposed by the turgor pressure ( $P_{\text{turgor}}$ ) of the cell. After the ring constricts and a septum is formed, the inner layer is digested by glucanases to release the two daughter cells.

After multiple decades of investigation into cytokinesis in *S. pombe*, the field has a clear and detailed understanding of the overall cytokinetic process. It is known what proteins are involved (Nurse *et al.*, 1976; Balasubramanian *et al.*, 1998), when they arrive and leave the ring (Wu *et al.*, 2003; Wu and Pollard, 2005), and even how many molecules of many proteins are present (Wu and Pollard, 2005). However, it remains unclear how 50+ protein components (Table 1-1) assemble into a functional division apparatus. The protein organization of the ring at the ultrastructural level is unknown, hampering our understanding of its inner workings. I will present the first detailed nanoscale map of the contractile ring in Chapter IV. Furthermore, how each component contributes biochemically toward a functional molecular machine is only beginning to become clear. One area in particular that remains elusive is how the contractile ring forms a tight link to the plasma membrane, a necessity for constriction. One class of proteins that are prime candidates for securing this link are F-BAR proteins, which I have investigated in Chapters II and III of this thesis. A comprehensive background on the biochemical activities and function of F-BAR proteins follows.

### **The F-BAR family of proteins link membranes to actin cytoskeletal rearrangements**

The Bin/Amphiphysin/Rvs (BAR) domain superfamily of proteins act to link the plasma membrane to the actin cytoskeleton in a variety of cellular processes, including endocytosis, cell motility, and cytokinesis. The family is defined by its membrane-binding BAR domain that folds into a dimeric, tightly interwound 6-helix bundle with a curved, crescent-like shape (Peter *et al.*, 2004; Henne *et al.*, 2007). Structural studies have determined BAR domains interact directly with anionic membranes through the concave face of their crescent-shaped structures (Peter *et al.*, 2004; Henne *et al.*, 2007).

Multiple varieties of BAR domains exist, including classical BAR domains whose membrane-binding face is highly curved (BAR, N-BARs) (Peter *et al.*, 2004), inverse BAR domains whose membrane-binding face bows outward to form a convex curve (I-BARs) (Millard *et al.*, 2005), and Fer/Cip4 homology (FCH) BAR domains that form an elongated, shallow curve (F-BARs) (Henne *et al.*, 2007). F-BAR domains are accompanied by a variety of other domains in proteins, including SH3,  $\mu$ HD, tyrosine kinase, or GTPase activating domains (GAPs) and consequently possess multiple functions that together link membranes to the actin cytoskeleton.

Domain Layout	Organism	F-BAR genes	Binding Partners
	<i>H. sapiens</i>	CIP4, FBP17, TOCA1 PACSN1/2/3 PSTPIP1/2 Nostrin FCHSD1/2 Gas7	Dynamin <sup>3,19</sup> , WASP <sup>3,26</sup> , Cdc42 <sup>97</sup> Dynamin <sup>98</sup> , WASP <sup>98</sup> , Caveolin <sup>24,54</sup> , ProSAP1 <sup>125</sup> Dynamin <sup>99</sup> , WASP <sup>64</sup> , PTP-PEST <sup>100,101</sup> , Pyrin <sup>75</sup> Dynamin <sup>55</sup> , WASP <sup>55</sup> , NOS3 <sup>56</sup> WASP <sup>457</sup>
	<i>S. pombe</i>	Cdc15, Imp2 Bzz1	Formin <sup>72,73</sup> , Fic1 <sup>39</sup> , Spa2 <sup>40</sup> , Paxillin <sup>39</sup> , Rgf3 <sup>40</sup>
	<i>S. cerevisiae</i>	Hof1 Bzz1	Inn1 <sup>65</sup> , Bnr1 <sup>70</sup> , Bni1 <sup>70</sup> Las17(WASP) <sup>102</sup> , Vrp1 <sup>102</sup> , Myo5 <sup>102</sup>
	<i>H. sapiens</i>	FCHO1/2	Eps15 <sup>2</sup> , Intersectin <sup>2</sup>
	<i>S. pombe</i> / <i>S. cerevisiae</i>	Syp1	Ede1(Eps15) <sup>11</sup> , Las17(WASP) <sup>103</sup>
			<b>Substrates</b>
	<i>H. sapiens</i>	SrGAP1/2/2b/2c/3 PARG1 Gmp RhoGAP4	Cdc42 <sup>84</sup> , Rac1 <sup>7</sup> RhoA <sup>89</sup> , Rap2 <sup>87</sup> RhoA <sup>89</sup>
	<i>S. pombe</i>	Rga7 Rga8 Rga9	Rho2 <sup>104</sup> Rho1 <sup>105</sup>
	<i>S. cerevisiae</i>	Rgd1 Rgd2	Rho3 <sup>106</sup> , Rho4 <sup>106</sup> Cdc42 <sup>107</sup> , Rho5 <sup>107</sup>
	<i>H. sapiens</i>	Fer, Fes	FAK <sup>26</sup> , $\beta$ -catenin <sup>81</sup> , $\gamma$ -catenin <sup>81</sup> , Cortactin <sup>82</sup>

**Figure 1-4. F-BAR proteins and binding partners.** Conserved domain layouts and select binding partners or substrates of human, *S. pombe*, and *S. cerevisiae* F- BAR proteins. Dashed lines indicate the domain is present only in a subset of the listed F-BAR proteins. \*Indicates data from *Drosophila* homologs. †Indicates data from mouse or rat homologs.

### *Membrane binding*

The crescent-shaped F-BAR domain binds directly to membranes, localizing F-BAR proteins to various sites of action in cells. Emphasizing this important characteristic, membrane binding activity is essential for F-BAR protein function in all cases tested. For instance, point mutations within the FCHo2 and FBP17 F-BARs that specifically disrupt membrane binding prevent the proteins from localizing to the plasma membrane and sites of endocytosis (Tsujita *et al.*, 2006; Frost *et al.*, 2008; Henne *et al.*, 2010). Proteins lacking the F-BAR domain entirely also fail to properly localize and function: srGAP2 $\Delta$ F-BAR and PACSIN $\Delta$ F-BAR fail to localize to the plasma membrane (Dharmalingam *et al.*, 2009; Guerrier *et al.*, 2009), while *Saccharomyces cerevisiae* Hof1 $\Delta$ F-BAR and Syp1 $\Delta$ F-BAR lose localization to the bud neck (Meitinger *et al.*, 2011; Oh *et al.*, 2013) and sites of endocytosis (Reider *et al.*, 2009), respectively.

F-BAR domains interact with negatively charged membranes primarily through the concave face of their crescent shaped dimers, utilizing multiple positively charged surface residues (Henne *et al.*, 2007; McDonald *et al.*, 2015, 2016; Moravcevic *et al.*, 2015). PACSIN F-BAR domains also contain a unique amphipathic “wedge-loop” that partially inserts into the lipid bilayer (Wang *et al.*, 2009); mutations in this region consequently disrupt membrane binding. The concave orientation of membrane binding is conserved in all F-BARs, though a few variations have been proposed. Under certain conditions in vitro, the FBP17 F-BAR domain associates with membranes through a side face (Frost *et al.*, 2008), and the *Drosophila* Nwk F-BAR has also been observed in a side conformation on membranes (Becalska *et al.*, 2013). It is not yet clear if these alternative orientations are important for function or if they occur in vivo; mutations that

disrupt this conformation must be tested for functionality in vivo to confirm that a sideways orientation is utilized in cells.

Given that F-BAR domains use positively charged residues for membrane binding, it is not surprising that they are generally capable of binding membranes containing negatively charged phospholipids. While most prefer phosphatidylserine (PS) or various phosphorylated phosphatidylinositol (PIP) lipid head groups, some F-BAR domains including srGAPs (Carlson *et al.*, 2011; Coutinho-Budd *et al.*, 2012) and *Drosophila* Nwk (Becalska *et al.*, 2013) bind membranes containing multiple species of PIPs. Other F-BAR domains display a preference for a certain lipid, though this preference appears less stringent than that of other lipid binding domains such as pleckstrin homology (PH) domains (Lemmon, 2008). FBP17 and CIP4 prefer PI(4,5)P<sub>2</sub> as well as PS (Itoh *et al.*, 2005; Tsujita *et al.*, 2006), PACSINs prefers PS (Itoh *et al.*, 2005), Fer prefers phosphatidic acids (Itoh *et al.*, 2009) and *S. cerevisiae* Rgd1p prefers PI(4,5)P<sub>2</sub> (Moravcevic *et al.*, 2015). However, in all of these cases the F-BAR domains can bind membranes containing only PS as a negatively charged lipid in vitro.

In healthy eukaryotic cells, PS and PI(4,5)P<sub>2</sub> are exclusively located in the inner leaflet of the plasma membrane (Di Paolo and De Camilli, 2006). PS comprises ~2-10% of the inner leaflet of the PM, while PI(4)P and PI(4,5)P<sub>2</sub> are present in trace amounts ( $\leq 1\%$ ) (Di Paolo and De Camilli, 2006). Therefore preferences for PS and PI(4,5)P<sub>2</sub> may be important to direct F-BAR proteins to specific areas enriched in these phospholipids, like the plasma membrane or endocytic sites. Conversely, some evidence suggests this relationship works in the opposite direction; F-BAR proteins may serve to cluster certain plasma membrane lipids into stable micro-domains (Zhao *et al.*, 2013). F-BAR domain-

mediated clustering of lipids could be important for generating distinct lipid environments at cellular structures like endocytic sites (Posor *et al.*, 2015), caveolae (Hansen *et al.*, 2011), or neuronal spines (Schneider *et al.*, 2014).

### *Oligomerization and membrane bending*

Since the earliest characterizations of F-BARs, multiple F-BAR domains were observed not only to bind, but also to bend membranes into thin tubules when present at high concentration (Kamioka *et al.*, 2004; Itoh *et al.*, 2005; Tsujita *et al.*, 2006). Tubulation has been observed when certain F-BAR domains are added to liposomes in vitro, or when overproduced in cultured cells. F-BAR-coated membrane tubules formed in this manner adopt a range of diameters from ~50 to ~200 nm (Frost *et al.*, 2008; McDonald *et al.*, 2016), indicating a degree of flexibility in the F-BAR coat. This heterogeneity initially precluded structural determination of the F-BAR coat; however, Frost and colleagues generated homogeneously coated tubules using careful in vitro slow-annealing methods. Using cryo-electron microscopy, the structure of F-BARs along these tubules was determined (Frost *et al.*, 2008), revealing that CIP4 F-BAR dimers oligomerize through complex lateral and tip to tip interactions to form a dense coat upon the membrane (Shimada *et al.*, 2007; Frost *et al.*, 2008). Accordingly, mutations that disrupt oligomerization of F-BAR domains prevent tubulation in overexpression assays (Frost *et al.*, 2008; McDonald *et al.*, 2016). Computational methods corroborate the oligomerization model of tubulation, as an assembly of oligomerized F-BAR domains can bend a flat membrane into a tubule in molecular dynamics simulations (Yu and Schulten, 2013). Attractive models proposing F-BAR domains oligomerize upon a membrane in order to collectively induce membrane curvature in endocytosis and other

processes have arisen from these structural studies (Frost *et al.*, 2009; Suetsugu *et al.*, 2010; Qualmann *et al.*, 2011; Mim and Unger, 2012).

Yet, the ability to induce inward-oriented membrane tubules isn't conserved in all F-BAR domains. srGAP F-BAR domains induce tubules of the opposite curvature, outward from the plasma membrane (Guerrier *et al.*, 2009; Coutinho-Budd *et al.*, 2012). This curvature generation is likely accomplished through similar mechanisms as I-BAR proteins, which also oligomerize to collectively bend a membrane (Saarikangas *et al.*, 2009). Recent evidence suggests even these two varieties of membrane tubulation do not adequately describe the functions of all F-BAR family members. In fact, multiple F-BAR proteins do not tubulate membranes in standard in vitro liposome binding or cultured cell overexpression assays. These include at the least: Fer (Tsujita *et al.*, 2006), *S. cerevisiae* Hof1 (Moravcevic *et al.*, 2015), and *Drosophila* Nwk (Becalska *et al.*, 2013). In Chapter II I will investigate the *S. pombe* Cdc15 F-BAR, which also cannot tubulate membranes.

Surprisingly, the importance of oligomerization for physiological function in the cases of tubulating F-BARs has rarely been directly tested, though it is clear that blocking oligomerization inhibits tubulation of liposomes in vitro and of the plasma membrane in mammalian cell overexpression assays (Frost *et al.*, 2008). In other words, whether the tubulation activity of F-BAR proteins in vitro is connected to their functions in vivo has not been rigorously established, a topic I will address in Chapter III.

#### *Scaffolding to signal to the actin cytoskeleton*

Once an F-BAR is bound and oligomerized upon a membrane, it utilizes additional domains to perform scaffolding and signaling functions. The majority of F-BAR proteins contain either a SH3 or  $\mu$ HD domain that they use to connect with other

proteins (Figure 1-4). In the cases of F-BAR proteins involved in endocytosis, they recruit partners that in turn have scaffolding and protein recruitment functions. For example, FCHo1/2 F-BAR proteins are two of the first components to localize at incipient sites of endocytosis (Henne *et al.*, 2010). FCHo2 uses a  $\mu$ HD domain to directly recruit Eps15 and Intersectin (Henne *et al.*, 2010), and an unstructured middle region to bind and allosterically activate AP2 (Hollopeter *et al.*, 2014; Umasankar *et al.*, 2014). In yeast, Syp1 acts similarly; it is present early at sites of endocytosis and recruits Ede1, an Eps15 homolog (Reider *et al.*, 2009; Stimpson *et al.*, 2009).

The tubulating activity of FCHo1/2 F-BAR domains (Henne *et al.*, 2007) led to the idea that they might induce the initial membrane curvature early at an endocytic site (Henne *et al.*, 2010). However, single-molecule imaging experiments suggest instead that FCHo1/2 “stabilize” the growing bud but do not initiate curvature (Cocucci *et al.*, 2012). Efficient recruitment of binding partners and activation of AP2 (Hollopeter *et al.*, 2014; Umasankar *et al.*, 2014), aided by clustering from oligomerization (Henne *et al.*, 2010), may instead explain how FCHo2 acts as a nucleator of clathrin-mediated endocytosis. Indeed, multiple other proteins at endocytic sites are likely responsible for curvature generation, including the FCHo2 binding partner Eps15 (Stachowiak *et al.*, 2013; Busch *et al.*, 2015), multiple classical BAR domain proteins (Qualmann *et al.*, 2011), and the triskelion clathrin coat (Ungewickell and Hinrichsen, 2007).

Slightly later in endocytosis, FBP17 and CIP4 F-BAR proteins bind the budding vesicle (Taylor *et al.*, 2011). FBP17 and CIP4 may contribute to branched actin network formation at the endocytic site through SH3 domain-mediated recruitment of Arp2/3 activators WASP (Tsujita *et al.*, 2006; Leibfried *et al.*, 2008; Hartig *et al.*, 2009) and, for



CIP4, WAVE (Fricke *et al.*, 2009). Both FBP17 and CIP4's SH3 domains also recruit the GTPase Dynamin (Kamioka *et al.*, 2004; Itoh *et al.*, 2005; Tsujita *et al.*, 2006; Taylor *et al.*, 2011), a critical component for vesicle scission (Ferguson and De Camilli, 2012). The PACSIN group of F-BAR proteins similarly scaffold WASP and Dynamin and are present in clathrin-mediated endocytosis in certain cells (de Kreuk *et al.*, 2012), as well as caveolar endocytic sites (Hansen *et al.*, 2011; Senju *et al.*, 2011). Nostrin also functions at caveolae by recruiting WASP, Dynamin, and a specific substrate, nitric oxide synthase, to regulate its internalization (Zimmermann *et al.*, 2002; Icking *et al.*, 2005). *Drosophila* Nwk proteins correspondingly recruit WASP (Coyle *et al.*, 2004), Dynamin (Rodal *et al.*, 2008), and sorting nexin Snx16 (Rodal *et al.*, 2011) in neurons to regulate synaptic growth receptor signaling at presynaptic neuromuscular junctions (O'Connor-Giles *et al.*, 2008; Rodal *et al.*, 2011). Therefore, multiple F-BAR proteins at endocytic sites in different cell types build branched actin networks through recruitment of WASP or WAVE, and assist in vesicle scission through recruitment of Dynamin.

In other cellular processes, F-BAR proteins perform similar scaffolding functions to bridge the membrane to the actin cytoskeleton. As examples, CIP4's binding and recruitment of WASP is also important in regulating lamellipodia during cell migration (Saengsawang *et al.*, 2012, 2013), and seems to be a critical component inducing invadopodia in cancer cells (Pichot *et al.*, 2010). In neurons, PACSIN2 interacts with ProSAP1 to form stable membrane-bound structures in neural spines (presumably through oligomerization) which regulate spine organization (Schneider *et al.*, 2014). Furthermore, the PSTPIP1 F-BAR protein scaffolds PTP-PEST phosphatases together

with substrates such as WASP (Wu *et al.*, 1998; Côté *et al.*, 2002) and Abl (Cong *et al.*, 2000) to modulate the actin cytoskeleton.

While many F-BAR proteins use  $\mu$ HD and SH3 domains for scaffolding functions, in certain cases F-BAR domains also interact directly with other proteins. For example, the *S. pombe* Cdc15 F-BAR domain directly binds and recruits the formin Cdc12 (Carnahan and Gould, 2003; Willet, McDonald, Bohnert, *et al.*, 2015), which is responsible for F-actin formation in the contractile ring (Chang *et al.*, 1997). Human PSTPIP1's F-BAR domain interacts with Pyrin (Shoham *et al.*, 2003); this interaction activates Pyrin to initiate pyroptosome formation and an inflammatory response (Yu *et al.*, 2007). It is possible that these two interactions occur simultaneously with membrane binding; the F-BAR domain could bind the membrane on its concave face and a partner on its opposite, cytoplasmic face. In contrast, the PACSIN2 F-BAR domain can interact directly with F-actin filaments *in vitro* through its concave face (Kostan *et al.*, 2014); this interaction excludes simultaneous membrane binding. The cytoplasmic face of F-BAR domains may represent a more generally utilized surface for F-BAR proteins to form linkages with other proteins upon the membrane than currently appreciated.

Based upon much work in the field since their original description, it is clear that many F-BAR family proteins serve as membrane bound scaffolds for a variety of binding partners (Figure 1-4). Oligomerization through their F-BAR domains aids scaffolding by locally concentrating the proteins upon membranes. SH3 domains have relatively low affinity ( $\sim 1-100 \mu\text{M}$ ) for substrates (Li, 2005); F-BAR oligomerization may therefore help to build a high density network of SH3 or  $\mu$ HDs to strongly link with actin cytoskeletal partners.

Other F-BAR proteins contain protein kinase or GAP domains (Figure 1-4) and act as signal transducers to the cytoskeleton. Fer and Fes are unique non-receptor tyrosine kinases whose F-BAR domains localize the proteins to the leading edges of migrating cells (Itoh *et al.*, 2009) or focal adhesions (Naba *et al.*, 2008), respectively. Fer and Fes F-BAR domain oligomerization impacts activation of their tyrosine kinase domains through trans-phosphorylation (Cheng *et al.*, 1999; Craig *et al.*, 1999), similar conceptually to how receptor tyrosine kinase clustering promotes trans-activation. When activated, Fer and Fes phosphorylate several substrates including FAK (Oh *et al.*, 2009),  $\beta$ - and  $\gamma$ -catenin (Kim and Wong, 1995), and cortactin (Kim and Wong, 1998) to modulate cell-cell and cell-matrix contacts (Greer, 2002).

The last class of F-BAR proteins contain GTPase activating domains (GAPs) that promote GTP to GDP catalysis by small GTPases. The most well studied of these in humans is the srGAP group. srGAP1/2/2b-c/3 participate in neural morphogenesis and migration (Wong *et al.*, 2001; Carlson *et al.*, 2011). srGAP1 is a critical effector of repulsive Slit-Robo signaling; ROBO1 bound to extracellular SLIT2 activates srGAP1's GAP domain at the membrane to specifically inactivate the Cdc42 GTPase, leading to actin cytoskeletal changes that decrease migration toward the SLIT2-displaying cells (Wong *et al.*, 2001). srGAP2 is important for the biogenesis of neurites (Guerrier *et al.*, 2009; Charrier *et al.*, 2012), as well as regulation of Slit-Robo mediated contact inhibition during cell migration through its GAP domain's inactivation of Rac1 (Fritz *et al.*, 2015). Additional F-BAR GAP proteins in humans include PARG1, Gmip, and RhoGAP4. PARG1 and Gmip's GAP domains target RhoA (Saras *et al.*, 1997; Aresta *et al.*, 2002; Myagmar *et al.*, 2005), while RhoGAP4's substrates are unknown. RhoGAP4

functions in inhibiting cell migration (Vogt *et al.*, 2007), but little is known about PARG1 and Gmip cellular function. Significant future study is required to understand the substrates of signaling F-BARs and integrate this functionally with their F-BAR domain activities.

### **Cdc15 and Imp2 F-BAR proteins are scaffolds within the contractile ring**

The *S. pombe* genome encodes 7 F-BAR proteins, as compared to the 22 F-BAR proteins present in human cells. As each of the 7 *S. pombe* F-BARs appears to have a unique function, the fission yeast model organism offers a simplified system to study the function of this protein family. Indeed in humans, multiple F-BAR proteins are involved in single processes and can possess partially redundant functions. During endocytosis in *S. pombe* two F-BAR proteins are utilized, Syp1 and Bzz1 (Roberts-Galbraith and Gould, 2010). In contrast, humans use 5 or more homologous F-BARS (FCHo1/2, FBP17, CIP4, and TOCA1) with overlapping functions (Taylor *et al.*, 2011). It is likely that discoveries about the mechanisms and regulation of F-BAR proteins in the simplified *S. pombe* system will have broad relevance to the larger human F-BAR family.

Three F-BAR proteins in *S. pombe* localize to the contractile ring and are involved in cytokinesis: Cdc15, Imp2, and Rga7 (Figure 1-5A-B) (Fankhauser *et al.*, 1995; Demeter and Sazer, 1998; Martín-García *et al.*, 2014). Cdc15 and Imp2 are most important for the formation and constriction of the contractile ring, while Rga7 plays a comparatively minor role in the later stages of septation (Martín-García *et al.*, 2014). Cdc15 is strictly essential for cytokinesis and cell viability; cells completely lacking Cdc15 cannot build a contractile ring and division fails (Fankhauser *et al.*, 1995;

Carnahan and Gould, 2003). Temperature sensitive mutations of Cdc15 (such as *cdc15-140*) allow a ring to form at restrictive temperatures, but the ring is unstable and unable to constrict and divide the cell (Figure 1-5C) (Laporte *et al.*, 2011). Imp2, on the other hand, is not strictly essential for viability, but in its absence most division events fail (Figure 1-5C) (Demeter and Sazer, 1998).

Cdc15 and Imp2 function as contractile ring scaffolds. Cdc15 is one of the first components to localize at cytokinesis precursor nodes and one of the most abundant components in the mature ring (Wu *et al.*, 2003; Wu and Pollard, 2005). Cdc15's membrane-binding F-BAR domain also directly binds the formin Cdc12 (Figure 1-5A), an interaction that is critical to robustly recruit the formin to the contractile ring (Carnahan and Gould, 2003; Willet, McDonald, Bohnert, *et al.*, 2015). Both Cdc15 and Imp2 possess homologous and redundant SH3 domains at their C termini (Ren *et al.*, 2015). These domains scaffold a variety of contractile ring accessory proteins including: Rgf3, Pxl1, Fic1, and Spa2 (Figure 1-5A) (Roberts-Galbraith *et al.*, 2009; Ren *et al.*, 2015). In the absence of either Cdc15 or Imp2's SH3 domain, cytokinesis can occur; however, cells lacking both SH3 domains cannot build a contractile ring and cytokinesis fails (Roberts-Galbraith *et al.*, 2009). Therefore, the SH3 protein network scaffolded by Cdc15 and Imp2 is essential for cytokinesis.

Cdc15's scaffolding functions are regulated by phosphorylation in a cell-cycle dependent manner (Roberts-Galbraith *et al.*, 2010). During interphase, Cdc15 is highly phosphorylated within its unstructured middle region between F-BAR and SH3 domains. This phosphorylation inhibits partner binding, as well as membrane binding and

oligomerization. At mitosis, Cdc15 is dephosphorylation, relieving inhibition to allow membrane binding at the medial cortex and scaffolding of its contractile ring partners.

Though our understanding of Cdc15 and Imp2's functions is extensive, mechanistic understanding of their activities is incomplete. Particularly, it is not understood how Cdc15 and Imp2's F-BAR domains bind membranes and oligomerize, and how these activities organize the proteins into the contractile ring.

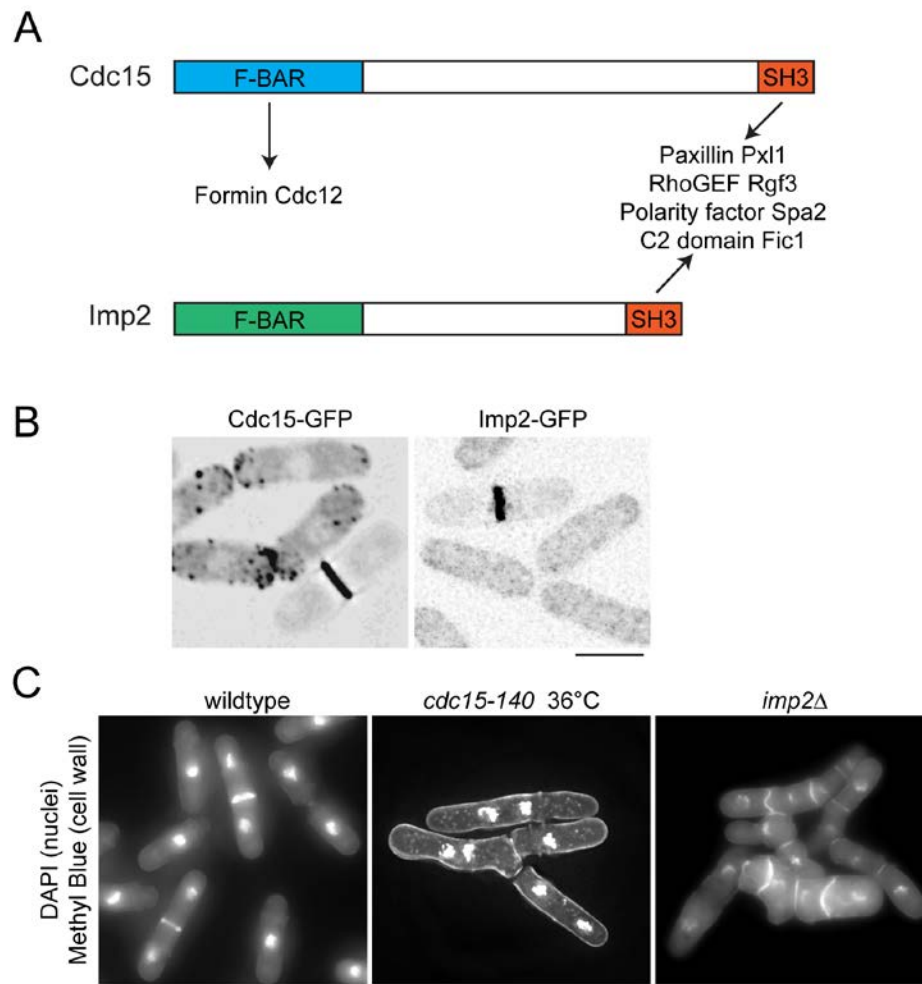


**Figure 1-5. Cdc15 and Imp2 are critical contractile ring scaffolds.** A) Schematic domain layouts of Cdc15 and Imp2. Binding partners of domains are indicated. B) Cdc15-GFP and Imp2-GFP localize to the contractile ring. C) Cdc15 and Imp2 are critical for cytokinesis. A *cdc15-140* temperature sensitive mutation fails cytokinesis and cells become multinucleate. Cells lacking *imp2* also fail cytokinesis, though after forming septa. Scale bars = 4  $\mu$ m.

## Summary

In this work I have examined the function of two critical F-BAR proteins in cytokinesis, as well as the nanoscale architecture of the contractile ring. In Chapter II, I explored how linear oligomerization by Cdc15's F-BAR domain is critical for cytokinesis, as well as how other F-BAR proteins oligomerize in non-canonical fashions. In Chapter III, I investigated the mechanism and importance of Imp2's helical oligomerization in cytokinesis. In Chapter IV, I determined the precise spatial organization of 29 components of the *S. pombe* actomyosin ring in order to construct a detailed nanoscale model of a eukaryotic contractile ring.

## CHAPTER II

### OLIGOMERIZATION BUT NOT MEMBRANE BENDING UNDERLIES THE FUNCTION OF CERTAIN F-BAR PROTEINS IN CELL MOTILITY AND CYTOKINESIS

McDonald N.A., Vander Kooi C.W., Ohi M.D., and Gould K.L. (2015)

*Developmental Cell*, 35(6):725–736

#### **Introduction**

Diverse membrane remodelers and scaffolds interact with and modulate the organization of biological membranes during many cellular processes including cell division, endocytosis, and motility (Bezanilla *et al.*, 2015). The Bin/Amphiphysin/Rvs (BAR) domain superfamily is a central player in many of these processes (Frost *et al.*, 2009). Structural studies have defined the family as crescent-shaped dimers of anti-parallel alpha-helix bundles (Peter *et al.*, 2004). Several families exist within the BAR domain superfamily: classical BAR domains, inverse BAR domains (I-BAR), and Fer/CIP4 homology BAR (FCH-BAR, F-BAR) domains, each of which exhibits structural variation on the canonical crescent theme (Qualmann *et al.*, 2011). F-BAR domains in particular are flatter elongated versions of classical BAR domains (Henne *et al.*, 2007; Shimada *et al.*, 2007) involved in many actin-driven processes (Roberts-Galbraith and Gould, 2010).

Multiple BAR and F-BAR domains possess the ability to deform membranes at high concentration (Peter *et al.*, 2004; Itoh *et al.*, 2005; Tsujita *et al.*, 2006). BAR domains do this by binding and imposing their intrinsic curvature on membranes, in some cases inserting amphipathic helices into the bilayer (Gallop *et al.*, 2006; Masuda *et al.*,



2006) or collaborating with adjacent membrane binding domains (Pang *et al.*, 2014). In contrast, F-BAR domain tubulation is thought to arise from a cooperative mechanism wherein assemblies of shallowly curved F-BARs bound to a membrane collectively impose a curvature (Shimada *et al.*, 2007; Frost *et al.*, 2008; Yu and Schulten, 2013). A pioneering structural study of CIP4 F-BAR-coated membrane tubules revealed numerous interactions between F-BAR dimers; lateral interactions between dimers were strictly essential for tubule formation, while tip-to-tip interactions stabilized the tilt of F-BAR assemblies to result in a consistent tubule diameter (Frost *et al.*, 2008).

Despite this detailed example and the tubulation model that has arisen from it (Frost *et al.*, 2009; Suetsugu *et al.*, 2010; Qualmann *et al.*, 2011; Mim and Unger, 2012), it remains unknown if contacts between F-BAR dimers are important for CIP4's *in vivo* functions. In fact, while the ability of multiple F-BAR domains to tubulate membranes has been noted since the earliest characterization of the domain (Kamioka *et al.*, 2004; Itoh *et al.*, 2005; Tsujita *et al.*, 2006; Shimada *et al.*, 2007), the connection between tubulation activity *in vitro* and protein function *in vivo* is not clearly established. A straightforward example is F-BAR domain function during endocytosis, where distinct membrane curvatures are generated and resolved as a vesicle is nucleated and budded from the plasma membrane (Doherty and McMahon, 2009). It was initially hypothesized that F-BAR domains would bind to or induce distinct membrane curvatures throughout this process (possibly predictable from their domain structure) (Qualmann *et al.*, 2011). However, the membrane curvatures induced by endocytic F-BARs *in vitro* fail to strictly correlate with endocytic vesicle size at the time of F-BAR protein association (Taylor *et al.*, 2011). In other processes requiring F-BAR proteins like cytokinesis, it is unclear how

thin membrane tubules might contribute. Despite inconclusive experimental evidence linking in vitro tubulation activity to physiological function, the importance of F-BAR domain oligomerization and membrane tubulation has become dogma in the field (Frost *et al.*, 2009; Qualmann *et al.*, 2011; Mim and Unger, 2012; Daumke *et al.*, 2014). In fact, it is unknown if all F-BAR domains oligomerize, if contacts between dimers are important for physiological F-BAR protein functions, and if membrane tubulation or deformation is a default consequence of these interactions.

To test the importance of inter-F-BAR domain interactions and F-BAR domain-induced tubulation in a cellular process, we studied *Schizosaccharomyces pombe* Cdc15, the founding member of the Pombe Cdc15 Homology (PCH) scaffolding family, a large subfamily of F-BAR domain containing proteins (Roberts-Galbraith and Gould, 2010). Cdc15 is essential for cytokinesis in *S. pombe*, directly binding the membrane and scaffolding multiple contractile ring (CR) proteins to ensure proper CR formation and stability (Fankhauser *et al.*, 1995; Carnahan and Gould, 2003; Wachtler *et al.*, 2006; Hachet and Simanis, 2008; Roberts-Galbraith *et al.*, 2009; Ren *et al.*, 2015; Willet, McDonald, Bohnert, *et al.*, 2015). Indeed, Cdc15 is proposed to be a major membrane tether for the CR in both *S. pombe* and *S. japonicas* (Roberts-Galbraith *et al.*, 2010; Gu *et al.*, 2015). Here, we find that the Cdc15 F-BAR domain binds but does not bend or tubulate membranes in vitro or in vivo, a characteristic we extend to six human F-BAR domains. Nevertheless, Cdc15 utilizes contacts between F-BAR dimers to organize into linear oligomers. We reveal the structural basis for oligomerization and membrane binding of Cdc15, and determine the importance of these functions in vivo using endogenous oligomerization and membrane binding mutants. As further examples, we

show F-BAR domain oligomerization interactions are critical for in vivo functions of the tyrosine kinase regulator of cell motility and adhesion, Fer (Greer, 2002; Itoh *et al.*, 2009), and RhoGAP4, an inhibitor of cell motility (Vogt *et al.*, 2007). Our results provide the first evidence for the importance of interactions between F-BAR dimers for in vivo function of F-BAR proteins in the absence of membrane tubulation.

## Results

### *The Cdc15 F-BAR domain binds membranes and is essential for function*

Although Cdc15 is the founding member of the PCH family and is essential for cytokinesis, the importance of its F-BAR domain has not been tested. Thus, we replaced one allele of *cdc15* in a diploid with a version lacking sequences encoding the F-BAR domain (Figure 2-1A). Tetrad dissection of the resultant heterozygous diploid showed that the truncation allele did not give rise to viable progeny (Figure 2-1B). Furthermore, a construct lacking the F-BAR domain did not rescue a *cdc15-140* strain at the restrictive temperature (Figure 2-1C). Together, these data indicate that the F-BAR domain is essential for Cdc15 function.

We next tested the membrane binding properties of the Cdc15 F-BAR domain (residues 19-312). We found that it pelleted with liposomes composed of Folch fraction lipids rich in phosphorylated phosphatidylinositols (PIPs) in a salt-dependent manner (Figure 2-1D), without any dependence on liposome size (Figure 2-1E). At low salt, the domain pelleted by itself, a behavior that will be explained below. Using a Bio-Layer Interferometry (BLI) binding assay (Abdiche *et al.*, 2008), the lipid specificity of the Cdc15 F-BAR was tested (Figure 2-1F). Liposomes enriched in phosphatidylserine (PS)

and PIP/PIP<sub>2</sub> increased Cdc15 binding, and Cdc15 particularly favored liposomes containing PIPs phosphorylated at the 4- and 5- positions of the inositol ring.

*Cdc15 represents a novel class of F-BARs that do not bend or tubulate membranes*

We used three assays to determine if the Cdc15 F-BAR domain is capable of remodeling or tubulating the membrane when present at high concentrations. First, GFP-Cdc15 F-BAR was mixed with giant unilamellar vesicles (GUVs) composed of a generic blend of lipids including negatively charged PS and PI(4)P (Figure 2-2A). The Cdc15 F-BAR bound and coated the GUVs, often clustering on the surface. However, unlike the previously characterized human FBP17 F-BAR domain (Tsujita *et al.*, 2006; Frost *et al.*, 2008), which formed tubules emanating from the GUVs, the Cdc15 F-BAR did not deform GUVs even when coating the surface at high concentration (Figure 2-2A, bottom panel; Figure 2-3). A similar binding experiment was performed with small (800 nm) liposomes and membrane deformation was examined by negative stain electron microscopy (EM). As with GUVs, tubules were observed when the FBP17 F-BAR domain was added, but not when Cdc15 was (Figure 2-2B). Third, whereas overexpression of the GFP-FBP17 F-BAR domain in mammalian COS-7 cells induced many short plasma membrane tubules as previously described (Kamioka *et al.*, 2004) (Figure 2-2C), overexpression of the GFP-Cdc15 F-BAR domain did not tubulate the membrane and instead concentrated in ribbon-like clusters. Taken together, these data

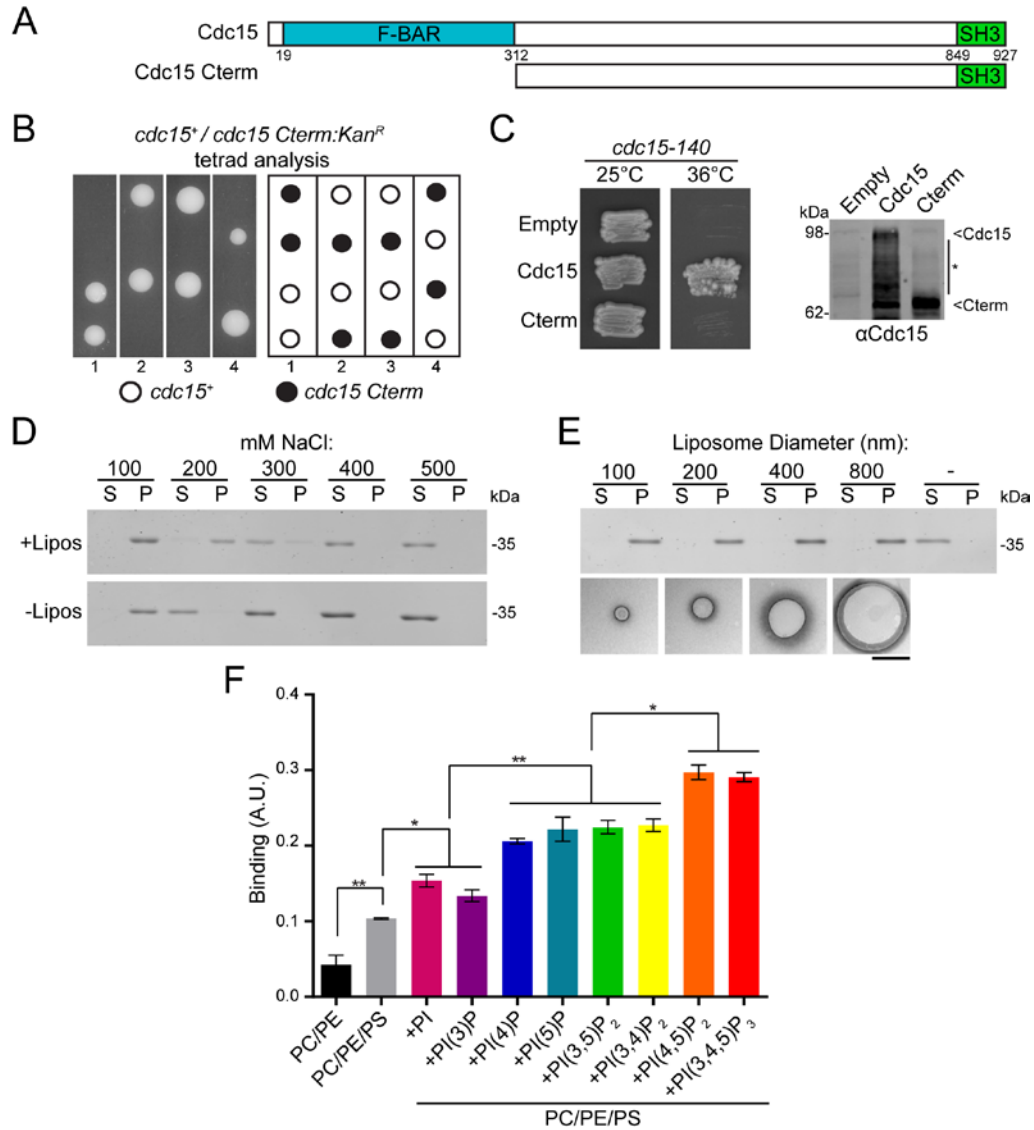


**Figure 2-1. The Cdc15 F-BAR domain binds membranes and is essential for function.** A) Cdc15 domains and alleles. B) Cdc15 alleles from (A) integrated into *cdc15/cdc15::ura4<sup>+</sup>* diploids were sporulated and tetrads were dissected. Relevant genotypes are indicated. C) Cdc15 constructs from (A) were expressed from the *nmt81* promoter in a *cdc15-140* strain. Right) Anti-Cdc15 immunoblot of construct-expressing cells. D) Co-pelleting between the Cdc15 F-BAR domain (19-312) and Folch fraction liposomes at different NaCl concentrations. S = supernatant, unbound; P = pellet, bound. E) Co-pelleting between the Cdc15 F-BAR domain and Folch fraction liposomes extruded to various diameters. Representative negative stain electron micrographs of liposomes are shown. Scale bar = 500 nm. F) Bio-Layer Interferometry binding assay between the Cdc15 F-BAR domain and synthetic liposomes composed of 69.9% DOPC, 0.1% Biotin-PE, 10% DOPS when indicated (PS), 5% of different phosphatidylinositols when indicated, and the remainder DOPE. \*,  $p < 0.05$ ; \*\*,  $p < 0.01$ , one-way ANOVA. Error bars indicate standard error of the mean (SEM).

indicate that the Cdc15 F-BAR domain binds membranes but does not deform or tubulate them.

Lack of membrane deformation in cell culture overexpression assays has been reported previously only for human Fer (Tsujita *et al.*, 2006) and *S. cerevisiae* Hof1 F-BAR domains (Moravcevic *et al.*, 2015). Out of 22 total F-BAR proteins in humans, 15 have been shown to tubulate membranes with either positive (CIP4, TOCA1, FBP17, PSTPIP1/2, FCHo1/2, PACSIN1/2/3) or negative (SRGAP1/2A/2B/2C/3) curvature in vitro and/or upon overexpression in vivo (Table 2-1). To determine the total number of human F-BAR domains that do not deform membranes, we tested the remaining seven (Fer, Fes, Nostrin, FCHSD1/2, Gas7, RhoGAP4) in vitro with GUVs and smaller liposomes, and in vivo by expression in COS-7 cells (Figures 2-3, 2-4, and 2-5; Table 2-1). The Nostrin F-BAR tubulated membranes in all assays, but the six other F-BAR domains did not tubulate membranes in any assay although Fer and RhoGAP4, like Cdc15, clustered on the GUVs' surface (Figure 2-3A). The assemblies formed by the 6 non-tubulating F-BARs in COS-7 cells were dynamic as determined by Fluorescence Recovery after Photobleaching (FRAP) (Figure 2-6A). Additional evidence that they fold correctly in vitro and in vivo was obtained by circular dichroism, wherein each GFP-F-BAR displayed a strong near-UV signal above that of GFP alone, indicative of folded molecules (Figure 2-6B). We conclude that a significant number of F-BAR domains bind but do not bend membranes.

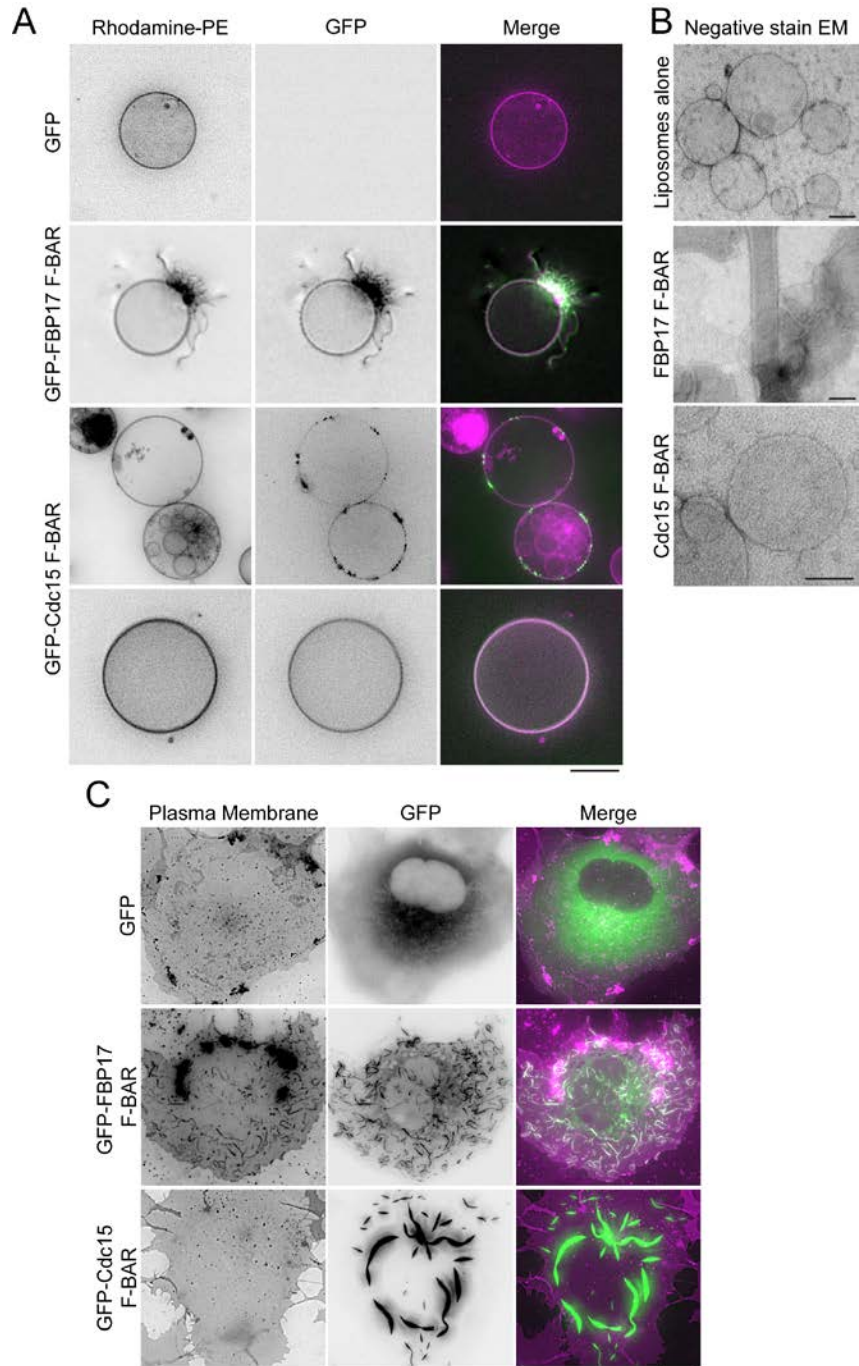


**Figure 2-2. The Cdc15 F-BAR domain binds but does not bend or tubulate membranes.** A) 10-30  $\mu\text{m}$  GUVs (composed of 69% DOPC / 15% DOPE / 10% DOPS / 5% PI(4)P / 1% Rhodamine-PE) mixed with 10  $\mu\text{M}$  GFP, GFP-FBP17 (1-319), or GFP-Cdc15 (19-312) F-BAR constructs. Scale bar = 10  $\mu\text{m}$ . B) 800nm extruded liposomes (composed of 70% DOPC / 15% DOPE / 10% DOPS / 5% PI(4)P) mixed with 10  $\mu\text{M}$  of the indicated F-BAR domain and examined with negative stain EM. Scale bars = 100nm. C) GFP, GFP-FBP17 (1-319), or GFP-Cdc15(19-312) expressed in COS-7 cells and co-stained with CellMask Orange plasma membrane dye. Scale bar = 10  $\mu\text{m}$ .

Gene	Protein	Tubulation (+/-/none)	Evidence (in vivo, in vitro)
CIP4	Cdc42-interacting protein 4	+	in vivo, in vitro (Tsujita <i>et al.</i> , 2006)
FBP17	Formin-binding protein 17	+	in vivo (Kamioka <i>et al.</i> , 2004) in vitro (Tsujita <i>et al.</i> , 2006)
TOCA1	Transducer of Cdc42-dependent actin assembly	+	in vivo (Kakimoto <i>et al.</i> , 2006) in vitro (Wang <i>et al.</i> , 2009)
FCHO1	FCH domain only protein 1	+	in vivo, in vitro (Henne <i>et al.</i> , 2010)
FCHO2	FCH domain only protein 2	+	in vitro (Henne <i>et al.</i> , 2007) in vivo (Henne <i>et al.</i> , 2010)
PSTPIP1	Proline-serine-threonine phosphatase interacting protein 1	+	in vivo, in vitro (Tsujita <i>et al.</i> , 2006)
PSTPIP2	Proline-serine-threonine phosphatase interacting protein 2	+	in vivo (Tsujita <i>et al.</i> , 2006)
NOSTRIN	Nitric oxide synthase trafficking	+	in vivo, in vitro (this study)
PACSIN1	Protein kinase C and casein kinase substrate in neurons protein 1	+	in vitro (Wang <i>et al.</i> , 2009)
PACSIN2	Protein kinase C and casein kinase substrate in neurons protein 2	+	in vivo (Shimada <i>et al.</i> , 2010) in vitro (Bai <i>et al.</i> , 2012)
PACSIN3	Protein kinase C and casein kinase substrate in neurons protein 3	+	in vitro (Bai <i>et al.</i> , 2012)
FER	Tyrosine protein kinase	none	in vivo (Tsujita <i>et al.</i> , 2006) in vitro (this study)
FES	Tyrosine protein kinase	none	in vivo, in vitro (this study)
SRGAP1	SLIT-ROBO Rho GTPase-activating protein 1	-	in vivo (Coutinho-Budd <i>et al.</i> , 2012)
SRGAP2A/B/C	SLIT-ROBO Rho GTPase-activating protein 2A/B/C	-	in vivo, in vitro (Guerrier <i>et al.</i> , 2009)
SRGAP3	SLIT-ROBO Rho GTPase-activating protein 3	-	in vivo (Carlson <i>et al.</i> , 2011)
GAS7	Growth arrest specific protein 7	none	in vivo, in vitro (this study)
RHOGAP4	Rho GTPase activating protein 4	none	in vivo, in vitro (this study)
FCHSD1	FCH and double SH3 domain protein 1	none	in vivo, in vitro (this study)
FCHSD2	FCH and double SH3 domain protein 2	none	in vivo, in vitro (this study)

**Table 2-1. Human F-BAR protein tubulation.**



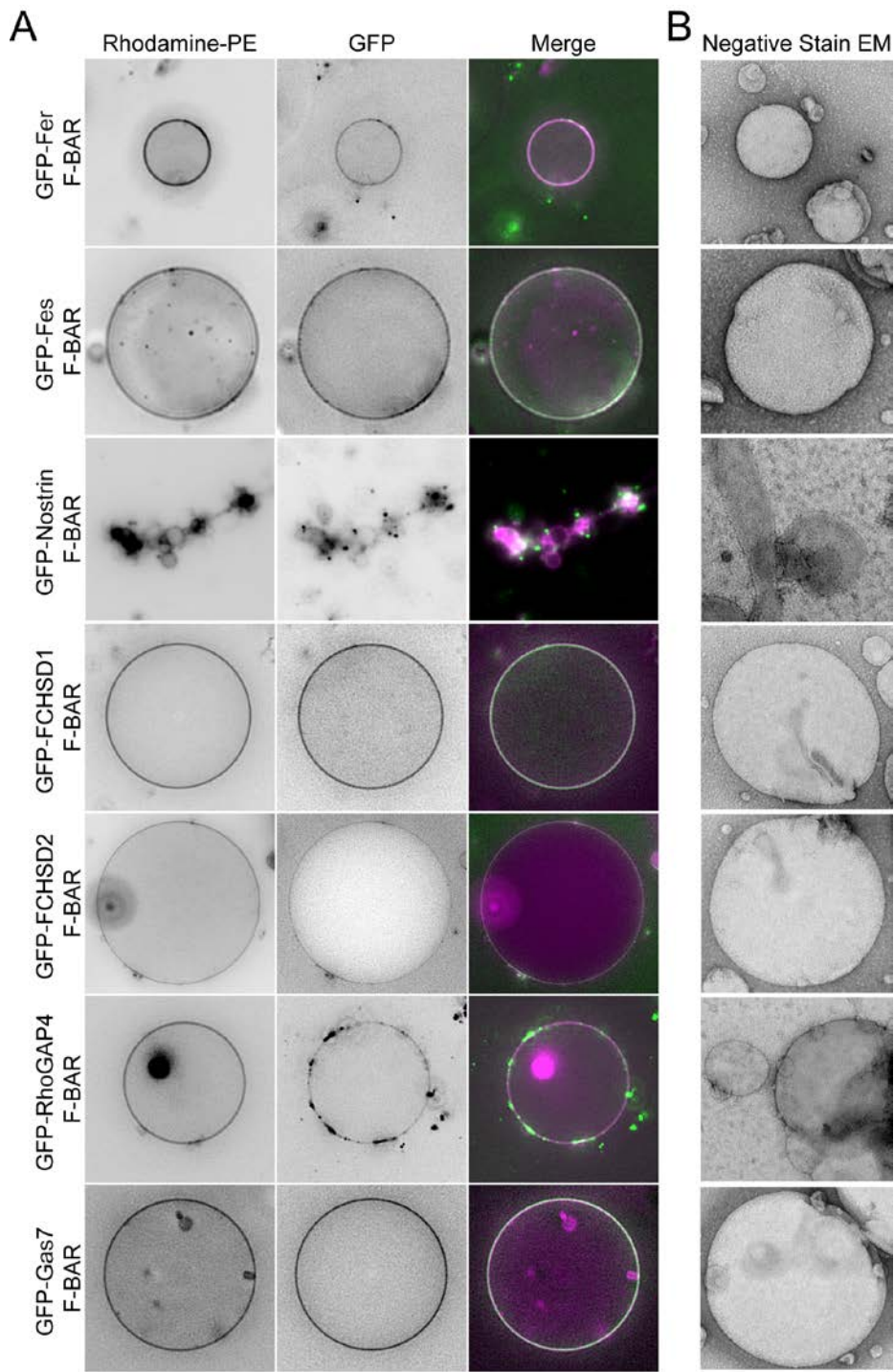


**Figure 2-3. A significant fraction of human F-BAR domains do not bend membranes.** A) 10-30  $\mu\text{m}$  GUVs (composed of 69% DOPC / 15% DOPE / 10% DOPS / 5% PI(4)P / 1% Rhodamine-PE) mixed with 10  $\mu\text{M}$  of the indicated GFP-F-BAR domain constructs. Scale bar = 10  $\mu\text{m}$ . B) 800nm extruded liposomes (composed of 70% DOPC / 15% DOPE / 10% DOPS / 5% PI(4)P) mixed with 10  $\mu\text{M}$  of the indicated F-BAR domain and examined with negative stain EM. Scale bar = 100nm.

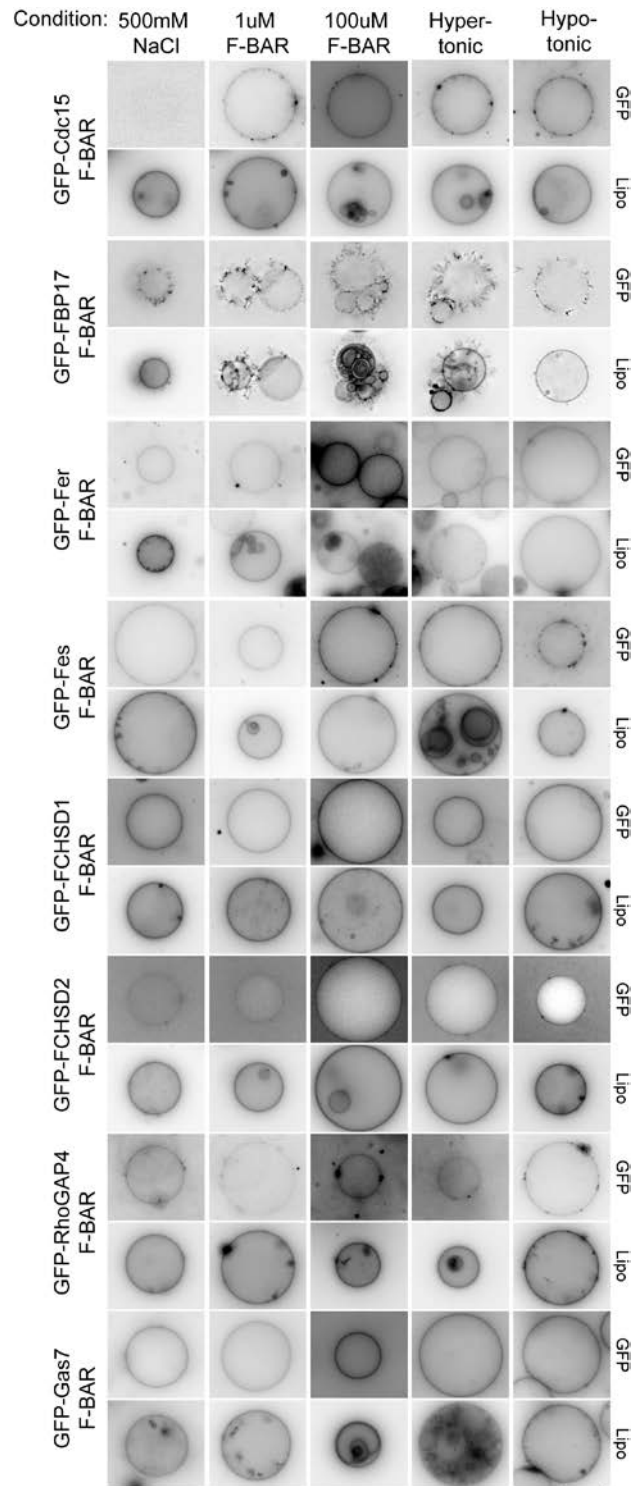


**Figure 2-4. Cdc15 and 6 human F-BARs do not tubulate membranes under a variety of conditions.** The indicated F-BAR domains were mixed with GUVs (composed of 69% DOPC / 15% DOPE / 10% DOPS / 5% PI(4)P / 1% Rhodamine-PE) in the indicated buffer condition. Concentrations of F-BARs were 10  $\mu$ M and NaCl 150 mM unless otherwise indicated. See supplemental experimental methods for details on hypertonic and hypotonic conditions. Scale bar = 10  $\mu$ m.

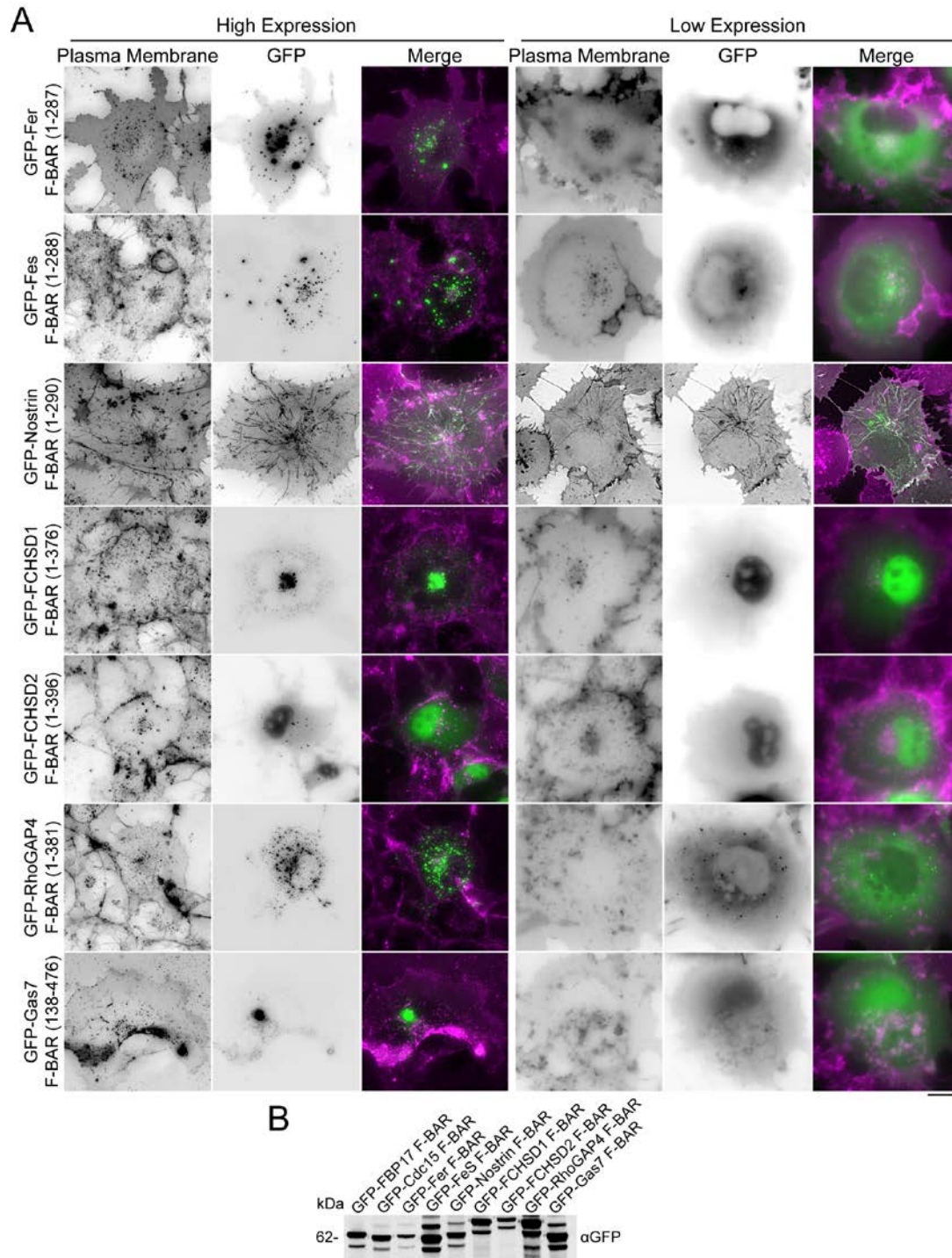


**Figure 2-5. A significant fraction of human F-BAR domains do not tubulate membranes in vivo.** A) Expression of the indicated GFP-F-BAR domains in COS-7 mammalian cells, co-stained with CellMask Orange plasma membrane stain. High and low expression example cells for each condition are shown. Scale bar = 10  $\mu$ m. B) Anti-GFP immunoblot showing expression of GFP-F-BAR domain constructs in COS-7 cell lysates.



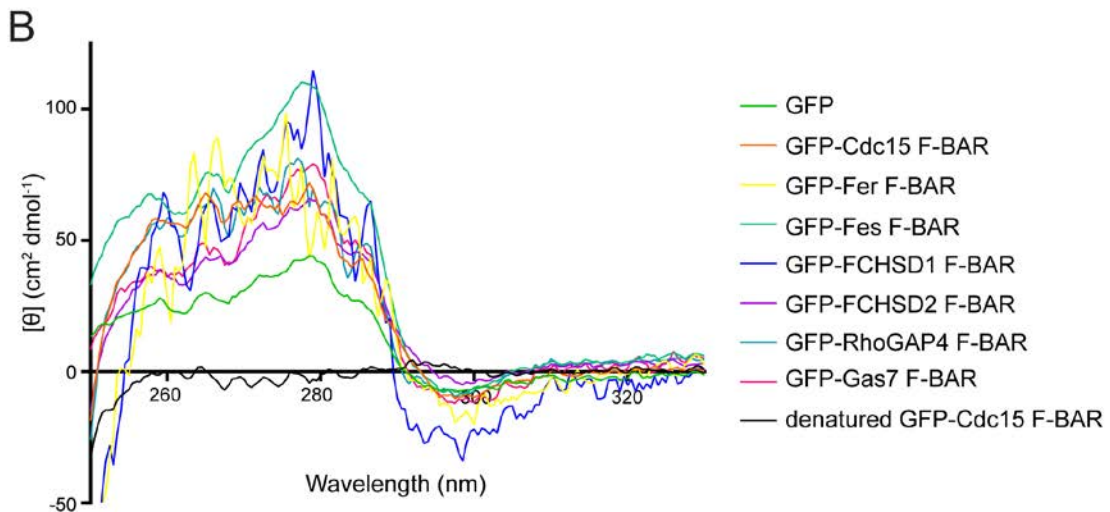
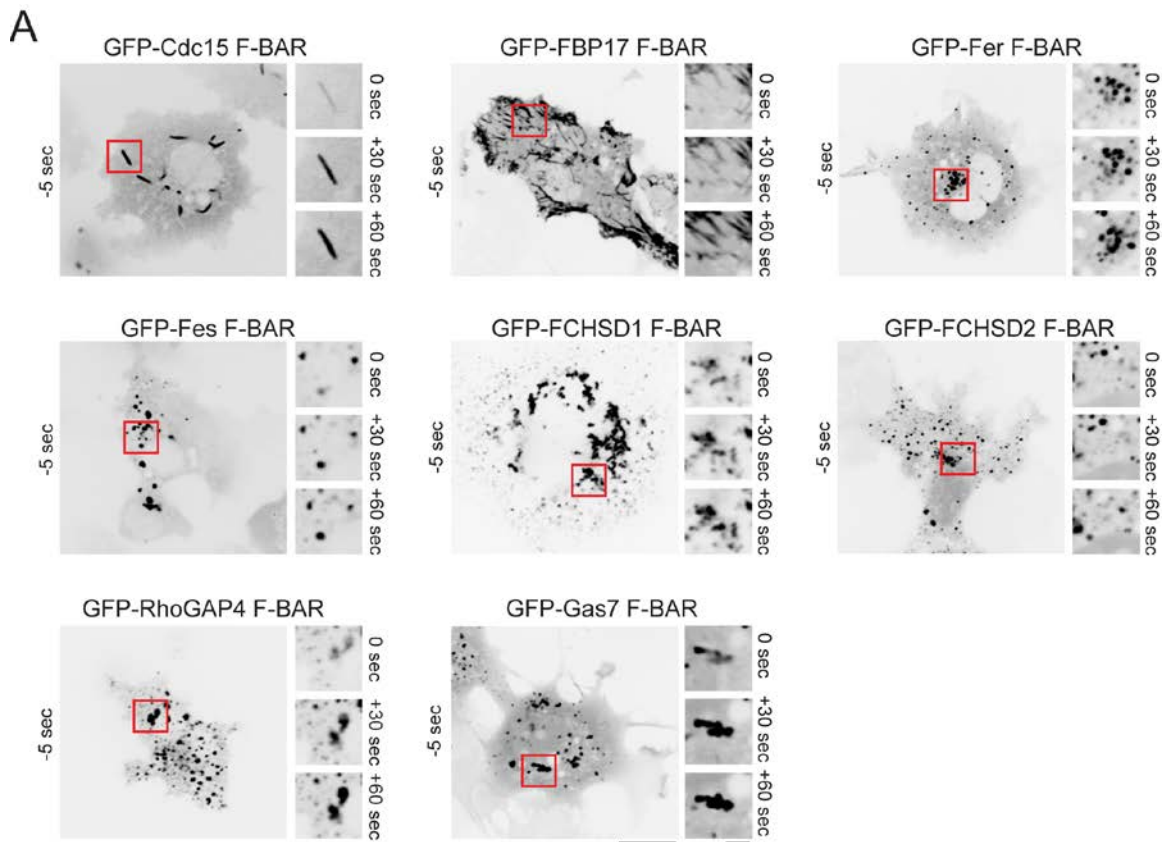


**Figure 2-6. Cdc15 and other F-BAR domains are folded and functional.** A) FRAP assay of the indicated transfected construct in COS-7 cells. The area in each red square was bleached. Scale bars = 10  $\mu\text{m}$  (main image) and 2  $\mu\text{m}$  (inset). B) Near-UV circular dichroism spectra of GFP and each GFP-F-BAR domain.

*The Cdc15 F-BAR oligomerizes in a tip-to-tip manner*

In membrane-tubulating F-BAR domains, interactions between adjacent F-BAR dimers, as identified in CIP4, are important for building the assemblies necessary to collectively bend membranes (Frost *et al.*, 2008). The Cdc15 F-BAR domain forms oligomers (Roberts-Galbraith *et al.*, 2010), suggesting similar interactions may exist despite a lack of tubulation activity. Indeed, as salt concentration was lowered, the Cdc15 F-BAR (Figure 2-7A) formed multiple oligomeric species when assayed by sedimentation velocity analytical ultracentrifugation (AU) (Figure 2-7B). A prominent peak comprising ~40% of the sample was present at ~240 kDa, corresponding to an assembly of four F-BAR dimers, while the remaining protein formed a heterogeneous mix of smaller and larger species (Figure 2-7B, arrows). The frictional ratio of the sample was 1.79, indicating a non-spherical shape of complexes in solution and negative stain EM of the sample revealed thin, linear oligomers (Figure 2-7C, left). These oligomers appeared to exist primarily via tip-to-tip interactions between F-BAR domain wings, as minimal branching and no sheet-like structures were observed (beyond the expected overlap from settling onto a 2D EM grid). The formation of these oligomers explains the F-BAR domain's sedimentation in the absence of liposomes at low salt concentrations (Figure 2-1D, 100 mM NaCl), and suggests a mechanism for Cdc15 F-BAR domain clustering on GUVs (Figure 2-2A). Cdc15 F-BAR oligomers were also visualized bound to liposomes by EM (Figure 2-7D). We also investigated the six human non-tubulating F-BAR domains for evidence of oligomerization in solution using AU (Figure 2-8). Each of these F-BAR domains exhibited oligomeric species of two (Fer) or more (Fes, FCHSD1, FCHSD2, RhoGAP4, Gas7) dimers in 50 mM NaCl.

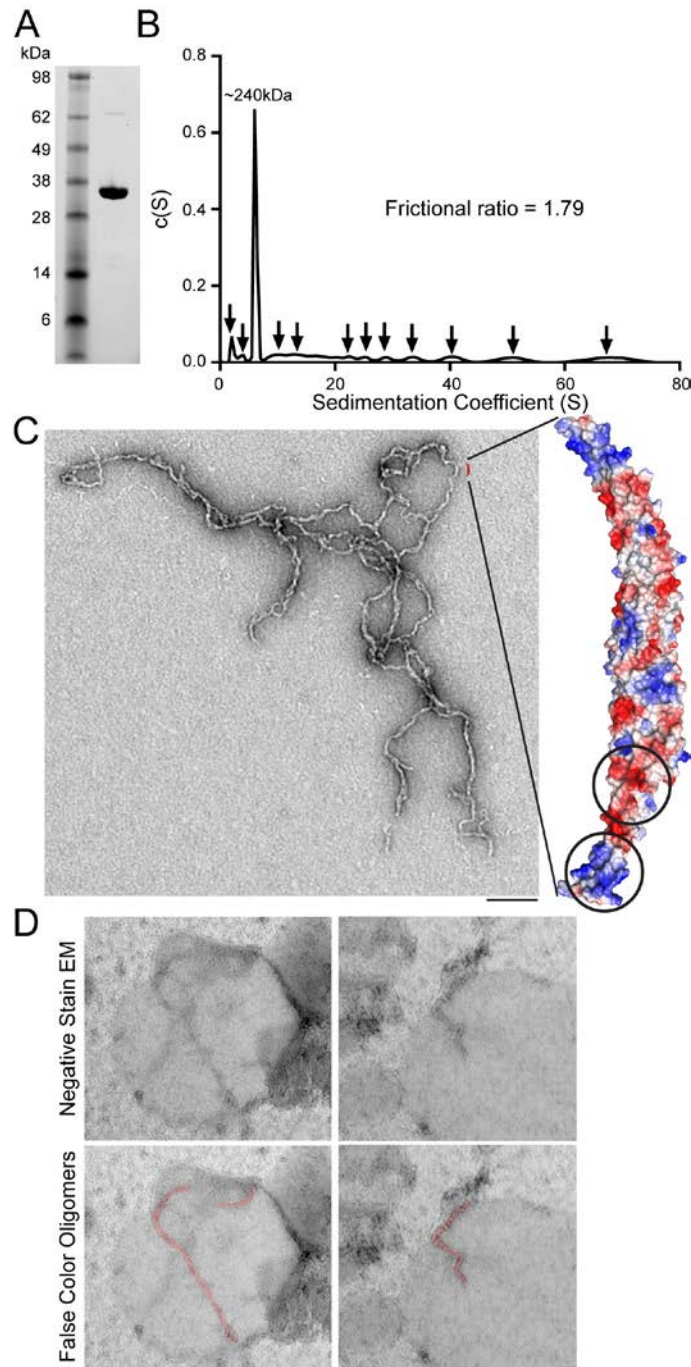


**Figure 2-7. The Cdc15 F-BAR domain organizes into tip-to-tip oligomers.** A) Coomassie stained SDS-PAGE of purified recombinant Cdc15 F-BAR domain (19-312). B) Analytical ultracentrifugation trace of the Cdc15 F-BAR domain in 50 mM NaCl. Multiple oligomer species are indicated by arrows. C) Negative stain electron micrograph of the Cdc15 F-BAR domain at 50 mM NaCl with electrostatic potential map of a Phyre2 structural homology model for scale. Putative patches interacting during oligomerization are circled. D) Cdc15 F-BAR domain mixed with liposomes and examined by negative stain EM. Bottom panels include false color highlighting of observable oligomers. All scale bars = 100 nm.

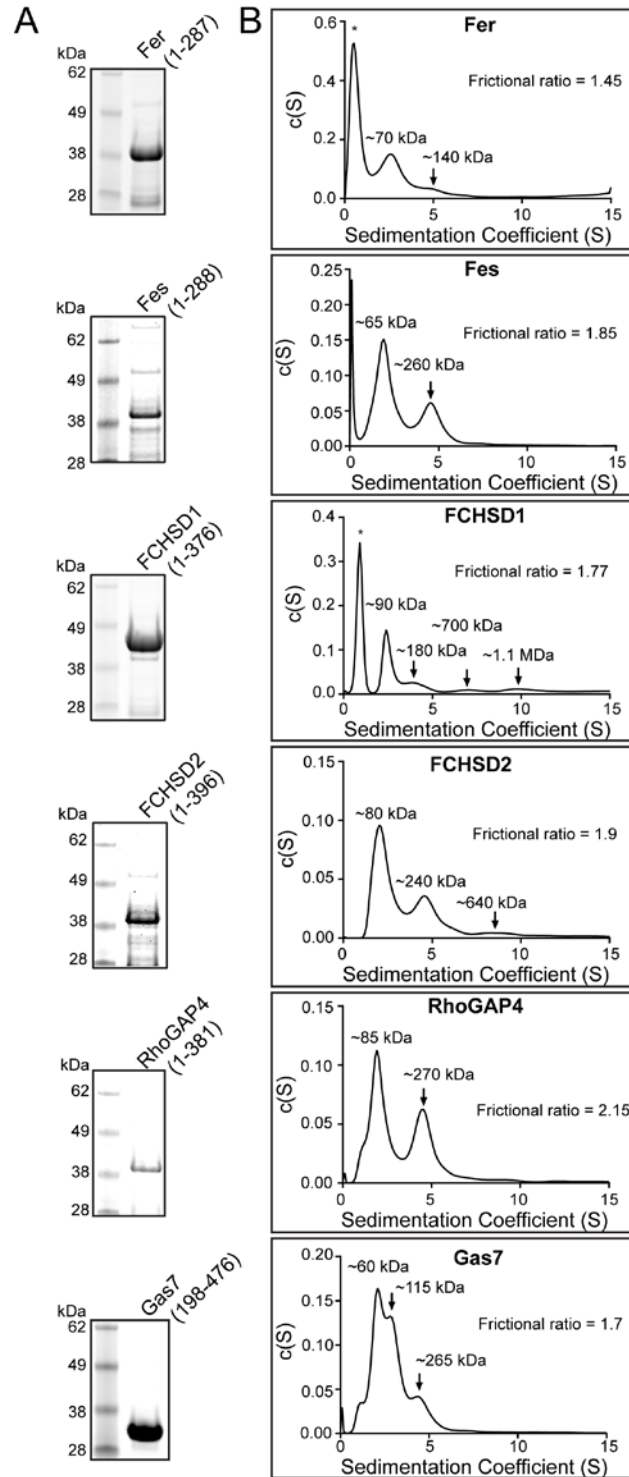


**Figure 2-8. Non-tubulating human F-BAR domains show evidence for oligomerization in solution.** A) Coomassie stained SDS-PAGE of the indicated purified F-BARs. B) Analytical ultracentrifugation traces of the indicated human F-BAR domains. Arrows indicate oligomerized species. \* indicates small MW contaminants.

To understand the structural basis for Cdc15's F-BAR domain oligomerization, we generated a model of the domain with the Protein Homology/analogy Recognition Engine v2.0 (Phyre<sup>2</sup>) (Kelley and Sternberg, 2009) using the homologous *S. cerevisiae* Hof1 F-BAR domain as a template structure, as Hof1 is the only non-tubulating F-BAR domain whose structure is available (Lippincott and Li, 1998; Moravcevic *et al.*, 2015) (Figure 2-7C, right). Based on the observed dependence of oligomerization on ionic strength and the appearance of the linear oligomer by EM, we reasoned that charged residues located on the sides of the F-BAR domain's wing tips might mediate F-BAR-to-F-BAR interaction. In an electrostatic potential map of the Cdc15 model, a prominent positively charged patch exists at the tip of the domain, wrapping around the concave face to one side, while a negatively charged cleft is located proximally on the wing (Figure 2-7C, circled on right). We hypothesized that interaction between these two patches could support oligomerization.

#### *Structural basis for Cdc15's F-BAR domain oligomerization and membrane binding*

To test this oligomerization model, we identified residues located in the positive (K163, R177, K181, and K185) and negative (E30, D31, and E152) patches on each F-BAR domain tip and wing, respectively (Figure 2-9A). Charge reversal mutations in the identified wing (E30K E152K) and tip (K163E) residues or a Tip-4A mutation (K163A, R177A, K181A, and K185A) abolished oligomerization of the F-BAR domain *in vitro* (Figure 2-9B and 2-10A). To ensure these mutations eliminated oligomerization *in vivo* as well, we purified the double E30K, E152K and single K163E mutants from *S. pombe*, and confirmed loss of oligomerization by AU (Figure 2-9C)



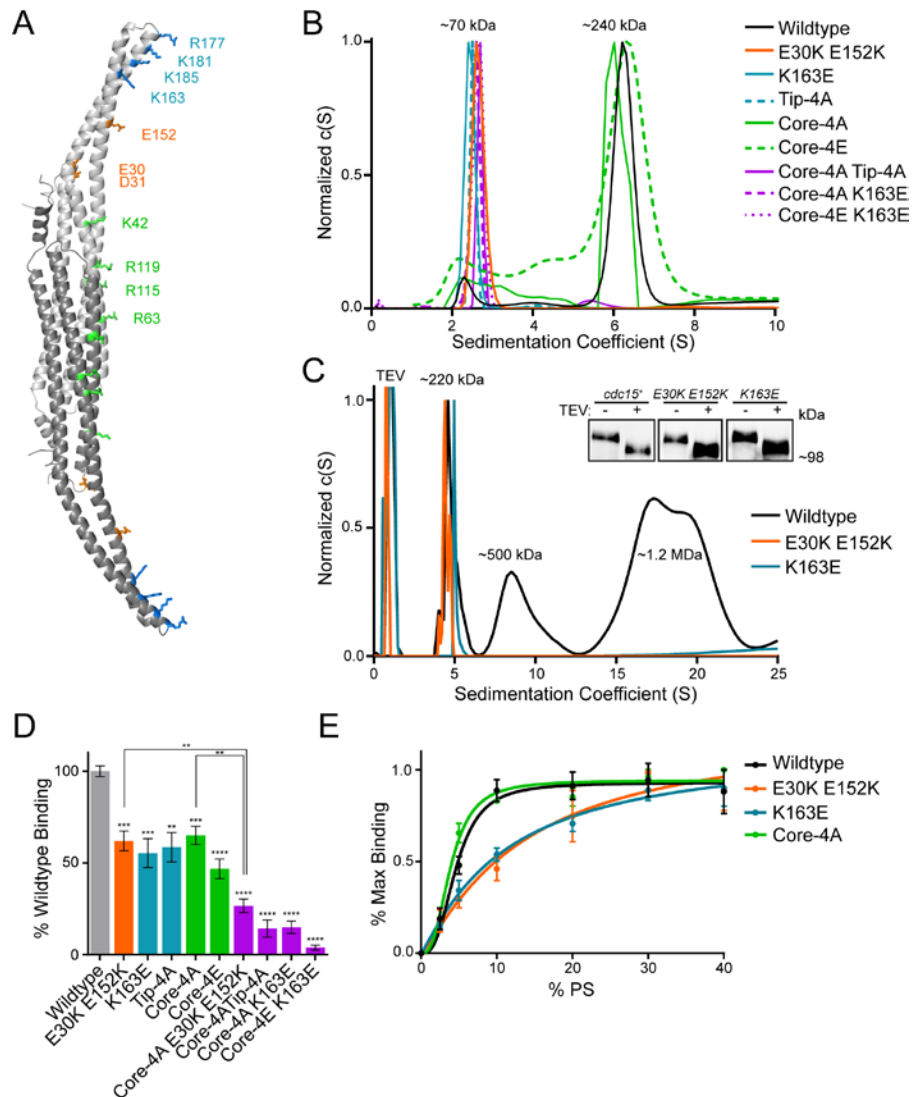


**Figure 2-9. Structural basis for Cdc15 F-BAR domain oligomerization and membrane binding.** A) Phyre2 homology model of the Cdc15 F-BAR (based on Hof1, PDB: 4WPE) with dimer subunits colored in dark and light grey. Putative charged residues involved in either oligomerization (blue and orange) or membrane binding (green and blue) are labeled. B) Analytical ultracentrifugation traces of Cdc15 F-BAR domain mutants. C) Analytical ultracentrifugation trace of purified full length Cdc15 and mutants purified from *S. pombe*. A TEV contaminant from the purification is indicated. Inset) Anti-Cdc15 Western blot of purified Cdc15-TEV-2xProtA and mutants before and after TEV cleavage. D) Bio-Layer Interferometry binding assay between 1  $\mu$ M Cdc15 F-BAR domain mutants and 100 nm liposomes composed of 69.9% DOPC / 15% DOPE / 10% DOPS / 5% PI(4)P / 0.1% Biotin-PE. \*\*,  $p < 0.01$ ; \*\*\*,  $p < 0.001$ ; \*\*\*\*,  $p < 0.0001$ , one-way ANOVA. E) Normalized saturation binding curves of Cdc15 and mutant F-BAR domains to liposomes composed of 50% DOPC, increasing amounts of DOPS, and the remainder DOPE. Tip-4A consists of K163A, R177A, K181A, K185A while Core-4A/E consist of K42A/E, R63A/E, R115A/E, R119A/E. All error bars indicate SEM.

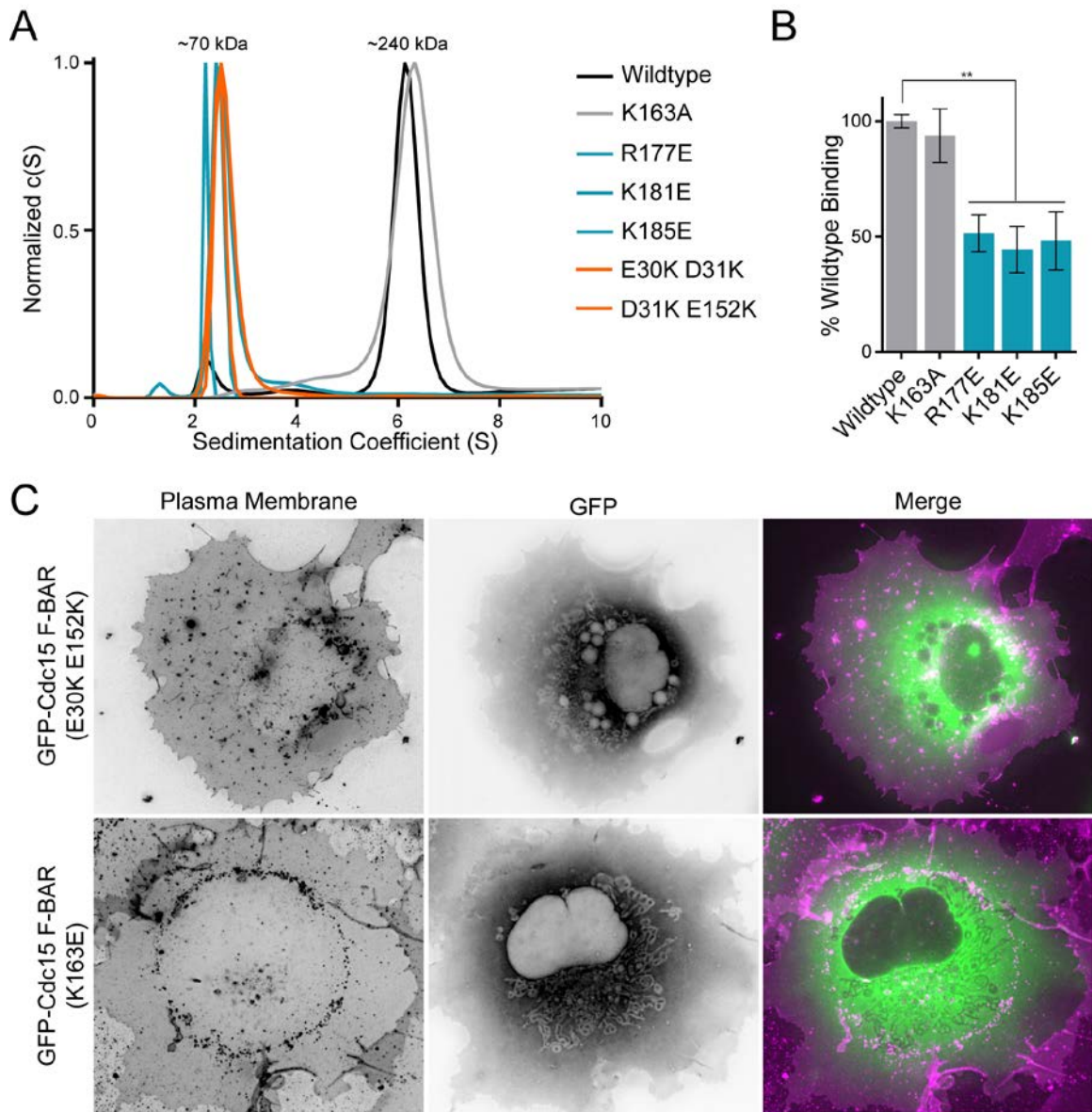


**Figure 2-10. F-BAR domain oligomerization and membrane binding.** A) Analytical ultracentrifugation traces of additional Cdc15 F-BAR domain mutants. B) Bio-Layer Interferometry binding assay between additional Cdc15 F-BAR domain mutants at 1  $\mu$ M and 100 nm liposomes composed of 69.9% DOPC / 15% DOPE / 10% DOPS / 5% PI(4)P / 0.1% Biotin-PE. Error bars indicate SEM. \*\*,  $p < 0.01$ , one-way ANOVA. C) GFP-Cdc15 F-BAR domain mutants were expressed in COS-7 cells and co-stained with CellMask Orange plasma membrane dye. Scale bar = 10  $\mu$ m.

(Roberts-Galbraith *et al.*, 2010). These two mutations also eliminated the clustering of the Cdc15 F-BAR domain when overexpressed in COS-7 cells (compare Figure 2-2C and 2-10C). That disruption of either of these two oppositely charged patches abolished oligomerization supports our reciprocal electrostatic interaction model of Cdc15 oligomerization.

We next determined the mechanism of Cdc15 F-BAR domain membrane binding and the interplay between this function and oligomerization. By analogy to other F-BAR domains, we reasoned that positively charged residues in the concave central core region (K42, R63, R115, and R119) might mediate membrane binding (Figure 2-9A, green residues). As predicted, mutation of these residues to alanine or glutamate (Core-4A and Core-4E) reduced binding of the F-BAR to liposomes *in vitro* (Figure 2-9D). However, membrane binding was not abolished, indicating the involvement of additional residues. Interestingly, mutations of either the positive or negatively charged tip patches that mediate oligomerization also decreased binding to membranes (Figure 2-9D and 2-10B). Since mutation of either positively (K163E) or negatively charged (E30K E152K) residues resulted in a similar decrease in equilibrium binding, this impairment likely arises from loss of oligomerization and a consequent decrease in the avidity of the Cdc15 F-BAR domain for the membrane. Supporting this idea, combining a strictly membrane binding mutation (Core-4A) with the acidic oligomerization mutant (E30K E152K) decreased equilibrium binding below the level of a Core-4A mutation alone (Figure 2-9D). Furthermore, oligomerization mutants displayed a loss of cooperative binding to membranes, with Hill coefficients of  $1.1 \pm 0.3$  (K163E) and  $1.2 \pm 0.4$  (E30K E152K) compared to  $2.9 \pm 0.8$  for wildtype (Figure 2-9E).

Since Core-4A and Core-4E mutants retained some membrane binding, we tested whether the basic residues at the F-BAR domain tips contributed both to oligomerization and also directly to membrane binding. Combination mutations (Core-4A Tip-4A, Core-4A K163E, and Core-4E K163E) decreased binding to very low levels, indicating that the residual membrane binding of core mutants is mediated by positive residues at the tips (Figure 2-9D). The positively charged patch, which extends from the concave face of wing tips around the sides of the wing, therefore, appears to have a dual function of binding membranes and mediating oligomerization.

#### *Cdc15 oligomerization defects impair cytokinesis*

Next, we investigated the function of the Cdc15 F-BAR domain's membrane binding and oligomerization activities in vivo by integrating mutants compromising one or both functions into Cdc15's endogenous locus. The most defective membrane-binding mutant (Core-4E K163E) was inviable (Figure 2-11A), indicating that membrane binding is strictly required for Cdc15's function. Although we were able to recover other strains producing Cdc15 mutants strongly deficient in membrane binding (e.g. Core-4A Tip-4A), they failed cytokinesis regularly and became multinucleate (Figures 2-12A-B), supporting the conclusion that membrane binding is an essential Cdc15 function.

To distinguish between the contribution of oligomerization as opposed to both oligomerization and direct membrane binding, we focused on the mutant of the negatively charged patch (E30K E152K) in further experiments but also assayed the basic charge reversal mutant K163E. mCherry-tagged E30K E152K and K163E were present at only ~31% or ~38%, respectively, of wildtype levels at the division site, while the Core-

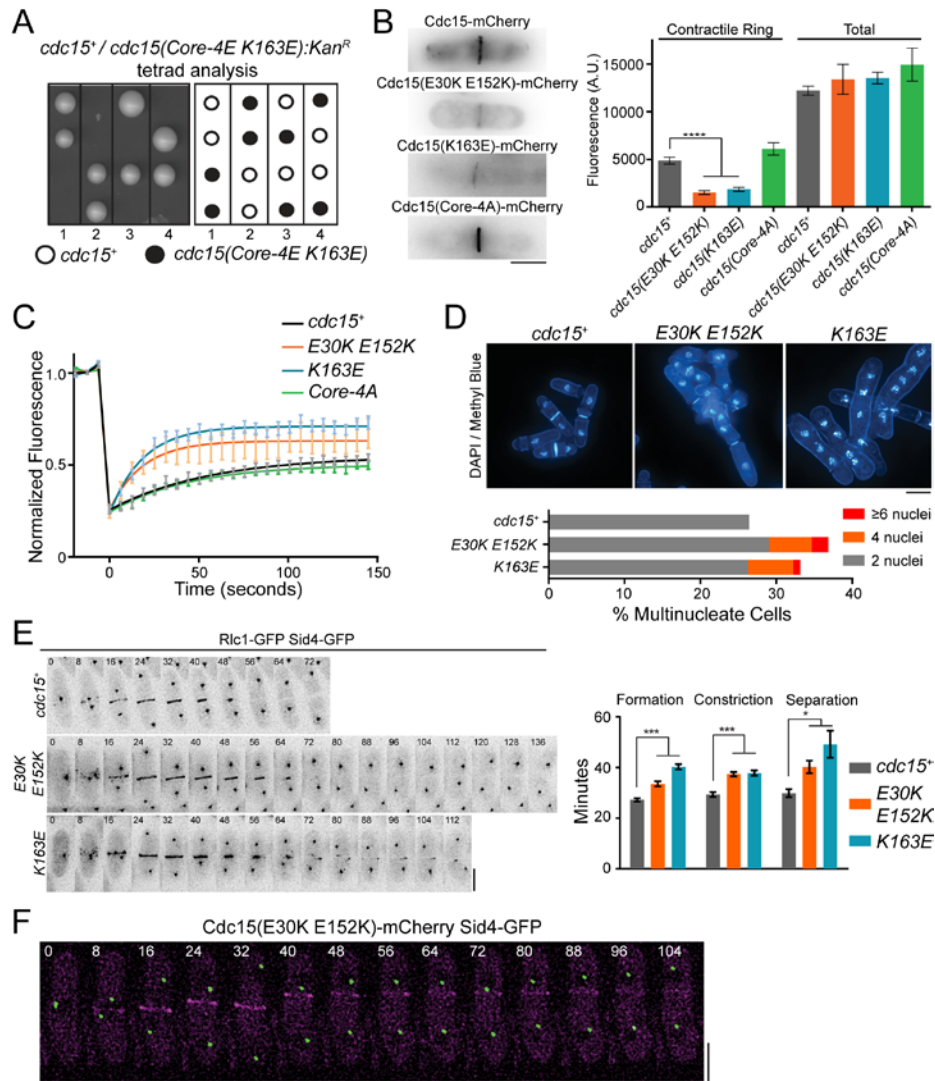


**Figure 2-11. Oligomerization is critical for a stable Cdc15 scaffold at the division site and robust cytokinesis.** A) A complete membrane binding Cdc15 mutant is inviable. The Cdc15(Core-4E K163E) mutation was integrated into a *cdc15/cdc15::ura4+* diploid, sporulated, and tetrads were dissected. Relevant genotypes are indicated. B) Comparison of *cdc15(E30K E152K)-mCherry*, *cdc15(K163E)-mCherry*, and *cdc15(Core-4A)-mCherry* to *cdc15<sup>+</sup>-mCherry* fluorescence at the division site. Right) Quantification of Cdc15-mCherry contractile ring and whole cell fluorescence intensities of the indicated strains.  $n > 50$  for each genotype. C) Recovery after photobleaching of Cdc15-GFP and mutants. Lines represent least squares fit of recovery,  $n > 30$  for each genotype. D) DAPI (DNA) and Methyl Blue (cell wall / septum) staining of *cdc15<sup>+</sup>* and *cdc15* mutants. Bottom) Number of nuclei per cell in *cdc15<sup>+</sup>* and *cdc15* mutants.  $n > 400$  for each genotype. E) Representative time-lapses (left) and quantification (right) of cytokinesis in the indicated strains.  $n > 30$  for each genotype. F) Time-lapse imaging of a *cdc15(E30K E152K)-mCherry sid4-GFP* cell as cytokinesis fails. All scale bars = 4  $\mu$ m. All error bars indicate SEM. \*,  $p < 0.05$ ; \*\*\*,  $p < 0.001$ ; \*\*\*\*,  $p < 0.0001$ , one way ANOVA.

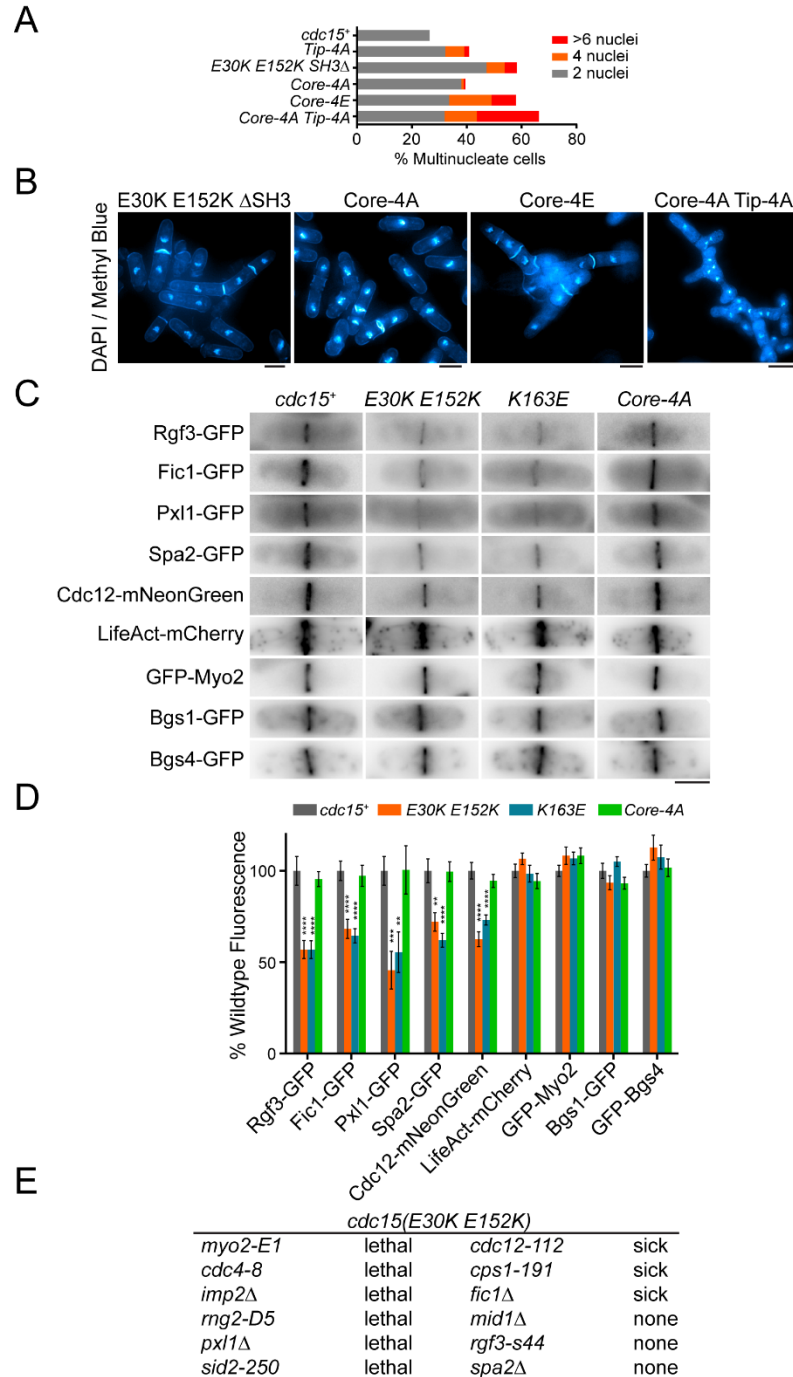


**Figure 2-12. Oligomerization is critical for Cdc15 function in cytokinesis.** A) Number of nuclei per cell in the indicated *cdc15* mutants. Wildtype data is from Figure 7B.  $n > 400$  for each genotype. B) DAPI (DNA) and Methyl Blue (cell wall / septum) staining of the indicated *cdc15* mutants. C-D) Representative sum projection images (C) and quantification (D) of contractile ring fluorescence intensity of the indicated fluorescently tagged proteins in *cdc15+*, *cdc15(E30K E152K)*, *cdc15(K163E)*, or *cdc15(Core-4A)* strains.  $n > 50$  for each condition. Error bars indicate SEM. \*\*,  $p < 0.01$ ; \*\*\*,  $p < 0.001$ ; \*\*\*\*,  $p < 0.0001$ , one-way ANOVA. E) Summary of *cdc15(E30K E152K)* synthetic genetic interactions. All scale bars = 4  $\mu\text{m}$ .

4A mutant defective in membrane binding but still capable of oligomerization was present at wildtype levels (Figure 2-11B). Wildtype Cdc15 is highly static in CRs with a mobile fraction ( $F_m$ ) of 29.5% and a slow recovery half time ( $t_{1/2}$ ) of 38.5 seconds, as determined by FRAP (Figure 2-11C) (Roberts-Galbraith *et al.*, 2009). This indicates that Cdc15 is stably “glued” on the membrane at the division site, which we hypothesized was due to extensive oligomerization and membrane interactions. To test this, we compared the dynamics of the oligomerization mutants to wildtype Cdc15 (Figure 2-11C) and found that oligomerization-defective Cdc15 mutants were significantly more dynamic with  $t_{1/2} = 12.7$  seconds (E30K E152K) and 12.9 seconds (K163E), and increasingly mobile with  $F_m = 37.6\%$  (E30K E152K) and 47.5% (K163E). This increased dynamicity is due to loss of oligomerization, as the Core-4A mutant deficient only in membrane binding (Figure 2-9B, D-E) resembled wildtype with  $F_m = 26.1\%$  and  $t_{1/2} = 30.8$  seconds. The Core-4A mutant therefore appears to retain enough membrane binding capability via electrostatic interactions of tip residues with the membrane and oligomerization to function normally in the CR.

Cdc15 partners with several other proteins at the CR; therefore, we tested whether reduced levels and increased dynamicity of the Cdc15 oligomerization mutants affected partner recruitment (Figure 2-12C-D). We found that the SH3 domain interactors Rgf3, Fic1, Pxl1, and Spa2 (Roberts-Galbraith *et al.*, 2009; Ren *et al.*, 2015), in addition to F-BAR domain interactor Cdc12 (Carnahan and Gould, 2003; Willet, McDonald, Bohnert, *et al.*, 2015), were all significantly diminished at pre-constriction CRs in both

*cdc15(E30K E152K)* and *cdc15(K163E)* mutants. However, CR proteins not known to directly bind Cdc15 including F-actin (measured by LifeAct-mCherry), Myo2, and  $\beta$ -glucan synthases Bgs1 and Bgs4 were unchanged in abundance at pre-constriction CRs. Decreased recruitment of binding partners was a function of oligomerization defects alone, as the *cdc15(Core-4A)* mutant had no effect on downstream recruitment levels (Figure 2-12C-D), as expected with normal levels and stability at the division site.

To further understand the importance of linear F-BAR oligomerization to Cdc15's function in cytokinesis, we studied oligomerization mutant cells using live cell microscopy. Oligomerization-defective mutants displayed phenotypes indicative of compromised cytokinesis (Figure 2-11D). Positive and negative residue charge reversal mutations exhibited identical phenotypes, supporting our previous conclusion that both are involved in mediating F-BAR domain oligomerization. Combining the E30K E152K mutation with truncation of the C-terminal SH3 domain exacerbated the cytokinesis defects as might be expected if SH3-domain interactions help to further stabilize Cdc15 at the CR (Figure 2-12A-B) (Roberts-Galbraith *et al.*, 2009). That cytokinesis defects result from loss of Cdc15 F-BAR domain oligomerization is further supported by synthetic lethal genetic interactions between oligomerization mutants and other mutations in cytokinesis genes including *myo2-E1*, *rng2-D5*, *imp2 $\Delta$* , *cdc4-8*, in addition to synthetic sickness in combination with *cps-191* and *cdc12-112* (Figures 2-12E). Interestingly, oligomerization mutants were also synthetically lethal in combination with *pxl1 $\Delta$*  and sick with *fic1 $\Delta$* , two Cdc15 SH3 binding partners.

To understand how impaired Cdc15 oligomerization compromises cytokinesis, we imaged *cdc15<sup>+</sup>*, *cdc15(K163E)*, and *cdc15(E30K E152K)* strains with Rlc1-GFP and



Sid4-GFP as markers of the CR and spindle pole body (SPB), respectively, to analyze the kinetics of cytokinesis (Figure 2-11E). We defined CR formation as the time from SPB separation to onset of CR constriction, constriction as the time from Rlc1-GFP ingress to disappearance at the division site, and separation as time from Rlc1-GFP disappearance to cell separation. In both E30K E152K and K163E mutants, each step of cytokinesis was extended (Figure 2-11E, right). We additionally observed cells that failed to divide, consistent with the 5-10% multi-nucleation rate. By imaging *cdc15(K163E)-mCherry* cells, we observed that in cells failing cytokinesis, Cdc15 rings were formed, but slid from the cell middle and disassembled during anaphase (Figure 2-11F). These data indicate that Cdc15 oligomerization facilitates its stable membrane binding and scaffolding function at the cell division site.

To determine if the importance of F-BAR oligomerization extends to any of the human F-BARs studied above that also do not tubulate membranes, we focused on Fer and RhoGAP4 because they have easily assayable functions in lamellipodia formation and cell migration, respectively (Vogt *et al.*, 2007; Itoh *et al.*, 2009). We generated structural models of the Fer and RhoGAP4 F-BAR domains with Phyre<sup>2</sup> (Figure 2-13A, F) and identified acidic patches on the side of each F-BAR. By testing each patch, we found specific ones that, when mutated, eliminated Fer and RhoGAP4 F-BAR oligomerization in vitro (Figure 2-13A-B, F-G). We then tested the functional consequence of these mutations in the context of their respective full-length proteins. Whereas exogenously expressed wildtype Fer drove lamellipodia formation as shown previously (Itoh *et al.*, 2009), the Fer E265K oligomerization mutation prevented this activity (Figure 2-13C-E). Furthermore, the E122K or E155K, E156K, E159K mutations

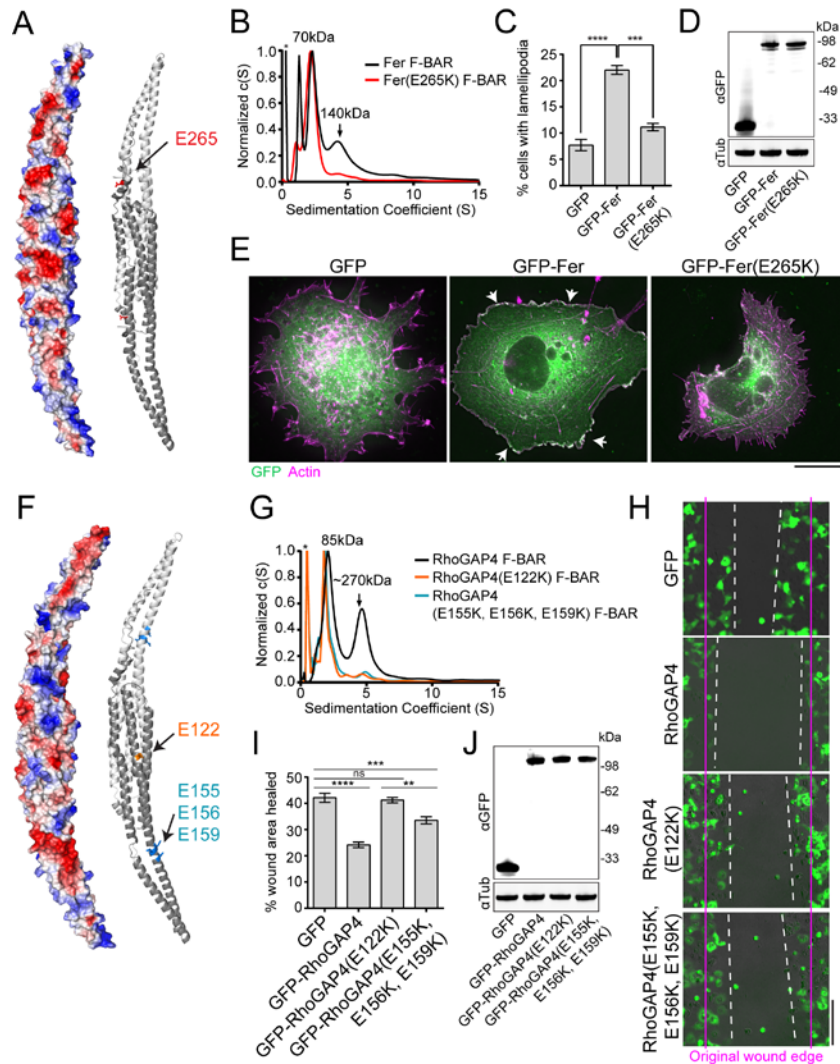


**Figure 2-13. Oligomerization is critical for Fer and RhoGAP4 function.** A) Phyre2 homology model (based on Fes, PDB:4DYL) of the Fer F-BAR domain with dimer subunits colored in dark and light grey. An electrostatic potential map (left) and a cartoon model (right) with oligomerization residues highlighted are shown. B) AU trace of purified Fer and Fer(E265K) F-BAR domains. Small MW contaminant indicated by \*. C-E) GFP, GFP-Fer, or GFP-Fer(E265K) were expressed in COS-7 cells (D), stained with Rhodamine-phalloidin (E), and quantified for the presence of lamellipodia (C). Scale bar = 10  $\mu$ m. F) Phyre2 homology model (based on CIP4, PDB:2EFK) of the RhoGAP4 F-BAR domain with dimer subunits colored in dark and light grey. An electrostatic potential map (left) and a cartoon model (right) with oligomerization residues highlighted are shown. G) AU trace of purified Fer and Fer(E265K) F-BAR domains. Small MW contaminant indicated by \*. H-J) GFP, GFP-RhoGAP4, GFP-RhoGAP4(E122K), and GFP-RhoGAP4(E155K, E156K, E159K) were expressed in COS-7 cells (J). A wound was formed with a P200 pipet tip (H) and migration into the wounded area was quantified after 8 hours (I). Scale bar = 100  $\mu$ m. All error bars indicate SEM from 3 experiments. \*\*\*,  $p < 0.001$ ; \*\*\*\*,  $p < 0.0001$ , one-way ANOVA.

in RhoGAP4 blocked its ability to inhibit cell migration in a wound healing assay (Vogt *et al.*, 2007) (Figure 2-13H-J). Together, these data demonstrate that F-BAR oligomerization but not membrane bending is functionally important in several biological contexts.

## Discussion

In this study, we found that the Cdc15 F-BAR domain, unlike many previously described F-BAR domains, binds but does not bend membranes *in vivo* or *in vitro*, challenging the widely held view that tubulation is a fundamental function of F-BAR domains. Six human F-BAR domains exhibit similar behavior, suggesting that a significant fraction of F-BAR proteins function primarily as molecular tethers. Tuned by post-translational modification, these F-BAR proteins transiently link different machinery to the membrane in a variety of biological contexts without changing membrane contour. Oligomerization is critical for these F-BAR domains' functions; Fer and RhoGAP4 rely upon F-BAR oligomerization for their functions in cell migration, while the Cdc15 F-BAR domain forms linear oligomers that are critical for efficient membrane binding and robust localization to the division site. Indeed, Cdc15 oligomers appear to serve as a major anchor for the CR at the membrane.

### *Diverse modes of F-BAR oligomerization*

Lateral and tip-to-tip interactions have been observed between dimers in CIP4 F-BAR domain *in vitro* tubule reconstructions (Frost *et al.*, 2008). Lateral interactions were essential in CIP4 for bending membranes into tubules, while tip-to-tip contacts performed

an organizational role of aligning dimers and resisting helical tilting of F-BAR domain assemblies (Shimada *et al.*, 2007; Frost *et al.*, 2008). In the Cdc15 F-BAR, tip-to-tip contacts between adjacent dimers organized them into linear strands. In Fer and RhoGAP4, residues on the wings and core of F-BAR dimers were important for oligomerization, suggesting lateral F-BAR to F-BAR contacts. Interestingly, the residues identified in Cdc15, Fer, and RhoGAP4 are distinct from those identified in CIP4 tubule reconstructions. This suggests that the F-BAR family possesses multiple distinct modes of oligomerization which we propose result in different organizations on the membrane, not all of which produce membrane deformation. Crystal structures of non-tubulating F-BAR domains may also reveal any primary structural differences that preclude their abilities to bend membranes.

Cdc15 F-BAR domain's linear mode of oligomerization is important for efficient membrane binding. Our data suggest two interconnected factors contribute to weakened membrane binding when oligomerization is impaired: 1) Loss of cooperativity effectively lowers the amount of protein bound to membrane at a given concentration and 2) loss of Cdc15 oligomers' avidity (as each oligomer subunit contains membrane binding contacts) destabilizes membrane association. Cooperative binding has been observed for human FBP17 and *Drosophila* Nwk F-BAR domains, which may also arise from oligomerization of F-BAR dimers (Becalska *et al.*, 2013; Itoh *et al.*, 2005). Cooperative membrane binding through oligomerization may serve as a mechanism to concentrate and stabilize F-BAR domain localization at sites of action, similar to Cdc15 concentration at the division site.

Diversity among F-BAR domains is also seen with the choice of residues used for membrane binding. Of F-BARs studied in mechanistic detail, *S. pombe* Cdc15 and human FBP17, CIP4, and FCHo2, utilize unique charged residues on their concave surfaces, located both in the core and wings, to associate with membranes (Henne *et al.*, 2007; Shimada *et al.*, 2007; Frost *et al.*, 2008). Human PACSIN F-BAR domains additionally utilize a small loop inserted into the membrane bilayer (Wang *et al.*, 2009), and *S. cerevisiae* Rgd1p contains a specific PIP binding patch at the base of each wing (Moravcevic *et al.*, 2015). This patch may be loosely conserved in additional F-BAR domains, though none have been shown to have the strong PIP specificity observed in Rgd1p.

#### *Cdc15 oligomerizes to robustly scaffold a network of cytokinesis proteins*

There are approximately ~16,100 copies, or 8050 dimers, of Cdc15 at the division site (Wu and Pollard, 2005), and F-BAR dimers are approximately 220 Å in length (Shimada *et al.*, 2007; Moravcevic *et al.*, 2015). Assuming a 3.5 µm inner cell diameter, linear oligomers of Cdc15 aligned perpendicular to the cell's long axis could, in a simple model, circle the division site ~16 times. Considering a ~25 Å width of one F-BAR dimer, oligomers lying next to each other would yield a scaffolding platform a minimum of ~40 nm wide, easily within estimates of CR width of 100-200 nm (Kamasaki *et al.*, 2007). The filamentous linear oligomerization of Cdc15, with each repeating F-BAR domain unit binding the membrane, generates a strong avidity for the membrane. Consequently, these oligomers serve as a stable scaffolding platform for the CR, reinforced by the many stabilizing interactions mediated by Cdc15's C-terminal SH3

domain (Roberts-Galbraith *et al.*, 2009; Ren *et al.*, 2015). Accordingly, when Cdc15 oligomerization is prevented, this platform weakens and becomes increasingly dynamic, leading to impairments in cytokinetic fidelity. The state of Cdc15 oligomerization is controlled during a normal cell cycle via cell cycle-regulated phosphorylation (Roberts-Galbraith *et al.*, 2010); dephosphorylation allows oligomerization while re-phosphorylation antagonizes it. Inhibition of oligomerization via phosphorylation during CR constriction could aid significantly in CR disassembly. In the future, it will be interesting to determine exactly how phosphorylation modulates F-BAR-to-F-BAR interactions within the context of the full-length protein.

CR sliding and/or instability have been observed in other situations with compromised Cdc15 levels or function (Wachtler *et al.*, 2006; Hachet and Simanis, 2008; Roberts-Galbraith *et al.*, 2009; Arasada and Pollard, 2014), as well as when glucan chain synthesis is compromised (Liu *et al.*, 2000; Pardo and Nurse, 2003; Muñoz *et al.*, 2013; Arasada and Pollard, 2014; Stachowiak *et al.*, 2014), suggesting an intimate link between the function of glucan synthase enzymes, Cdc15, and CR integrity. In *S. pombe*, it is essential that a primary and secondary septum forms behind the constricting CR (Liu *et al.*, 1999; Proctor *et al.*, 2012; Muñoz *et al.*, 2013). Considering these data and our results, we propose two factors contribute to CR instability when Cdc15 function is defective. First, the physical connection between the plasma membrane and the CR is weakened. Second, Cdc15's direct binding partners that influence septum formation (Tajadura *et al.*, 2004; Morrell-Falvey *et al.*, 2005; Roberts-Galbraith *et al.*, 2009; Bohnert and Gould, 2012; Ren *et al.*, 2015) including the Rho-GEF Rgf3, essential for activating Rho1 and the Bgs1 glucan synthase, are reduced in abundance at the CR. A

weakened membrane anchor and insufficient septum deposition likely contribute to CR instability, allowing CR sliding from the cell middle.

*A significant fraction of F-BARs do not deform membranes*

With the addition of our data, all human F-BAR domains have been tested for their ability to bend membranes into tubules at high concentration (Table 2-1). Eleven domains positively bend membranes into tubules, five induce negative curvature tubules, and here we find an additional six (Fer, Fes, FCHSD1/2, RhoGAP4, and Gas7) that bind but are unable to bend or tubulate membranes, similar to *S. pombe* Cdc15. Fer and Fes are non-receptor protein-tyrosine kinases with broad roles in actin cytoskeletal arrangement during cell motility and in cell-cell adhesions (Greer, 2002; Itoh *et al.*, 2009). FCHSD1/2 are the apparent human orthologs of *Drosophila* nervous wreck 1/2 proteins; interestingly, *Drosophila* Nwk1 is able to bend membranes into “ridges and scallops” (Becalska *et al.*, 2013), which we did not observe for human homologs FCHSD1/2. RhoGAP4 contains a GTPase activating domain and is involved in cell motility and axon growth (Vogt *et al.*, 2007). Gas7 is primarily expressed in quiescent cells and is involved in forming actin-based protrusions (Ju *et al.*, 1998; You and Lin-Chao, 2010). The lack of a functional connection between these proteins suggests the membrane binding and oligomerization properties of each F-BAR domain are tuned to its specific cellular function. It will be interesting to clarify the diverse structural mechanisms and roles of F-BAR oligomerization in other F-BAR proteins in their respective physiological functions.

## CHAPTER III

### THE TUBULATION ACTIVITY OF THE FISSION YEAST F-BAR PROTEIN IMP2 IS DISPENSIBLE FOR ITS FUNCTION IN CYTOKINESIS

McDonald N.A., Takizawa Y., Feoktistova A., Xu P., Ohi M.D., Vander Kooi C.W.,  
and Gould K.L. (2016) *Cell Reports*, 14(3):534-46

#### **Introduction**

The Fer/CIP4 Homology-Bin/Amphiphysin/Rvs (F-BAR) protein family is characterized by the presence of a N-terminal membrane-binding F-BAR domain and conserved roles in linking cellular membranes to the actin cytoskeleton (Roberts-Galbraith and Gould, 2010). F-BAR family proteins are found throughout eukaryotes, with 22 members in humans, 4 in *Saccharomyces cerevisiae*, and 7 in *S. pombe*. They are involved in a diverse array of actin-driven cellular processes including endocytosis, motility, and cytokinesis (Frost *et al.*, 2009).

Even within a single biological process, such as mammalian endocytosis, several different F-BAR proteins collaborate (Qualmann *et al.*, 2011). Studies of the relative timing of recruitment to endocytic sites indicate that multiple F-BARs assemble in a defined order (Taylor *et al.*, 2011). One hypothesis for this observation has been that each F-BAR protein senses or induces a different membrane curvature and/or membrane composition through its F-BAR domain (Mim and Unger, 2012; Qualmann *et al.*, 2011). Structurally, F-BAR domains are shallowly curved, crescent-shaped alpha-helical dimers with membrane binding capacity (reviewed in Frost *et al.*, 2009; Mim and Unger, 2012; Qualmann *et al.*, 2011; Suetsugu *et al.*, 2009). Several F-BAR domain proteins, such as those at sites of endocytosis (e.g. human FBP17, CIP4, Pacsin2, and FCHo2), are able to



bend membranes into thin tubules when present at high concentration (Itoh *et al.*, 2005; Tsujita *et al.*, 2006; Henne *et al.*, 2007). This process is thought to be accomplished through the formation of oligomeric assemblies of F-BAR domains on membranes which collectively enforce a curvature (Shimada *et al.*, 2007; Frost *et al.*, 2008; Yu and Schulten, 2013). Other F-BAR domains can induce outward curvature in membranes, i.e. protrusions rather than invaginations (Guerrier *et al.*, 2009; Carlson *et al.*, 2011). Additionally, multiple F-BAR domains lack the ability to deform membranes altogether (Tsujita *et al.*, 2006; McDonald *et al.*, 2015; Moravcevic *et al.*, 2015). It is not clear what properties of a F-BAR domain confer diverse membrane binding behaviors in vitro, and how these in vitro activities correspond to F-BAR protein physiological functions.

As in mammalian endocytosis, cytokinesis in the fission yeast *S. pombe* involves multiple F-BAR proteins (three) that arrive in a defined order as a medially placed actomyosin-based contractile ring (CR) is assembled and constricts. To further our understanding of cytokinesis, and of the multiple functions of F-BAR proteins in a single biological process, a clear understanding of the shared and distinct features of these proteins must be obtained. Of the three, Cdc15 (Fankhauser *et al.*, 1995), Imp2 (Demeter and Sazer, 1998), and Rga7 (Arasada and Pollard, 2011; Martín-García *et al.*, 2014), Cdc15 has been most thoroughly characterized. Essential for cytokinesis (Nurse *et al.*, 1976; Fankhauser *et al.*, 1995), Cdc15 is one of the first components detected at the incipient CR (Wu *et al.*, 2003) and is one of the most abundant CR elements (Wu and Pollard, 2005). It acts as a key anchor of the CR (Roberts-Galbraith *et al.*, 2009, 2010; Laporte *et al.*, 2011) and a platform for assembling additional CR components. Specifically, Cdc15 binds membranes and the cytokinetic formin Cdc12 through its F-

BAR domain (Carnahan & Gould 2003; Willet et al. 2015; McDonald et al., 2015), other proteins involved in cytokinesis through its SH3 domain (Roberts-Galbraith et al. 2009; Ren et al. 2015), and these interactions are modulated by Cdc15's phosphostatus (Roberts-Galbraith *et al.*, 2010). *rga7* $\Delta$  cells have only mild septation defects and it therefore appears that Rga7 is the least important of the three F-BAR proteins for cytokinesis (Martín-García *et al.*, 2014; Arasada and Pollard, 2015). Cells lacking the Cdc15 paralog, Imp2, on the other hand, are strikingly defective in cell division, specifically in the final stages of CR constriction and disassembly (Demeter and Sazer, 1998), consistent with its recruitment to the division site later than Cdc15 (~10 min. after spindle pole body separation) (Wu *et al.*, 2003; Ren *et al.*, 2015). Finally, whereas Cdc15 localizes to cell tips during interphase (Carnahan and Gould, 2003; Arasada and Pollard, 2011), Imp2 localizes solely at the CR during cytokinesis (Demeter and Sazer, 1998). Thus, although Imp2 and Cdc15 are paralogs, there are significant differences in their behaviors and functions during the cell cycle.

Because Cdc15 and Imp2's SH3 domains are functionally interchangeable, collaborating to recruit proteins required to stabilize the CR (Roberts-Galbraith *et al.*, 2009; Ren *et al.*, 2015), we tested whether the unique function of Imp2 is dictated, at least in part, by distinct structural and functional properties of its F-BAR domain. We found that the Imp2 F-BAR preferentially bound phosphoinositol-containing membranes and showed no preference for a specific membrane curvature. The Imp2 F-BAR robustly tubulated membranes *in vitro* and when overexpressed in cultured cells. We determined the crystal structure of the Imp2 F-BAR domain and used it to identify the molecular basis for membrane binding and tubulation. As expected, membrane binding via the F-

BAR is strictly required for Imp2's function in cytokinesis but, surprisingly, despite Imp2's prodigious membrane tubulation ability in vitro, tubulation activity is dispensable in vivo. Accordingly, the Imp2 F-BAR can be functionally replaced by the Cdc15 or *S. cerevisiae* Hof1 F-BAR domains, which do not have the ability to tubulate membranes (McDonald *et al.*, 2015; Moravcevic *et al.*, 2015). These results indicate that membrane tubulation via F-BAR proteins is not required for cytokinesis, raise the possibility that membrane tubulation may not be an essential physiological function of other F-BAR domain proteins that exhibit this activity in vitro, and indicate that the unique function of Imp2 in cytokinesis is dictated by properties of its central domain rather than its F-BAR.

## Results

### *The Imp2 F-BAR is critical for CR constriction and disassembly*

To test the importance of Imp2's F-BAR domain for function, we replaced *imp2*<sup>+</sup> with a truncated version that lacked its F-BAR domain at the endogenous *imp2* locus (Figure 3-1A). Cells producing only Imp2(C) (residues 321-670) were phenotypically similar to *imp2*Δ with both alleles displaying a high percentage of multi-nucleate and multi-septated cells, indicative of failures in cytokinesis (Figure 3-1A-B). Loss of *imp2* function via F-BAR truncation was not due to lack of Imp2(C) localization because GFP-Imp2(C) was detected at the division site in *imp2*Δ cells (Figure 3-2A). The incorporation of GFP-Imp2(C) into the CR where its central and SH3 domains could contribute to CR function (Roberts-Galbraith *et al.*, 2009) is a plausible explanation for why the phenotype of F-BAR domain loss is not quite as severe as that of *imp2*Δ. Consistent with this interpretation, GFP-Imp2(C) CR localization was abolished with a mutation that prevents

the SH3 domain from binding partners, W644S (Figure 3-2A) (Hongtao *et al.*, 1994). To identify exactly how *imp2(C)* cells fail during cytokinesis, we imaged cells producing Sid4-GFP (a spindle pole body component) and Rlc1-GFP (a CR component), to visualize mitotic and cytokinetic progression, respectively. Similar to phenotypes seen previously when *imp2* is deleted (Figure 3-2B, (Demeter and Sazer, 1998)), *imp2(C)* cells often failed to constrict their CRs, disassemble CR remnants, and separate daughter cells (Figure 3-1C). We quantified the percentage of cells that completed cytokinesis, failed during constriction (defined as cells that build a CR but do not fully constrict it), or failed separation (defined as cells which fully constrict the CR but do not physically separate) (Figure 3-1C). As cells lacking the Imp2 F-BAR domain fail cytokinesis >60% of the time, we conclude that the domain is required for Imp2's contribution to recruiting proteins for CR constriction and disassembly such as Rgf3, Fic1, and Px11 (Morrell-Falvey *et al.*, 2005; Bohnert and Gould, 2012; G. Cortés *et al.*, 2015; Ren *et al.*, 2015). Further evidence for the importance of Imp2's F-BAR domain was obtained through genetic analysis. We crossed *imp2(C)* into a *cdc15-140* cytokinesis mutant, which is synthetically lethal with *imp2Δ* (Demeter and Sazer, 1998). *imp2(C)* showed a strong negative genetic interaction with *cdc15-140* (Figure 3-1D), confirming genetically a major loss of protein function in the absence of the F-BAR domain. Though essential, the Imp2 F-BAR domain alone is not sufficient for function, as an *imp2(N)* allele (Figure 3-1A) displayed identical phenotypes to *imp2Δ* (Figure 3-1A-B).

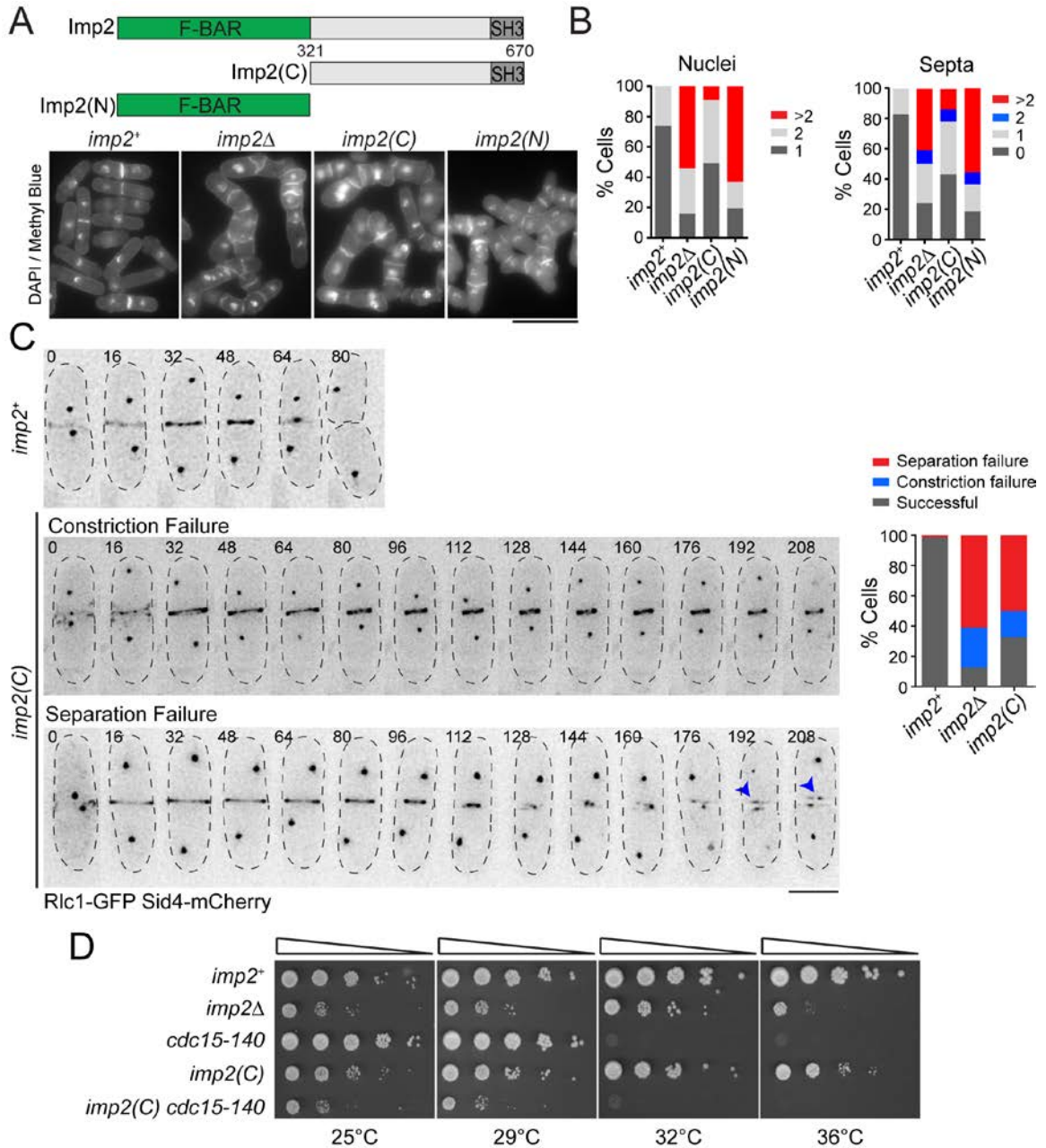


**Figure 3-1. The Imp2 F-BAR domain is important for cytokinesis.** A) Schematic of Imp2 and truncation alleles Imp2(C) and Imp2(N). Bottom) DAPI- and Methyl Blue-stained cells of the indicated *imp2* genotype. Scale bar, 10  $\mu$ m. B) Cytokinesis phenotype quantifications of cells in (A).  $n \geq 300$  for each strain. C) Representative images (left) and quantification (right) of cytokinesis defects in *imp2+*, *imp2 $\Delta$* , and *imp2(C)*.  $n > 30$  for each strain. Blue arrowheads indicate persistent contractile ring remnants. Numbers indicate time from spindle pole body duplication. Scale bar, 5  $\mu$ m. D) Serial dilutions of *imp2* strains at the indicated temperatures.

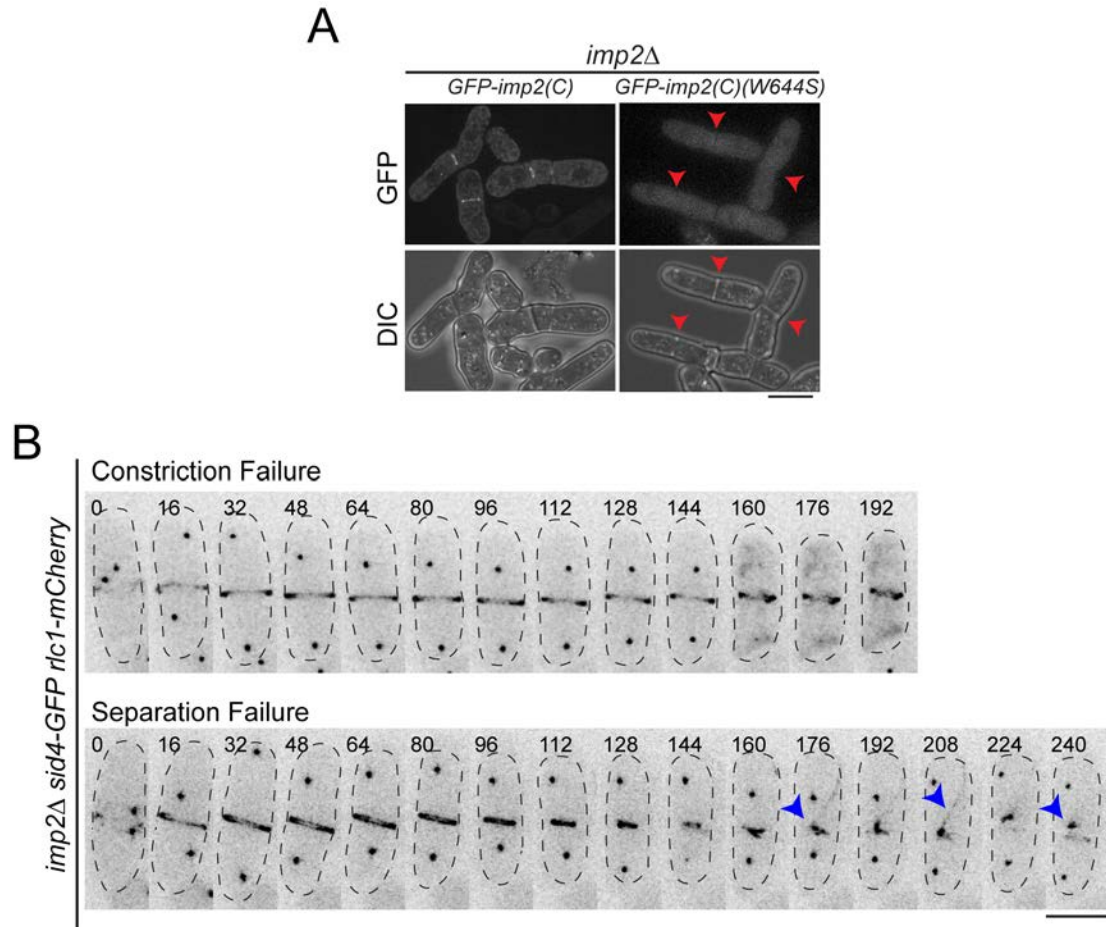


**Figure 3-2. The Imp2 F-BAR domain is important for cytokinesis; supplement.** A) GFP-*Imp2(C)* localizes to the contractile ring, while GFP-*Imp2(C)*(W644S) deficient in SH3 partner binding does not. Red arrowheads indicate division sites lacking GFP-*Imp2* signal. *Imp2(C)* constructs were produced from the *nmt1* promoter in *imp2Δ* cells. Scale bar, 5  $\mu$ m. B) Representative images of *imp2Δ rlc1-GFP sid4-mCherry* cytokinesis defects. Blue arrowhead indicates persistent contractile ring remnants. Scale bar, 5  $\mu$ m.

### Structure of the Imp2 F-BAR domain

To determine what properties of the Imp2 F-BAR domain drive its cytokinetic function, we took a structural approach. The X-ray crystal structure of the Imp2 F-BAR domain was determined using seleno-methionine phasing, and fully refined to a resolution of 2.35 Å. The Imp2 F-BAR domain adopts a characteristic tightly interwound dimeric BAR-domain architecture, with 5911 Å<sup>2</sup> interface area (Figure 3-3A).

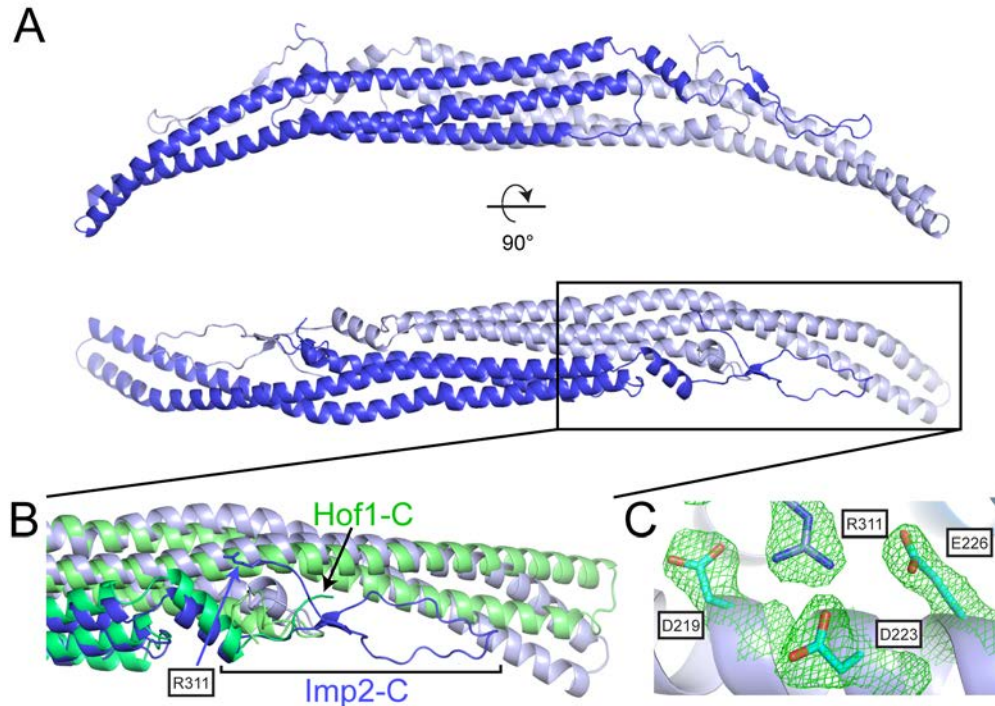


**Figure 3-3. Structure of the Imp2 F-BAR domain.** A) Crystal structure of the Imp2 F-BAR domain dimer with subunits colored in dark and light blue. B) Close up view of the wing-tip orientation and C-terminal residues of Imp2 (blue) which diverge significantly from Hof1 (green). C) Close up view of the intermolecular salt-bridge network formed by the F-BAR C-terminus (2Fo-Fc contoured at 1.1 $\sigma$ ).

The domain consists of a six-helical dimeric bundle with extended wings that adopt a bent conformation relative to the helical core. Dali server search (Holm and Rosenström, 2010) indicates that the closest structural homologue of Imp2 is the F-BAR domain of *S. cerevisiae* Hof1 (Moravcevic *et al.*, 2015), with a R.M.S.D. (Root Mean Square Deviation) of 2.7 Å. However, the two structures differ significantly in the overall shape of the F-BAR domain, particularly in wing tip orientation, with Imp2 exhibiting a significantly higher tip angle (Figure 3-3B). Additionally, the thirty C-terminal residues of the Imp2 F-BAR domain are well ordered and form an extension of the F-BAR-domain compared to Hof1 (Figure 3-3B). Residues in the extended C terminus make important contacts back to the core of the protein, explaining why a construct encoding a shorter fragment (residues 15-295) was unstable. In particular, a  $\beta$ -strand is formed by residues 282-284 and 304-306, and R311 forms inter-molecular salt bridges to D219, D223, and E226, located in the core six-helical bundle interface (Figure 3-3C).

#### *Structural basis for Imp2 membrane binding*

Recombinantly produced and purified Imp2 F-BAR domain (Figure 3-4A) binds biological membranes rich in phosphorylated phosphatidylinositols (PIPs) in a salt-dependent manner (Figure 3-4B). The domain bound maximally to synthetic liposomes containing at least 20% phosphatidylserine (PS) (Figure 3-4C) and showed no preference for membrane curvature, binding liposomes between 100-800 nm in diameter equally well (Figure 3-4D). The domain bound liposomes of various compositions in a



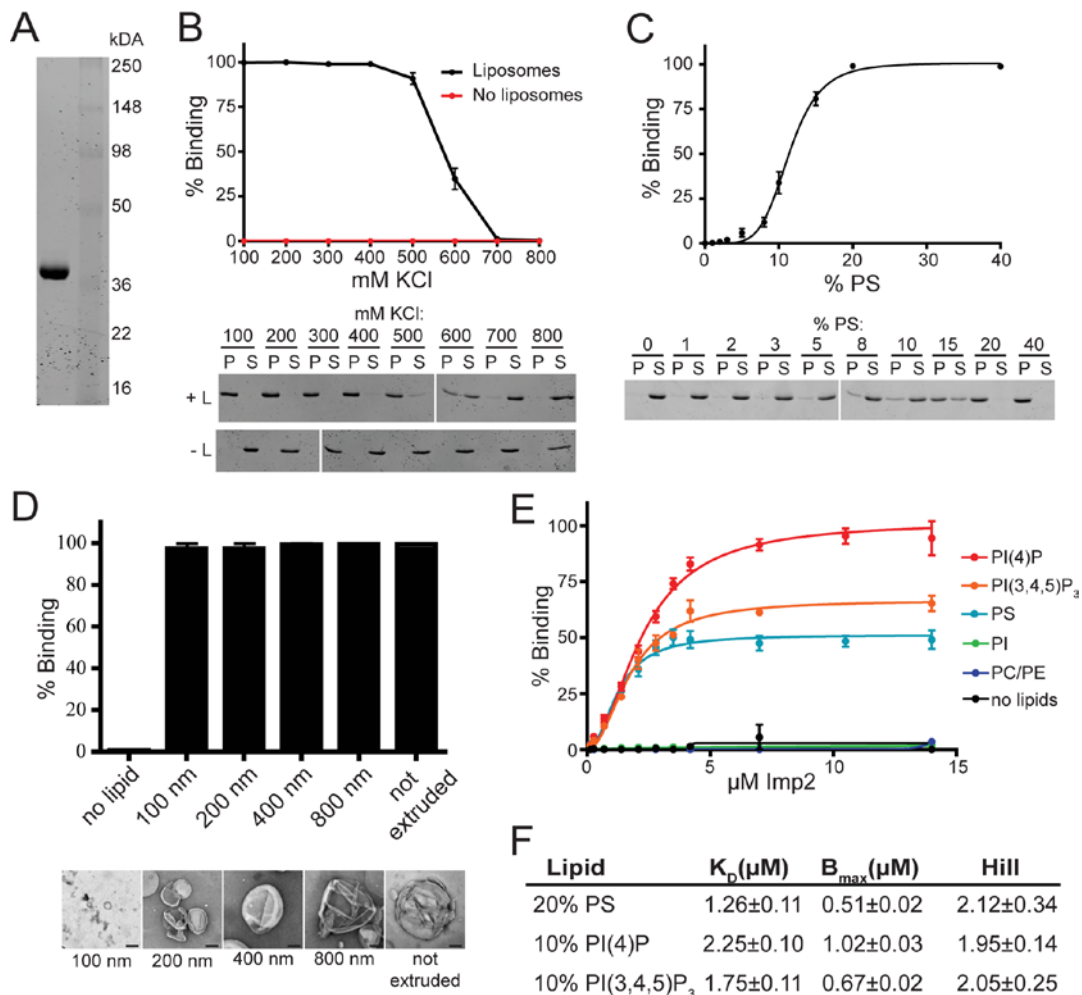


**Figure 3-4. The Imp2 F-BAR domain binds biological membranes.** A) SDS-PAGE and Coomassie Blue stain of purified His6-Imp2 F-BAR domain. B) Liposome co-pelleting assay between Folch fraction liposomes and the Imp2 F-BAR domain in different concentrations of KCl. P = pellet, bound fraction; S = supernatant, unbound fraction. C) Liposome co-pelleting assay between Imp2 F-BAR domain and liposomes composed of 20% PE, increasing concentrations of PS, and the remainder PC. D) The Imp2 F-BAR domain binds membranes independent of membrane curvature. Top) Quantification of 3 liposome co-pelleting assays between Folch fraction liposomes extruded to the indicated sizes and the Imp2 F-BAR domain. Bottom) Representative negative stain EM images of liposomes extruded to the indicated size. Scale bars, 100 nm. E) Saturation binding assays performed with increasing concentrations of the Imp2 F-BAR domain and liposomes composed of 20% PE, either 20% PS / 10% PI / 10% PI(4)P / 10% PI(3,4,5)P<sub>3</sub>, and the remainder PC. F) Saturation binding curves from fit with a specific binding model including a Hill slope. The calculated apparent kinetic parameters reflect the affinity of the Imp2 F-BAR domain for liposomes of the indicated compositions. Error bars in all panels indicate SEM from at least 3 experiments.

cooperative manner with a preference for liposomes containing negatively charged PIPs and PS (Figure 3-4E-F). Interestingly, this F-BAR domain bound most strongly to liposomes containing PI(4)P compared with PI(3,4,5)P<sub>3</sub>, indicating a mild preference for the PI(4)P lipid head group.

To identify how the Imp2 F-BAR binds to negatively charged phospholipids, the electrostatic surface of the dimer was examined. The concave surface of the dimer contains extensive positive charge, particularly in the domain's bent wings, and an additional positively charged patch was present near the base of each wing in the dimeric core (Figure 3-5A). These basic regions are composed of clusters of lysine residues, similar in position to those used by the FBP17 and FCHo2 F-BARs to bind membranes (Henne *et al.*, 2007; Frost *et al.*, 2008). To determine the role of these lysine residues in Imp2 F-BAR function, several mutations were generated: K159A, K148A/K152A, and K173A/K177A/K181A/K184A (Lipid-4A) (Figure 3-5A). We also generated a mutation that disrupted the basic patch at the base of the wing, K122A (Figure 3-5A). Mutations of these basic residues, particularly the Lipid-4A combination, K159A, and K122A, resulted in decreased affinity of the F-BAR domain for liposomes, confirming the important role of these basic surfaces in Imp2 F-BAR domain membrane binding (Figure 3-5B). Interestingly, the K122 patch appears to be responsible for the PI(4)P preference, as binding to PI(4)P-containing liposomes decreased more than binding to PS-containing liposomes in the K122A mutant.

To further reduce membrane binding, we designed a Lipid-5A mutant consisting of Lipid-4A and K159A, and a Lipid-7A mutant comprised of all 7 basic wing residues to alanine. F-BAR domains containing these mutations proved difficult to purify; however,

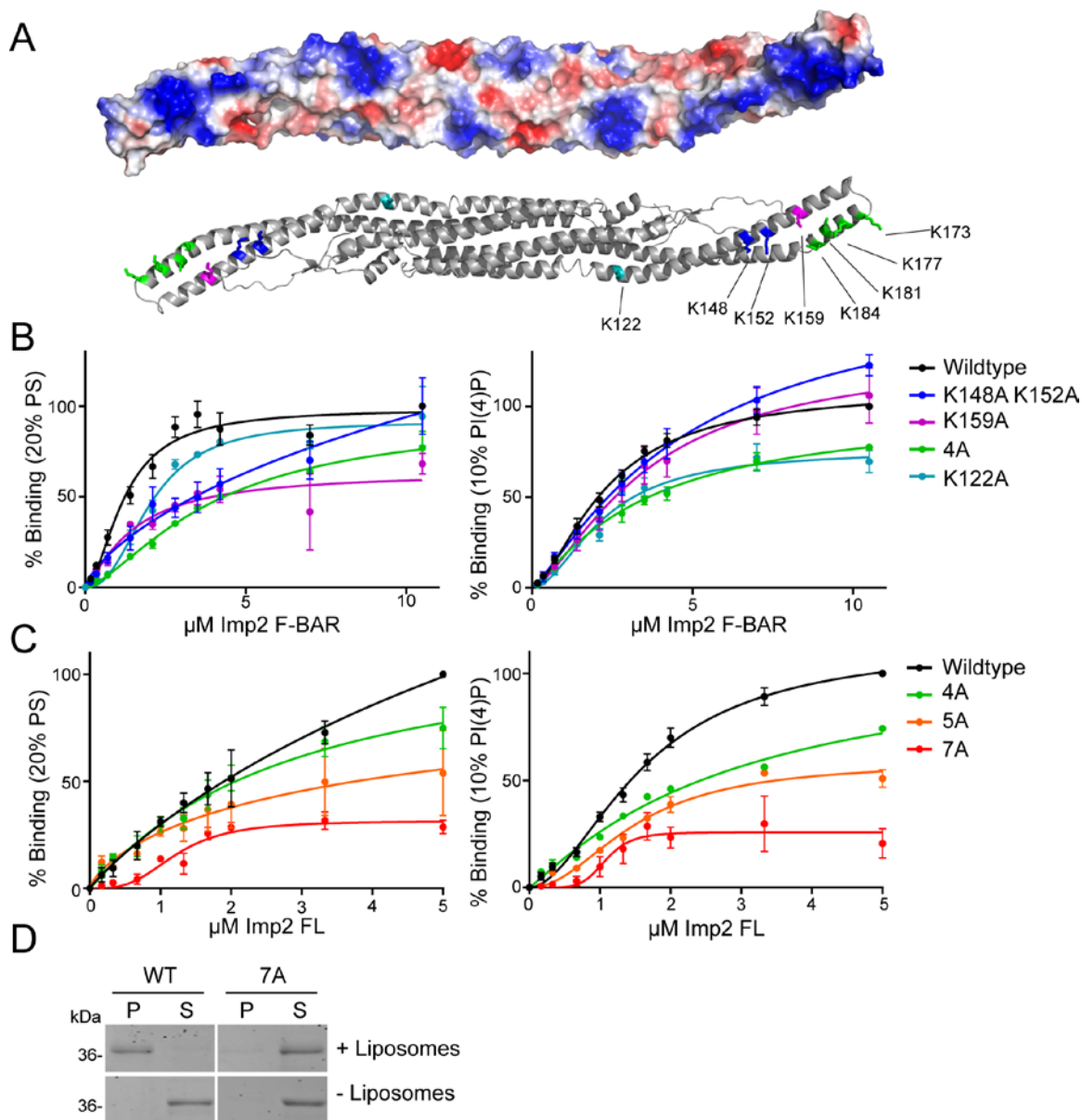


**Figure 3-5. Mechanism of Imp2 F-BAR domain membrane binding.** A) Electrostatic potential map of the concave surface of the Imp2 F-BAR domain. Blue, positive potential; Red, negative potential; White, near neutral. Bottom) Ribbon model depicting predicted membrane binding residues. B) Binding assays of wildtype (WT) or membrane binding mutant Imp2 F-BAR domains and liposomes composed of 60% PC / 20% PE / 20% PS or 70% PC / 20% PE / 10% PI(4)P. 4A consists of K173A, K177A, K181A, and K184A. C) Binding assays of wildtype or multi-site membrane binding mutations in full-length purified Imp2. 4A as in (B); 5A = 4A + K159A; 7A = 5A + K148A and K152A. D) Representative liposome co-pelleting assay between 1 $\mu$ M full-length Imp2(7A) and Folch fraction liposomes. Error bars in all panels indicate SEM from at least 3 experiments.

full length Imp2-Lipid-4A, -5A, and -7A were readily purified. Testing the full length proteins in liposome binding assays showed that Imp2 bound membranes whereas Imp2-Lipid-4A, -5A, and -7A had reduced binding (Figure 3-5C). Despite retaining a low level of binding to synthetic liposomes at saturating concentrations, the 7A combination mutant completely abolished co-pelleting with Folch fraction liposomes (Figure 3-5D). We conclude that the basic residues within the wing of the Imp2 F-BAR domain are necessary for Imp2 to associate with membranes.

Having identified how the Imp2 F-BAR domain binds membranes, we next tested the importance of membrane binding for Imp2 function in vivo by replacing the wildtype gene with lipid binding mutants at the *imp2* endogenous locus. *imp2-Lipid-4A*, *-5A*, and *-7A* mutants displayed progressively worsening phenotypes similar to *imp2(C)* (Figure 3-6A), with cells often failing cytokinesis to become multinucleated and multiseptated (Figure 3-6A-C). Also like *imp2(C)*, the *imp2* membrane binding mutants showed severe negative genetic interactions with *cdc15-140* (Figure 3-6D). When Imp2 cannot bind membranes, Imp2 levels at the ring were decreased, though total cellular amounts remained near wildtype levels (Figure 3-7A-B). Recruitment of important Imp2 SH3 domain interactors to the CR was impaired in accord with Imp2 reduction (Figure 3-6E-F). We conclude that membrane binding is a necessary function of the Imp2 F-BAR domain in cytokinesis to form an efficient scaffold for its partners.

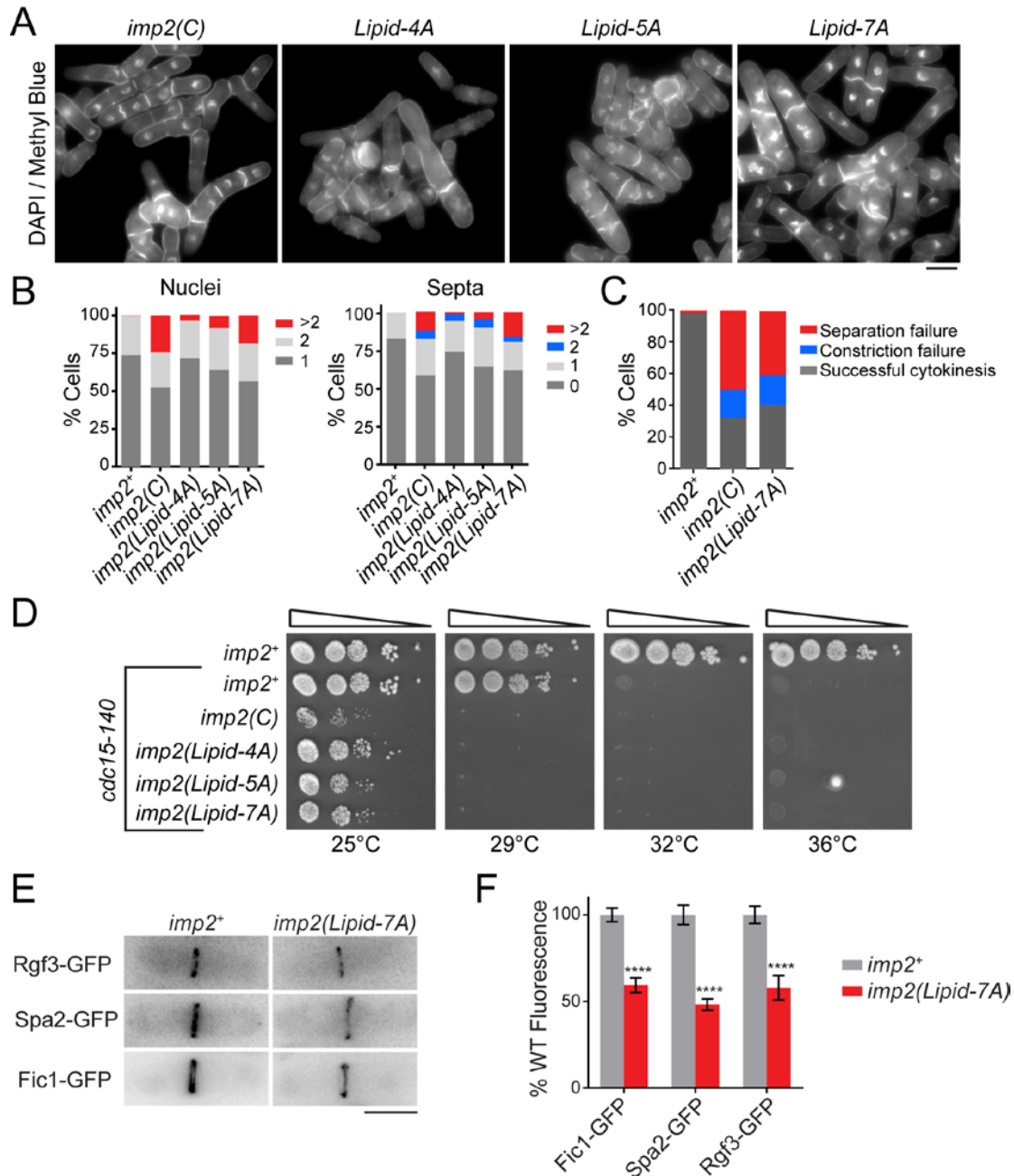


**Figure 3-6. Membrane binding is an essential function of the Imp2 F-BAR domain.**

A) DAPI- and Methyl Blue-stained cells of the indicated *imp2* genotype. Lipid mutations are described in Figure 3C. Scale bar = 4  $\mu$ m. B) Quantification of cytokinesis phenotypes of cells in (A).  $n \geq 300$  for each strain. C) Cytokinesis failure phenotype quantifications from time-lapse imaging of Rlc1-GFP Sid4-GFP in the indicated *imp2* strains.  $n \geq 30$  for each strain. Data for *imp2<sup>+</sup>* and *imp2(C)* is from Figure 1C. D) Serial dilution assay of *imp2* membrane binding mutants at the indicated temperatures. E) Representative images of GFP-tagged Imp2 SH3 interactors in the indicated *imp2* strains. Scale bar, 5  $\mu$ m. F) Quantification of Imp2 SH3 binding partners in the contractile ring from (E). Error bars indicate SEM.  $n > 60$  for each condition. \*\*\*\*,  $p < 0.0001$ .

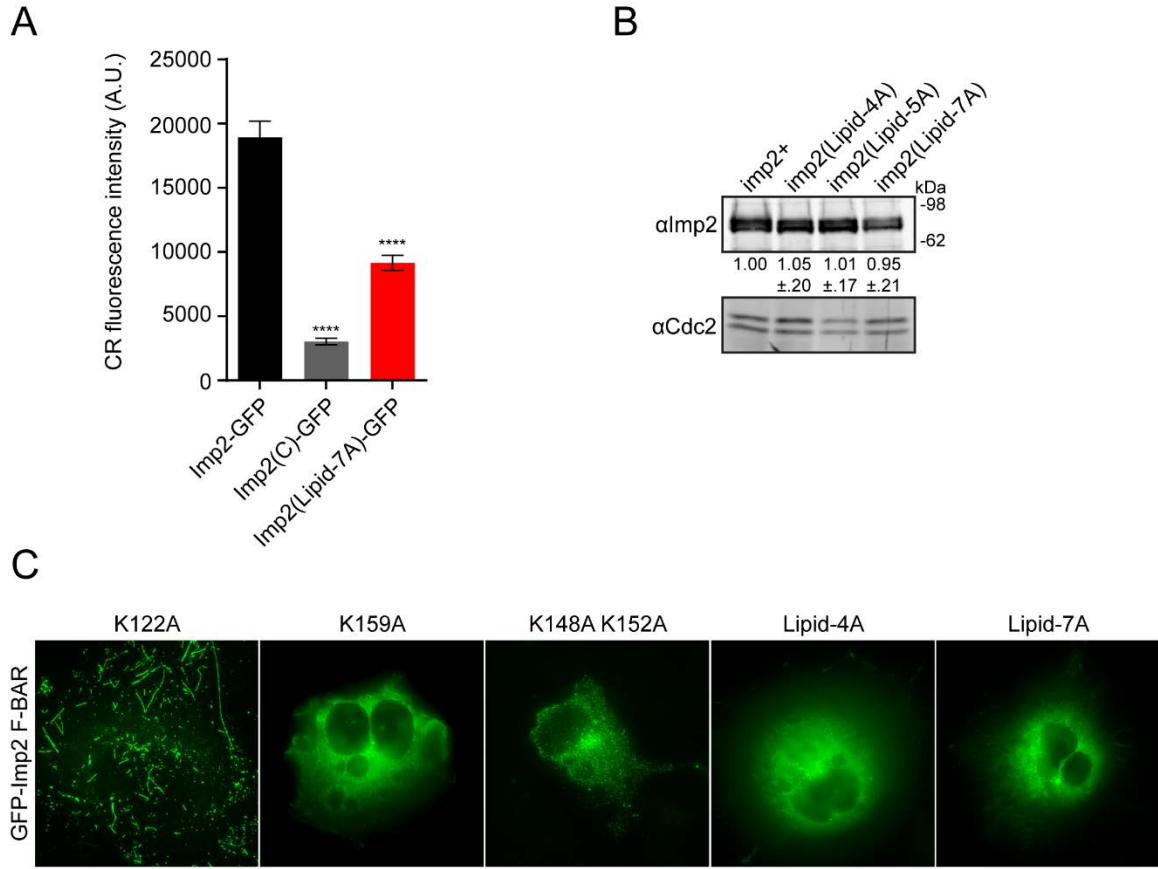


**Figure 3-7. Imp2 membrane binding mutants.** A) Fluorescence intensity of the indicated Imp2 mutants at the contractile ring. \*\*\*\*,  $p < 0.0001$ .  $n > 50$  for each genotype. B)  $\alpha$ Imp2 western blot for Imp2 protein levels in the indicated strains from Figure 4A. Numbers indicate relative band intensity versus *imp2+* from 3 biological replicates  $\pm$  SD. C) GFP-Imp2 F-BAR domains with the indicated mutations were expressed in COS-7 cells. Scale bar, 10  $\mu$ m.

### *The Imp2 F-BAR tubulates membranes by forming higher order structures*

Several F-BAR domains not only bind membranes, but bend and tubulate them when present at high concentration (Itoh *et al.*, 2005; Tsujita *et al.*, 2006; Frost *et al.*, 2008). Indeed, F-BAR domains have been hypothesized to induce or stabilize the curvature present at the division site during *S. pombe* cytokinesis (Frost *et al.*, 2009). As Cdc15 does not tubulate membranes (McDonald *et al.*, 2015), we tested whether tubulation was an activity of the Imp2 F-BAR and if this activity is in fact important during cytokinesis. We found that the Imp2 F-BAR tubulated the plasma membrane of COS-7 cells when overexpressed (Figure 3-8A). It also tubulated synthetic liposomes *in vitro* as detected by negative stain electron microscopy (EM) (Figure 3-8B).

To investigate how the Imp2 F-BAR domain tubulates membranes in detail, the organization of Imp2 F-BAR coats on membranes was more closely examined using cryo-EM (Figure 3-8C). Images of tubules in vitrified ice showed that, similar to the CIP4 F-BAR (Frost *et al.*, 2008), the Imp2 F-BAR forms tubules spanning a range of diameters (Figure 3-8D). The Imp2 F-BAR domain could be seen coating the membrane of individual tubules (Figure 3-8E) and class averages of Imp2-coated tubules of similar widths revealed an ordered pattern on the membrane (Figure 3-8F). Despite this ordered pattern, a high degree of heterogeneity of the Imp2 F-BAR tubules precluded determination of a high resolution structure. This heterogeneity, which included differences in diameter and F-BAR lattice packing even within individual tubules, was not improved using low temperature annealing protocols that have been used previously to determine an F-BAR tubule structure (Frost *et al.*, 2008).



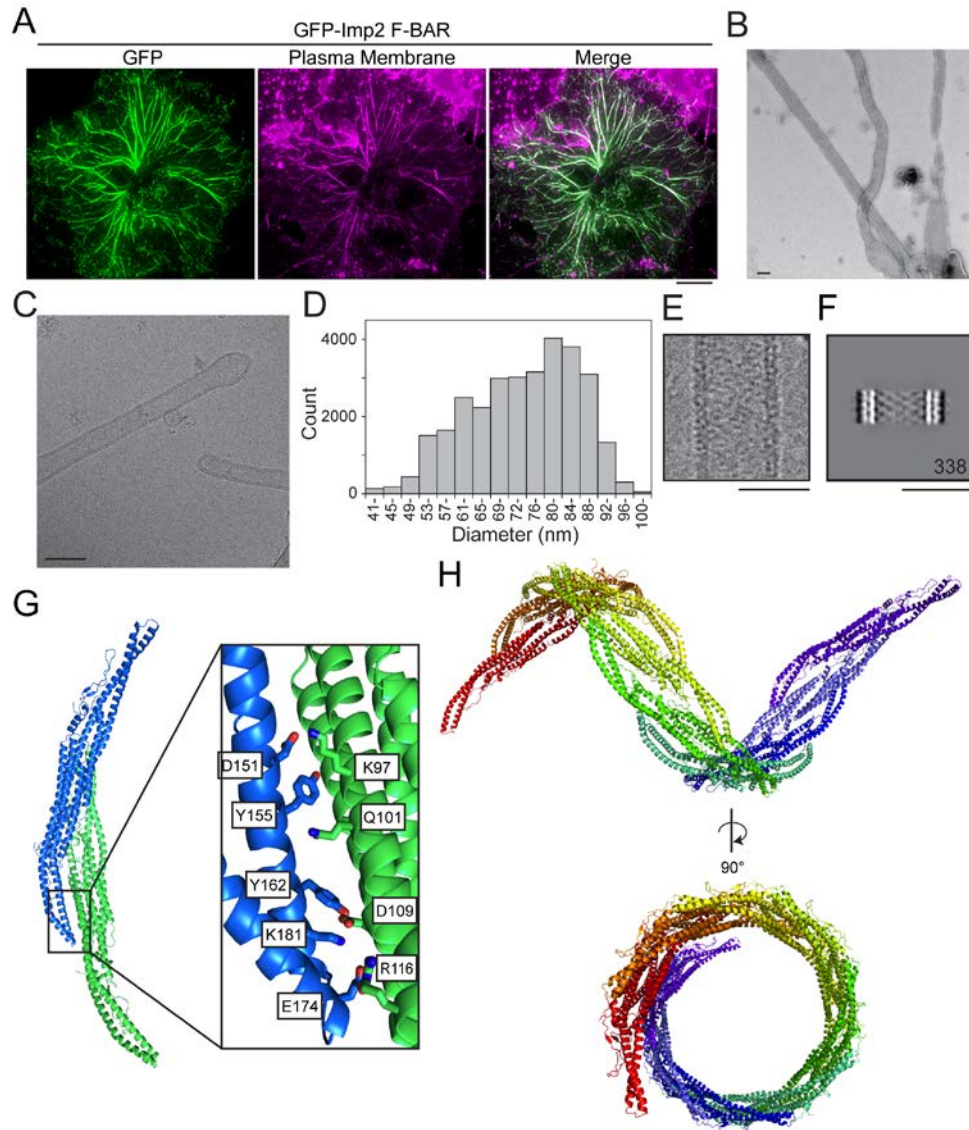


**Figure 3-8. The Imp2 F-BAR domain tubulates membranes through helical oligomerization.** A) GFP-Imp2 F-BAR domain expressed in COS-7 cells and co-stained with Cellmask Orange plasma membrane dye. B) Imp2 F-BAR domain incubated with liposomes composed of 50% PS / 35% PC / 10% PE / 5% PI and visualized with negative stain EM. Left scale bar, 500 nm; Right scale bar, 100 nm. C) Cryo-EM image of an Imp2 F-BAR domain-coated membrane tubule in vitrified ice. Scale bar, 100 nm. D) Size distribution of Imp2 F-BAR domain-induced liposome tubules measured from cryo-EM images. E) Representative Imp2 liposome tubule as used to generate class average in (F). Scale bar, 50 nm. F) Class average of Imp2 F-BAR domain-coated tubules with a diameter of 50 nm. 338 images were included in the average. Scale bar, 50 nm. G) Packing of the dimer-of-dimers present in Imp2 F-BAR domain crystals. Individual dimers are represented as blue and green. Inset shows key interface residues. H) Extending the dimer-dimer contacts between Imp2 F-BARs results in a helical-filament structure. Each dimer is depicted in a different color.



Membrane tubulation by F-BAR domains is expected to rely upon membrane binding. Therefore, we tested if mutations of the membrane binding residues on the wing and core interfered with membrane tubulation by Imp2 F-BAR domains. The K122A core patch mutant retained tubulation activity though at a much reduced level, while the wing patch mutants lacked tubulation activity (Figure 3-7C). Therefore, membrane binding is required for the Imp2 F-BAR domain to tubulate membranes.

#### *Imp2 F-BAR helical oligomerization supports membrane tubulation*

Membrane tubulation by F-BARs is proposed to occur through a scaffolding mechanism where F-BAR domains organize into defined oligomers that collectively deform the membrane (Shimada *et al.*, 2007; Frost *et al.*, 2008; Yu and Schulten, 2013). To determine the mechanism of Imp2 F-BAR oligomerization, we analyzed the packing of the Imp2 F-BAR domain in crystals. The domain organized into a higher order dimer-of-dimers in the crystal (Figure 3-8G), formed by reciprocal packing of the wing of one dimer with the core of the next. The interaction surface was significant, with 804Å<sup>2</sup> of interface area. The dimer-of-dimers showed a systematic shift in register with addition of each dimer subunit that could support the formation of an oligomeric filament. We computationally extended the dimer-of-dimers, assuming symmetric wing to core interactions, to produce a model of an Imp2 F-BAR filament (Figure 3-8H). Strikingly, the filament is helical, suggesting this conformation of Imp2 F-BAR oligomers on a membrane may be responsible for its tubulation activity.

A detailed examination of the dimer-of-dimers crystal packing showed that the interface is formed by a series of salt-bridges and hydrogen bonds between wing tip

residues (D151, Y155, Y162, E174, K181) and dimer core residues (K97, Q101, D109, R116) (Figure 3-8G). To test this helical oligomerization model and the role of tip to core dimer-dimer interactions on Imp2 membrane tubulation, alanine point mutations in the dimer core residues (D109A, R166A and K97A, Q101A, D109A, R116A (Dimer-Dimer-4A)) were produced. Dimer-dimer mutants were completely deficient in their ability to tubulate membranes when overexpressed in COS-7 cells (Figure 3-9A), supporting our model of tubulation. Additionally, these mutations abolished the ability of the Imp2 F-BAR to tubulate GUVs in vitro (Figure 3-9B). Mutation of these residues had no significant effect on the affinity of the Imp2 F-BAR for membranes, indicating constructs containing these point mutants (K97A, Q101A, D109A, and R116A) were properly folded and were not deficient in membrane binding (Figure 3-10A).

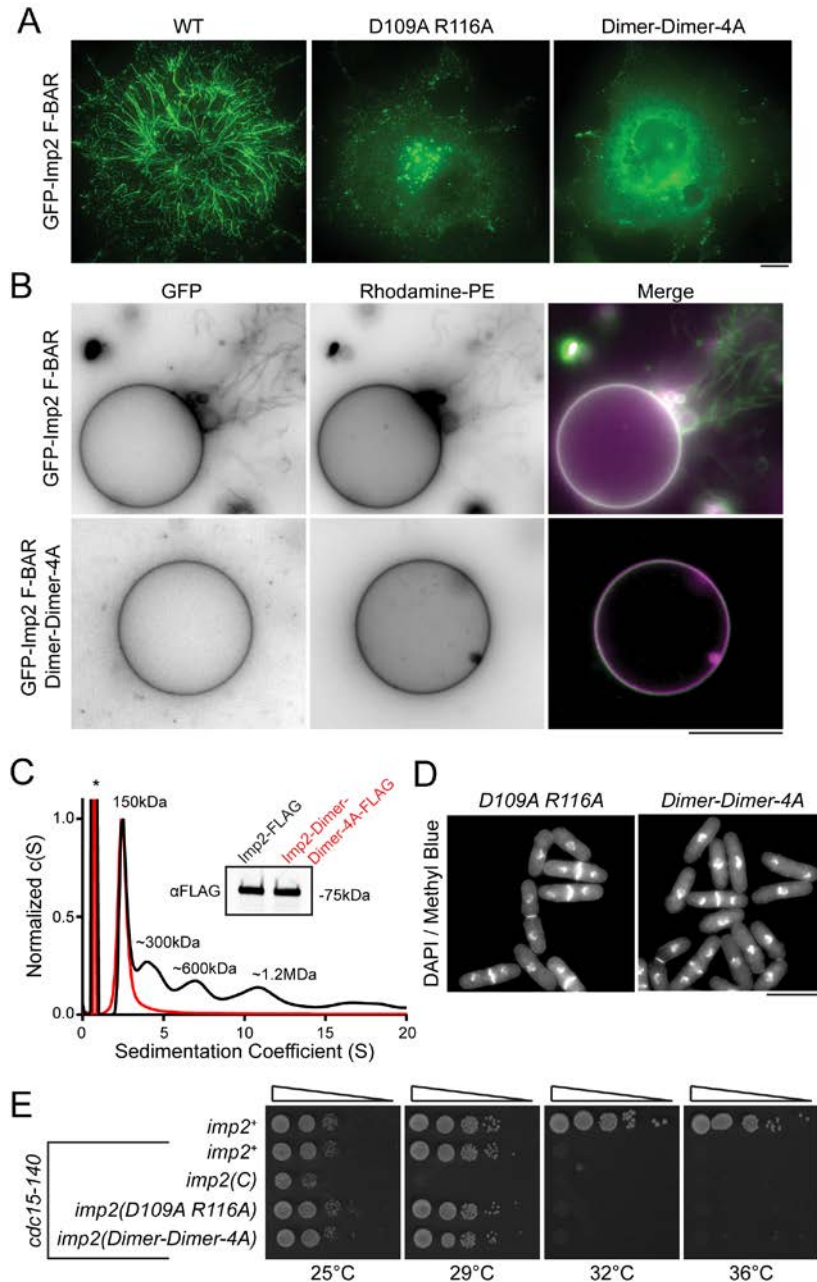


**Figure 3-9. Imp2 oligomerization is essential for tubulation but dispensable for cytokinesis.** A) GFP-Imp2 F-BAR domains with the indicated mutations were expressed in COS-7 cells. Scale bar, 10  $\mu$ m. B) Dimer-dimer contact mutations abolish tubulation activity of the GFP-Imp2 F-BAR domain on giant unilamellar vesicles (GUVs) composed of 64% PC / 20% PE / 10% PS / 5% PI(4)P / 1% Rhodamine-PE. Scale bar = 10  $\mu$ m. C) Sedimentation velocity analytical ultracentrifugation trace of full length Imp2 and Imp2(Dimer-Dimer-4A) purified from *S. pombe*. \* indicates 3X FLAG peptide contaminant. Inset)  $\alpha$ FLAG western blot of Imp2 and Imp2(Dimer-Dimer-4A) samples. D) DAPI- and Methyl Blue-stained cells of the indicated *imp2* genotype. Scale bar, 10  $\mu$ m. See Figure S4B for quantification. E) Serial dilutions of *imp2* mutant strains at the indicated temperatures. Dimer-Dimer 4A = K97A, Q101A, D109A, R116A.

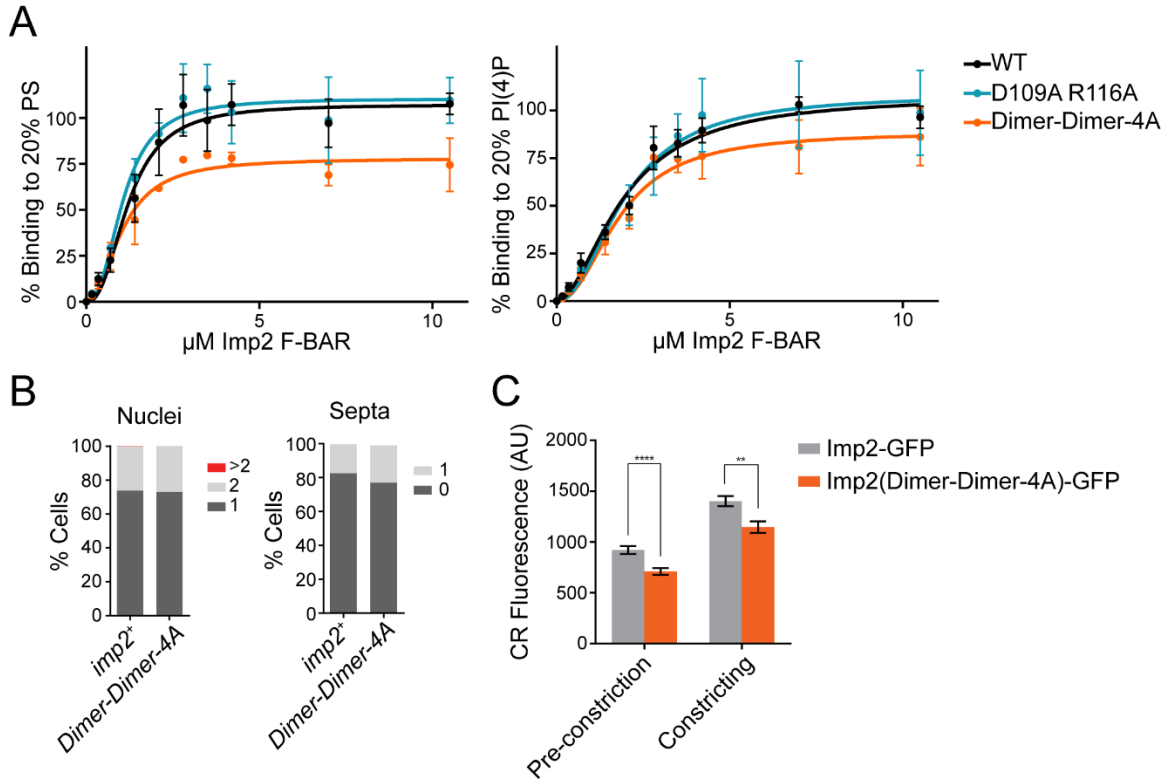


**Figure 3-10. Imp2 F-BAR domain dimer-dimer mutant properties.** A) Liposome binding assays performed between Imp2 F-BAR domain mutants and liposomes composed of 20% PE, either 20% PS / 10% PI / 10% PI(4)P / 10% PI(3,4,5)P3, and the remainder PC. B) Cytokinesis phenotype quantifications of cells in Figure 8C.  $n \geq 300$  for each strain. C) Quantification of Imp2-GFP and Imp2(Dimer-Dimer-4A) fluorescence at the contractile ring.  $n > 60$  for all conditions. \*\*,  $p < 0.01$ ; \*\*\*\*,  $p < 0.0001$ . All error bars indicate SEM.

*The Imp2 F-BAR domain's cytokinetic function does not require tubulation or oligomerization*

Despite multiple F-BAR proteins' ability to tubulate membranes in vitro, the importance of tubulation activity for the physiological function of any F-BAR is unknown. We directly tested the importance of membrane tubulation on Imp2's physiological function in cytokinesis by integrating both tubulation-deficient dimer-dimer mutants (D109A, R116A and Dimer-Dimer4A) into the *imp2* endogenous locus. Though we determined these mutants can no longer tubulate membranes in vivo or in vitro (Figure 3-9A-B), we first tested whether the mutants retained any oligomerization activity in *S. pombe*. To this end, Imp2 and the Imp2-Dimer-Dimer-4A mutant were purified from *S. pombe* cell lysates and assayed by analytical ultracentrifugation. Whereas wildtype Imp2 was present in multiple oligomeric species, the Dimer-Dimer-4A mutant was strictly dimeric (Figure 3-9C), confirming complete loss of oligomerization in vivo along with loss of tubulation activity. Surprisingly, these mutant cells had wildtype morphologies with no evidence of cytokinetic defects (Figure 3-9D and 3-10B). The absence of compromised cytokinetic function was confirmed genetically as dimer-dimer mutants displayed no synthetic genetic interactions with *cdc15-140* (Figure 3-9E). We observed a minor decrease in the levels of Imp2-Dimer-Dimer-4A at the contractile ring (Figure 3-10C), but this did not result in observable cytokinetic phenotypes. Therefore, despite a strong ability to tubulate membranes in vitro or when overexpressed in vivo, tubulation and oligomerization are not necessary for Imp2's function in cytokinesis.

To rigorously test this conclusion, we created synthetic fusion proteins that replaced Imp2's F-BAR domain with the F-BAR domains from Imp2's paralog Cdc15 or homolog *S. cerevisiae* Hof1 (Figure 3-11A, top), which unlike Imp2's F-BAR domain do not tubulate membranes (McDonald *et al.*, 2015; Moravcevic *et al.*, 2015). Both Cdc15 and Hof1 F-BAR domains successfully replaced Imp2 F-BAR domain function in cytokinesis (Figure 3-11A-B) and in growth (Figure 3-11C) and the fusion proteins localized to the division site normally (Figure 3-12). We conclude that Imp2's F-BAR domain does not need to bend the membrane, but instead operates as a temporally restricted bridge between the membrane and other proteins that bind Imp2.

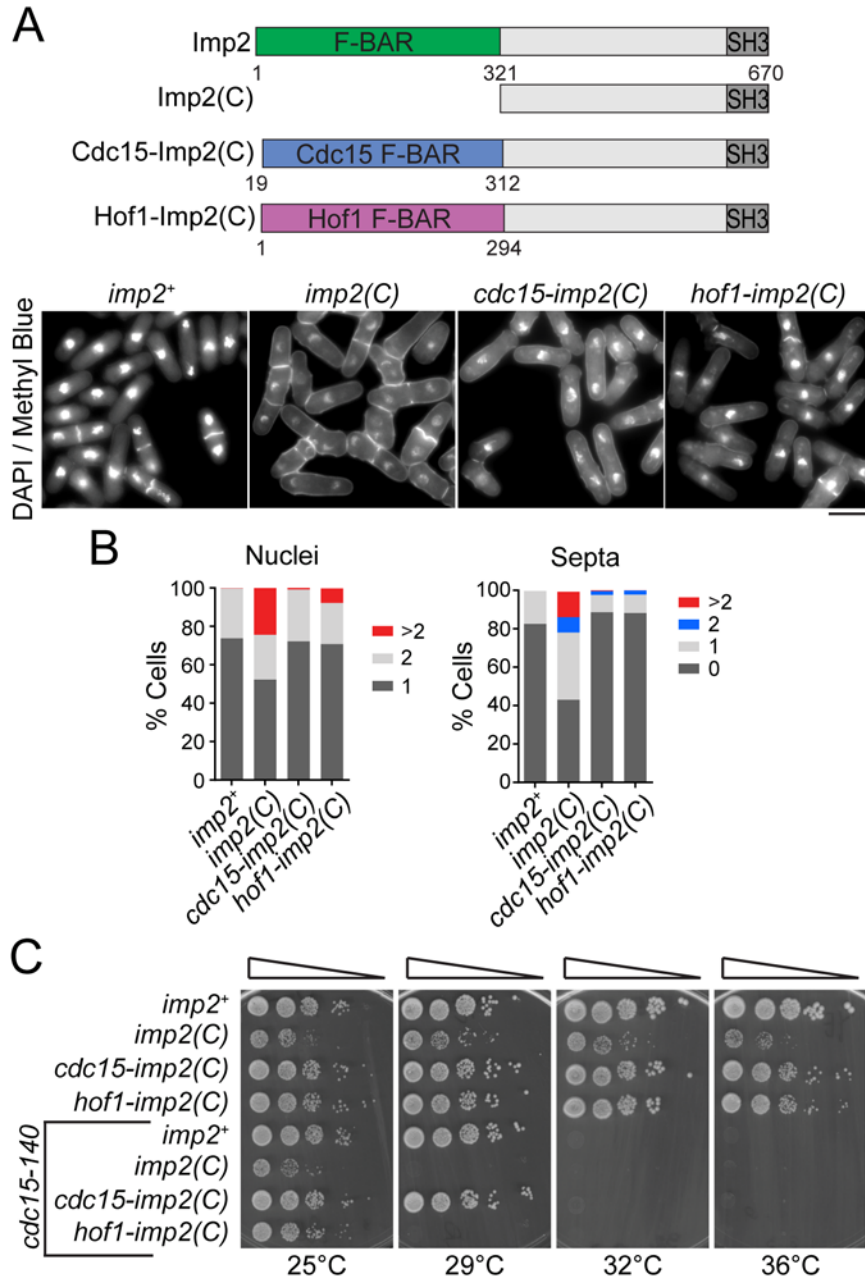


**Figure 3-11. Non-tubulating F-BAR domains can complement Imp2 F-BAR domain function.** A) Schematic of Imp2 F-BAR domain replacement constructs. Bottom) DAPI- and Methyl Blue-stained cells of the indicated *imp2* genotype. Scale bar, 5  $\mu$ m. B) Cytokinesis phenotype quantifications of cells in (A).  $n \geq 300$  for each strain. C) Serial dilutions of *imp2* strains at the indicated temperatures.

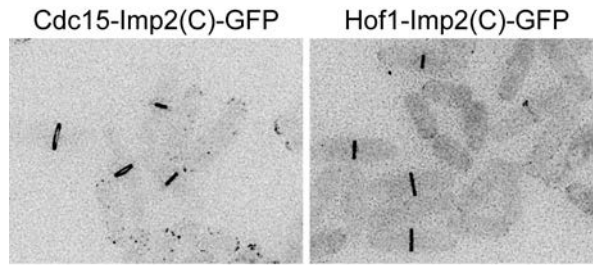


**Figure 3-12. Both F-BAR fusions are present at the contractile ring.** Images of the indicated GFP-tagged fusion proteins integrated at the *imp2* locus. Scale bar, 4  $\mu$ m.

## Discussion

We have determined that the Imp2 F-BAR domain is critical for proper CR constriction, septation, and CR disassembly during cytokinesis. We determined the structure of the domain, as well as the domain's mechanism of membrane binding and helical oligomerization-based tubulation. Using separate sets of mutations that affected either Imp2 membrane binding or tubulation activities, we surprisingly found that Imp2's cytokinetic functions rely only on F-BAR membrane binding, rather than tubulation activity and can be replaced by other non-tubulating cytokinetic F-BAR domains. Our data suggest that the Imp2 F-BAR domain acts only as a membrane bound tether to properly orient and scaffold cytokinetic partners that interact with Imp2's other domains.

### *Diverse modes of F-BAR oligomerization drive tubulation*

Our model of Imp2 F-BAR super-molecular assembly derived from the Imp2 crystal structure predicts that the Imp2 F-BAR domain can oligomerize to form a helical structure with a diameter of  $\sim 130$  Å. The diameters of tubules formed by the Imp2 F-BAR range from  $\sim 50$ - $100$  nm in vitro to  $\sim 100$ - $300$  nm in cultured cells. This variability in tubule diameter induced by the Imp2 F-BAR domain suggests that the dimer-dimer



contact interfaces have significant flexibility. The wing angles of individual Imp2 F-BAR dimers may also be flexible, introducing another degree of freedom to helical filaments. Flexibility at the Imp2 F-BAR to F-BAR interfaces was also suggested by our EM data of Imp2 F-BAR domain-coated tubules. Though striations of a helical Imp2 F-BAR domain coat were visible on individual tubules, this membrane coat was irregular and varied down a tubule's length. Whether structural flexibility is important for Imp2 F-BAR function outside the context of an oligomeric structure awaits further analysis.

We defined mutations that disrupt the observed super-helical oligomeric interface of Imp2 and demonstrated that these mutant proteins completely lack tubulation activity. Our model, therefore, provides additional evidence for a “scaffolding” mechanism of F-BAR domain membrane tubulation (Shimada *et al.*, 2007; Frost *et al.*, 2008; Yu and Schulten, 2013) that could be relevant to other F-BAR domains. Indeed, our model is similar in principal to EM reconstructions of CIP4 membrane tubules (Frost *et al.*, 2008), but diverges in the physical mechanism of F-BAR to F-BAR interactions. Multiple interactions were present in CIP4 tubule reconstructions between F-BARs, including lateral interactions between adjacent dimers and tip-to-tip interactions between F-BAR domain wings. Imp2 F-BAR to F-BAR interactions, on the other hand, occur between the tip of one dimer and the core of an adjacent dimer. Mutation of this single interface is sufficient to disrupt all oligomerization and subsequent tubule formation. Unsurprisingly, the residues involved in CIP4 oligomerization are distinct from those identified in Imp2. Therefore, this common in vitro ability of F-BARs to tubulate membranes using a scaffolding mechanism can be mediated by diverse F-BAR to F-BAR interactions.

Of the 13 F-BAR domain structures available (Henne *et al.*, 2007; Shimada *et al.*, 2007; Edeling *et al.*, 2009; Reider *et al.*, 2009; Wang *et al.*, 2009; Rao *et al.*, 2010; Moravcevic *et al.*, 2015), the Imp2 crystal structure is most similar to that of its homolog in *S. cerevisiae*, Hof1, with an R.M.S.D. of 2.7 Å. Despite this considerable similarity, the Hof1 F-BAR domain was not observed to tubulate membranes when expressed in cultured cells (Moravcevic *et al.*, 2015). Neither the interaction interface we identified in the Imp2 F-BAR, nor the one identified in CIP4 (Frost *et al.*, 2008), are conserved in Hof1 and this may explain why Hof1 does not tubulate membranes when overexpressed (Moravcevic *et al.*, 2015). As the sole cytokinetic F-BAR in *S. cerevisiae*, Hof1's inability to tubulate membranes is consistent with our conclusion that membrane tubulation by F-BAR proteins is not required during cytokinesis in yeast.

*Is F-BAR domain oligomerization and tubulation important in vivo?*

Our results show that although the Imp2 F-BAR domain can tubulate membranes *in vitro*, it doesn't require this activity for its function *in vivo*. In contrast to prevailing models derived from *in vitro* analyses (Frost *et al.*, 2009; Suetsugu *et al.*, 2010; Qualmann *et al.*, 2011; Mim and Unger, 2012), these results combined with the findings that the *Drosophila* Nwk1 F-BAR, the Cdc15 F-BAR and six other human F-BAR domains also do not tubulate membranes (Becalska *et al.*, 2013; Kelley, Becalska, *et al.*, 2015; McDonald *et al.*, 2015) indicate that membrane tubulation is not an essential physiological function of all F-BAR domains. It is possible that the observed membrane tubulation by some F-BAR domains is due to their overexpression, with membrane deformation unnecessary for their biological function, as in the case of Imp2. High levels

of molecular crowding can lead to membrane tubulation by certain proteins when locally concentrated at membranes (Stachowiak *et al.*, 2012). On the other hand, it not yet clear what function, if any, lateral F-BAR to F-BAR contacts perform in vivo, if not membrane tubulation. It is possible that less extensive oligomeric membrane-bound structures exist, such as the clusters of F-BAR proteins at dendritic spines (Schneider *et al.*, 2014), that could reinforce certain structures or cluster specific phosphoinositides (Zhao *et al.*, 2013). Our data indicate that Imp2 is present as oligomeric species in solution that may play a minor role in recruitment to the CR, since oligomerization mutants localize less robustly. However the decrease in CR localization when oligomerization was inhibited did not lead to any observable phenotype. It will be important to clarify the extent to which other F-BAR domains utilize their lateral contacts in normal physiological function.

#### *Function of F-BAR proteins in cytokinesis*

Combining our results with those from other studies (Nishihama *et al.*, 2009; Roberts-Galbraith *et al.*, 2009, 2010; Oh *et al.*, 2013; Moravcevic *et al.*, 2015; Ren *et al.*, 2015) leads us to suggest that the F-BAR proteins participating in cytokinesis serve as regulatable linkers between the membrane and additional division machinery rather than direct engines of membrane deformation. The results of our F-BAR domain swapping experiments further indicate that considerable plasticity is allowed in the membrane binding module offered by different F-BAR proteins. Given that Cdc15 and Imp2's SH3 domains are functionally interchangeable (Ren *et al.*, 2015) and Cdc15's F-BAR can substitute for Imp2's, the central region of these two proteins must specify important functional distinctions. Cdc15's unstructured central region controls the conformation of

the protein through extensive regulatory phosphorylation (Roberts-Galbraith *et al.*, 2010) and is also proposed to mediate an undefined interaction with the Golgi network (Arasada and Pollard, 2014). The central region of *S. cerevisiae* Hof1 binds septins and Myosin II (Meitinger *et al.*, 2011; Oh *et al.*, 2013), and tunes these interactions with cell cycle-regulated phosphorylation (Meitinger *et al.*, 2011, 2013). Imp2's central domain is also differentially phosphorylated throughout the cell cycle (unpublished data), hinting that Imp2 function may also be regulated via phosphorylation. Future work will be directed at understanding whether differential phosphoregulation underlies the distinct temporal requirements of Cdc15 and Imp2 in cytokinesis, and the contribution of Imp2's central region to regulation of its membrane and protein binding domains.

## CHAPTER IV

### NANOSCALE ARCHITECTURE OF THE SCHIZOSACCHAROMYCES POMBE CONTRACTILE RING

#### Introduction

In many eukaryotes, including animals and fungi, cell division is accomplished by an actin and myosin based contractile ring apparatus (Green *et al.*, 2012). This complex structure is tightly linked to the plasma membrane and uses myosin motors to constrict a F-actin ring (Cheffings *et al.*, 2016), pulling opposing sides of the membrane together.

Studies in *S. pombe* have led the cytokinesis field in identifying components and regulators of the contractile ring (Pollard and Wu, 2010; Goyal *et al.*, 2011; Willet, McDonald and Gould, 2015; Cheffings *et al.*, 2016; Rincon and Paoletti, 2016). Genetic screens as well as genome-wide and targeted localization studies have determined a complete “parts list” of protein components that comprise the ring, many of which are conserved in higher eukaryotes (Nurse *et al.*, 1976; Chang *et al.*, 1996; Balasubramanian *et al.*, 1998; Matsuyama *et al.*, 2006). 318 proteins are annotated as localizing to the *S. pombe* division site (Matsuyama *et al.*, 2006; Wood *et al.*, 2012), which includes both the contractile ring and the lining of the division septum formed during ring constriction. Only a subset of these proteins (38 according to PomBase annotation (Wood *et al.*, 2012)) make up the contractile ring itself.

Though the proteins that comprise the contractile ring have been identified, how these components are knit together into a functional division machine remains unclear despite several substantive efforts towards unraveling this complex question. The *S. pombe* contractile ring forms in the middle of the cell from precursor “nodes”,

membrane-tethered protein foci that contain anillin Mid1, IQGAP Rng2, myosin-II heavy chain Myo2 and light chains Cdc4 and Rlc1, F-BAR Cdc15, and formin Cdc12 (Wu *et al.*, 2006). Precursor nodes coalesce into a contiguous ring which recruits many additional components before constriction after mitotic exit. The orientation of 5 components within these nodes has been determined (Laporte *et al.*, 2011), and quantitative fluorescence studies have even been used to estimate the number of molecules of many proteins per node as well as in the fully-formed ring (Wu and Pollard, 2005; Laporte *et al.*, 2011). Knowledge from these studies has been incorporated into mathematical models that attempt to understand ring formation and constriction. A search-capture-pull-release model of node condensation was found to recapitulate basic ring formation (Vavylonis *et al.*, 2008; Ojkic *et al.*, 2011), while biophysical tension measurements of the ring have been used to model ring constriction (Stachowiak *et al.*, 2014). Though these models are becoming increasingly complex and explanatory, the field is hampered by sparse information about the fundamental molecular architecture of the ring.

Ultimately, the resolution limit of conventional fluorescence microscopy (~250 nm) restrains the spatial information attainable by studies of *S. pombe* nodes and contractile rings, each only 100-200 nm in width (Wu *et al.*, 2006; Laplante *et al.*, 2016). At higher resolution, one electron microscopy study revealed the ring is composed of a dense array of 1000-2000 F-actin filaments with mixed directionality (Kamasaki *et al.*, 2007); however, additional protein components could not be detected with this technique. New super-resolution microscopy technologies, based on the precise (<50 nm) localization of single photoactivated fluorescent molecules (Betzig *et al.*, 2006; Hess *et*

*al.*, 2006; Rust *et al.*, 2006), have the potential to drive our understanding of the contractile ring to a truly molecular level.

Super-resolution methods have recently been effective at determining the molecular architecture and revealing the inner mechanics of multiple cellular structures (Sydor *et al.*, 2015). In focal adhesions, the plasma membrane and F-actin were found to be separated by distinct layers of proteins: an integrin signaling layer, a force transduction layer, and an actin regulatory layer (Kanchanawong *et al.*, 2010), revealing a potential mechanism of force-induced focal adhesion formation and maintenance. At centrosomes, the pericentriolar matrix (PCM) was found to organize into two structural layers: one directly apposed to the centriole wall and a second extending radially outward (Mennella *et al.*, 2012), scaffolded by the N- and C-termini of pericentrin-like protein, respectively. Furthermore, super-resolution microscopy has revealed previously unresolvable structures, such as actin-spectrin periodic repeats which coat the membranes of axons in animals (Xu *et al.*, 2013; He *et al.*, 2016). Super-resolution microscopy has also recently been applied to *S. pombe* cytokinesis, in a study that investigated 6 proteins' orientations within precursor nodes relative to each other (Laplante *et al.*, 2016).

Using fluorescence photoactivation localization microscopy (fPALM) we approached the question of the molecular architecture of the contractile ring by comprehensively mapping 29 protein components' spatial organization relative to the underlying plasma membrane. We determined that the contractile ring is composed of layers of protein components at distinct positions interior to the plasma membrane, similar to other membrane-tethered actin structures like focal adhesions (Kanchanawong *et al.*, 2010) and cadherin junctions (Bertocchi *et al.*, 2017), a conclusion verified by

fluorescence resonance energy transfer (FRET) experiments. Moreover, we find certain components are uniformly distributed laterally within the ring, while others form clusters of various sizes and variable spacing. These data provide a structural framework for understanding the formation, mechanics, and regulation of the contractile ring.

## Results

### *fPALM strategy for determining the spatial organization of contractile ring components*

To determine the molecular architecture of the contractile ring using fPALM, we measured the precise spatial distribution of 29 proteins endogenously tagged with mMaple3 relative to the plasma membrane marked with the membrane-binding probe mCling-ATTO647N (Revelo *et al.*, 2014) (Figure 4-1A). The photoactivatable mMaple3 fluorophore was chosen because it has multiple advantages over the commonly used mEos3.2 (Zhang *et al.*, 2012), most importantly a faster maturation time (49 versus 330 minutes) (Wang *et al.*, 2014). The mMaple3 fluorophore is ~5 nm in size and was connected to protein termini with a short 11 amino acid linker, minimizing positional uncertainty. In many cases, the spatial distribution of both protein termini was interrogated to determine exact molecular orientations. We imaged synchronized cells that contained fully formed contractile rings (e.g. no precursor nodes remaining) that had not begun constriction (evidenced by membrane ingression and septum formation). We imaged the middle focal plane of cells and utilized optical astigmatism to precisely measure the Z positions of each photoactivated molecule in order to restrict our analysis to a 500 nm Z section (B. Huang *et al.*, 2008). This imaging scheme resulted in a significant increase in resolution from conventional fluorescence (Figure 4-1B) to



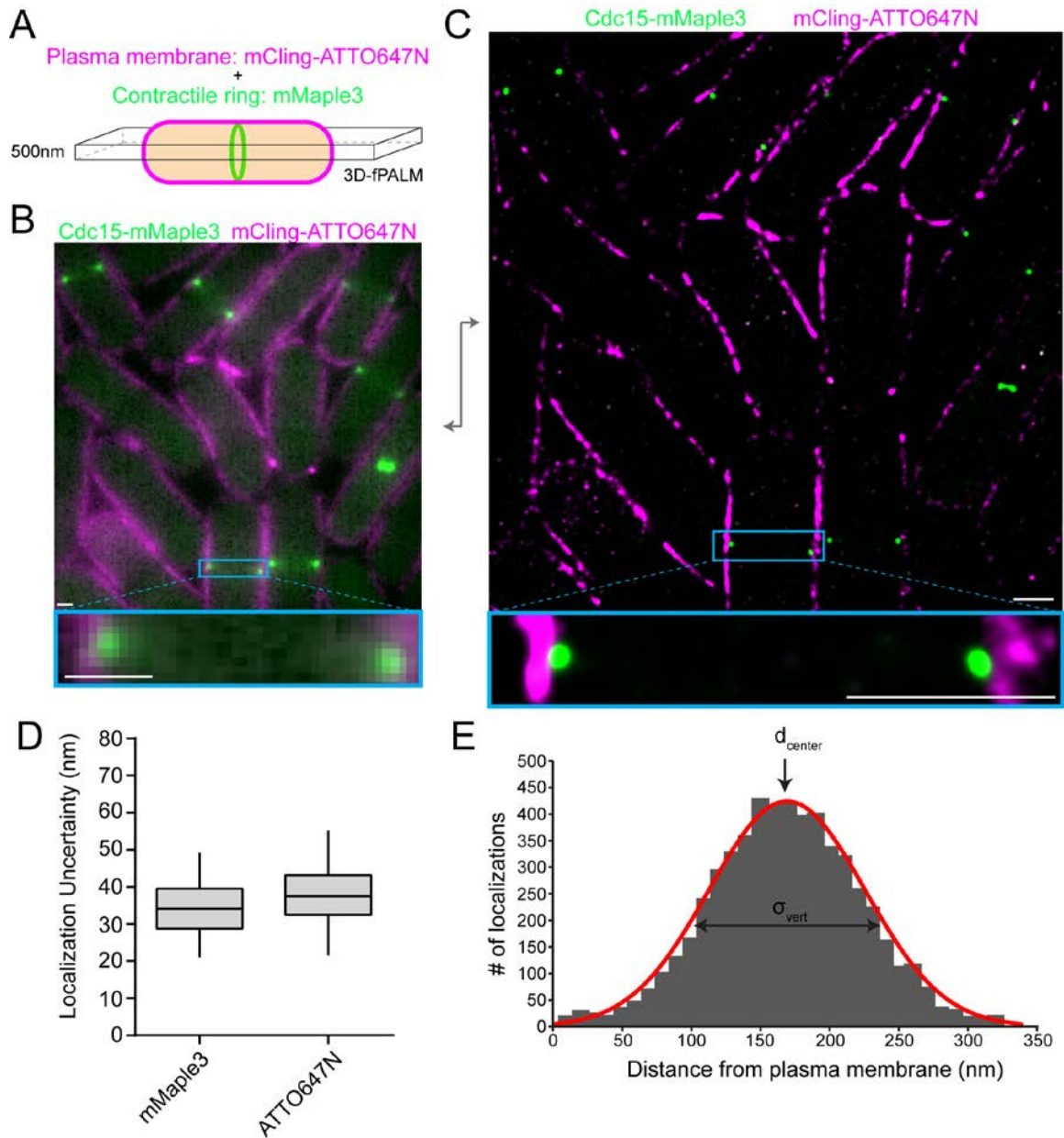


**Figure 4-1. fPALM strategy to localize contractile ring proteins with nanometer resolution relative to the plasma membrane.** A) Schematic of fPALM sample setup. Contractile ring proteins were endogenously tagged with mMaple3 while the plasma membrane was labeled with mCling-ATTO647N. A 3D-fPALM system was used to restrict the imaging plane to a narrow 500 nm Z section. B) Conventional fluorescence microscopy images of a contractile ring protein and membrane dye. C) Resulting 2 color fPALM image after localization analysis. Particles are visualized as normalized Gaussians with standard deviation = localization uncertainty. D) Localization uncertainty achieved with mMaple3 and ATTO647N fluorophores for all data in this study. E) Example histogram of Cdc15-mMaple3 localization distances from the mCling-ATTO647N membrane edge. A Gaussian curve was fitted to the data and  $d_{center}$  and  $\sigma_{vert}$  parameters were extracted. Scale bars = 1  $\mu$ m.

fPALM images (Figure 4-1C). Overall, we achieved an average of 34 and 37 nm localization uncertainty for mMaple3 and ATTO647N fluorophores, respectively (Figure 4-1D).

Before examining contractile ring proteins, we evaluated the mCling-ATTO647N probe's ability to identify the plasma membrane by comparison to membrane-bound Acyl-mMaple3 (Figure 4-2A). These images revealed the mCling-ATTO647N signal is wider than the ~10 nm plasma membrane alone (Figure 4-2B). However, the interior edge of the mCling signal aligns well the edge of Acyl-mMaple3 signal, validating this method for identifying the plasma membrane (blue line, Figure 4-2A-B). It is likely that the wide mCling signal reflects nonspecific binding to the cell wall as well as incorporation into the plasma membrane.

To quantify the spatial distribution of each protein component relative to the plasma membrane, we performed an analysis similar to that performed on focal adhesion and cadherin junction proteins (Kanchanawong *et al.*, 2010; Bertocchi *et al.*, 2017). The plasma membrane was defined as the edge of the mCling-ATTO647N signal, and the distance from this line was calculated for each individual localization in a contractile ring side-view "spot". The average distance from the membrane ( $d_{\text{center}}$ ) and a signal width parameter ( $\sigma_{\text{vert}}$ ) were determined (Figure 4-1E) (Kanchanawong *et al.*, 2010), and these values were then averaged across multiple rings.

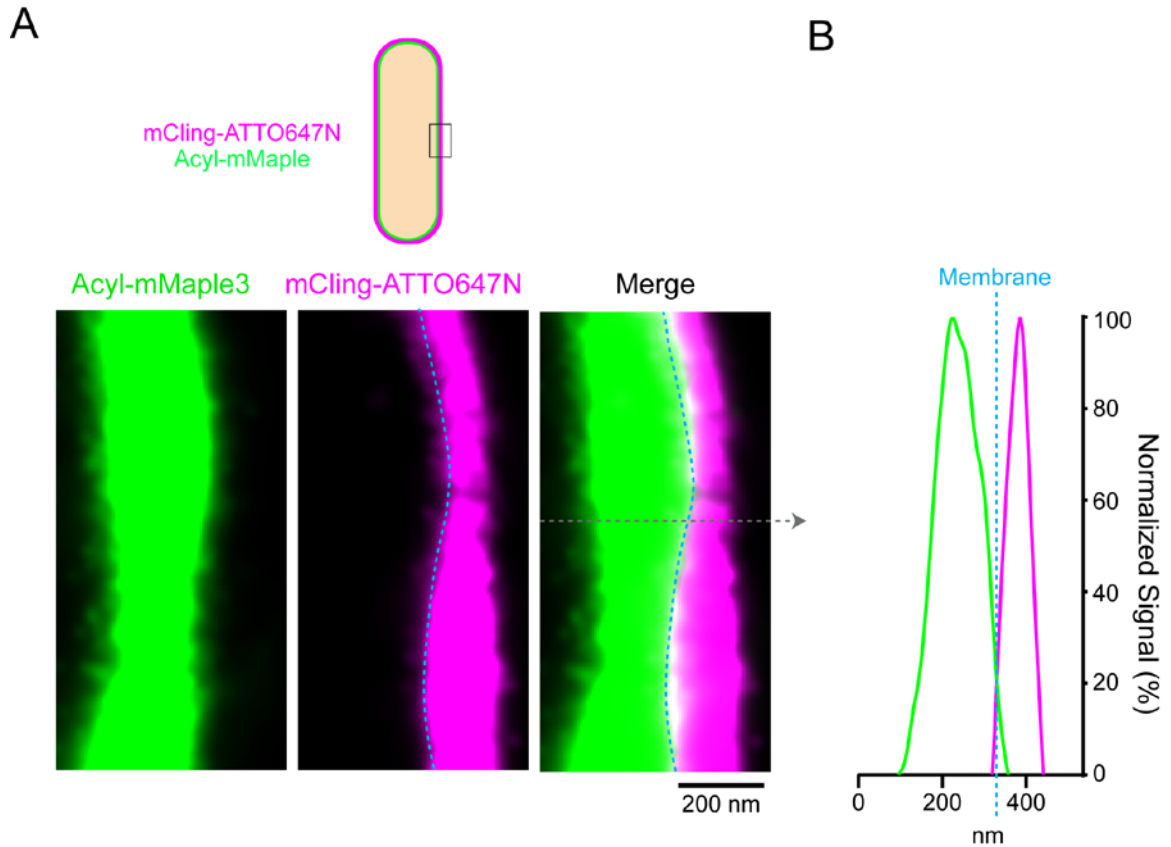


**Figure 4-2. The mCling-ATTO674N plasma membrane marker accurately identifies the plasma membrane edge.** A) Schematic of image orientation in (B). B) Representative image of mCling-ATTO647N membrane marker in an Acyl-mMaple3 expressing cell. Blue line indicates membrane identification. C) A linescan across the membrane in (B) shows the edges of the mCling-ATTO647N and Acyl-mMaple3 signals align.

### Spatial distribution of structural contractile ring components

We first determined the spatial distribution of 19 structural components of the contractile ring relative to the membrane (Figure 4-3A-B and 4-4). Endogenous mMaple3

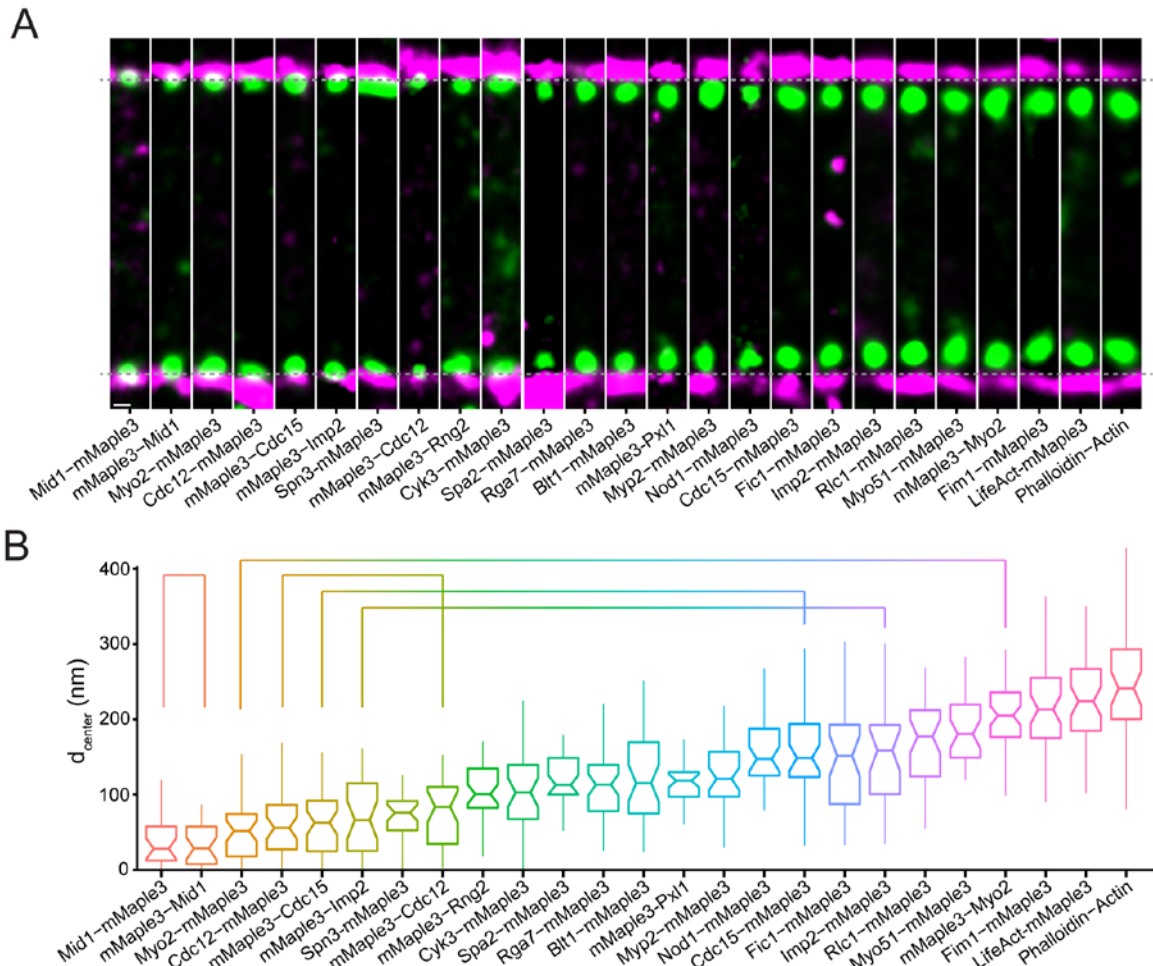
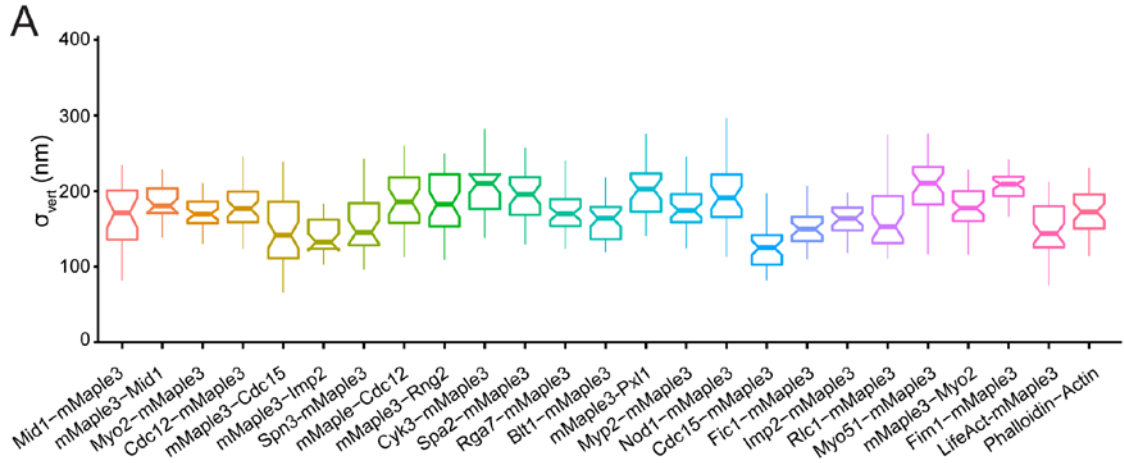


**Figure 4-3. Nanoscale organization of contractile ring structural components.** A) Representative fPALM images of structural contractile ring components. Scale, 100 nm. Particles are visualized as normalized Gaussians with standard deviation = localization uncertainty. B) Distance from the plasma membrane ( $d_{center}$ ) of structural contractile ring components. Box plots depict 1st and 3rd quartiles and median; Whiskers, minimum and maximum; Notches, 95% confidence intervals. Lines connect proteins labeled on opposite termini.



B

Protein	$d_{center} \pm SD$	$\sigma_{vert} \pm SD$	n rings	Total localizations	Avg localizations / ring	Uncertainty $\pm SD$
Blt1-mMaple3	123.8 $\pm$ 60.4	160.9 $\pm$ 28.0	38	35507	934	36.8 $\pm$ 7.9
Cdc12-mMaple3	59.6 $\pm$ 49.2	180.5 $\pm$ 32.8	40	23931	598	37.7 $\pm$ 13.6
Cdc15-mMaple3	158 $\pm$ 65	127.2 $\pm$ 30.8	41	212238	5177	30.5 $\pm$ 11.9
Cyk3-mMaple3	100.5 $\pm$ 58.3	200.0 $\pm$ 33.6	34	59280	1744	36.7 $\pm$ 7.0
Fic1-mMaple3	151.8 $\pm$ 72.5	151.8 $\pm$ 28.1	38	119188	3137	35.8 $\pm$ 17.7
Fim1-mMaple3	217.8 $\pm$ 61.6	205.0 $\pm$ 18.8	44	65912	1498	37.5 $\pm$ 7.1
Imp2-mMaple3	152.1 $\pm$ 68.0	167.4 $\pm$ 29.2	28	87349	3120	40.2 $\pm$ 21.5
LifeAct-mMaple3	225.7 $\pm$ 59.0	151.1 $\pm$ 37.3	44	466218	10596	33.2 $\pm$ 8.2
mMaple3-Cdc12	76.3 $\pm$ 43.8	186.2 $\pm$ 36.7	33	6771	205	37.2 $\pm$ 9.5
mMaple3-Cdc15	58.8 $\pm$ 45.4	149.5 $\pm$ 47.9	45	105301	2340	33.7 $\pm$ 11.5
mMaple3-Imp2	67.3 $\pm$ 58.2	141.5 $\pm$ 22.8	30	97869	3262	31.9 $\pm$ 17.0
mMaple3-Mid1	37.0 $\pm$ 46.7	185.0 $\pm$ 30.9	28	25662	917	37.8 $\pm$ 7.5
mMaple3-Myo2	204.0 $\pm$ 50.7	178.1 $\pm$ 28.5	54	102292	1894	36.9 $\pm$ 7.4
mMaple3-Pxl1	114.0 $\pm$ 25.3	202.9 $\pm$ 44.3	35	7225	206	36.5 $\pm$ 7.2
mMaple3-Rng2	102.5 $\pm$ 36.5	186.6 $\pm$ 44.8	41	8446	206	39.0 $\pm$ 8.7
Mid1-mMaple3	36.1 $\pm$ 44.9	165.1 $\pm$ 40.6	26	16777	645	40.9 $\pm$ 24.0
Myo2-mMaple3	48.0 $\pm$ 38.7	173.1 $\pm$ 27.8	42	55891	1331	35.8 $\pm$ 10.0
Myo51-mMaple3	191.4 $\pm$ 52.8	209.3 $\pm$ 37.2	34	19716	580	38.6 $\pm$ 10.8
Myp2-mMaple3	125.9 $\pm$ 41.0	178.4 $\pm$ 32.1	40	36421	911	35.8 $\pm$ 7.2
Nod1-mMaple3	156.1 $\pm$ 45.5	200.9 $\pm$ 50.3	36	7031	195	40.6 $\pm$ 10.2
Phalloidin-Alexa488	248.2 $\pm$ 75.3	172.2 $\pm$ 32.2	41	179411	4376	34.4 $\pm$ 18.5
Rga7-mMaple3	114.4 $\pm$ 48.2	173.4 $\pm$ 27.2	46	125349	2725	36.1 $\pm$ 7.9
Rlc1-mMaple3	169.7 $\pm$ 64.5	164.3 $\pm$ 40.2	38	111388	2931	34.0 $\pm$ 7.7
Spa2-mMaple3	122.4 $\pm$ 43.5	196.7 $\pm$ 40.6	36	19179	533	38.4 $\pm$ 8.2
Spn3-mMaple3	75.77 $\pm$ 29.1	145.5 $\pm$ 39.2	32	94600	2956	36.7 $\pm$ 8.2

**Figure 4-4. Vertical width parameters ( $\sigma_{vert}$ ) and localization values for strains in Figure 4-3.** A) Vertical width parameters ( $\sigma_{vert}$ ) for structural contractile ring components in Figure 2. B) Complete particle statistics for proteins in Figure 4-3.

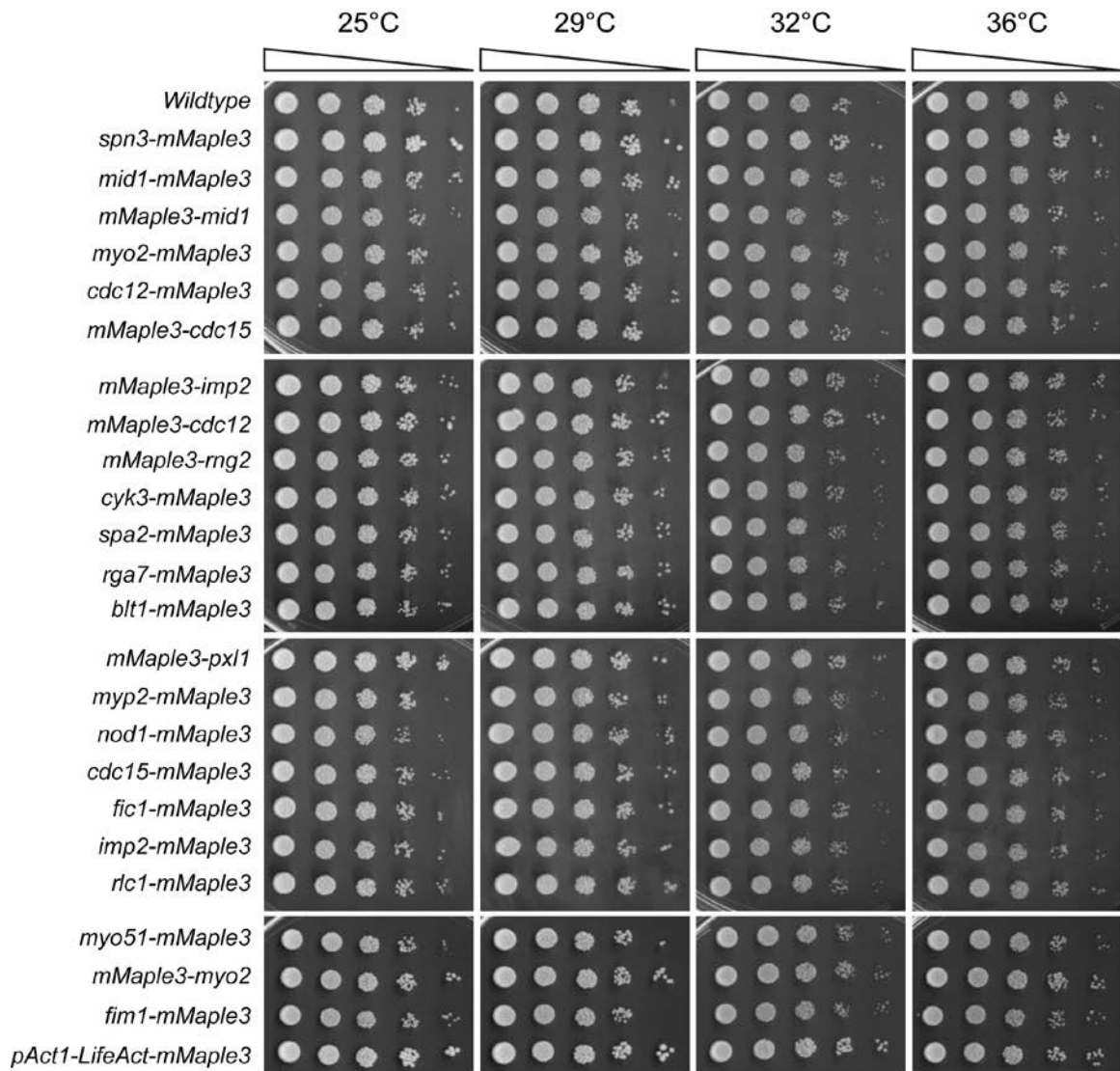


**Figure 4-5. Endogenous mMaple3 tags on structural components do not perturb normal growth and division.** Serial dilutions of the strains used in Figure 4-3 were grown at the indicated temperatures.

fusions of these proteins were functional and had no impact on growth or division (Figure 4-5 and 4-8). The resolution of the mMaple3 probe (Figure 4-1D) was sufficient to distinguish differences in distance from the membrane between components. Overall, we found the fully-formed contractile ring is made up of components  $181\pm 33$  nm wide and extends from the plasma membrane  $386\pm 72$  nm into the cytoplasm.

Multiple membrane binding proteins including Mid1, the F-BAR proteins Cdc15 and Imp2, and the septin Spn3 are positioned within 80 nm of the plasma membrane. Both termini of the anillin Mid1 are within 50 nm of the membrane, consistent with direct membrane binding through its C2 domain (Celton-Morizur *et al.*, 2004; Rincon and Paoletti, 2012; Sun *et al.*, 2015). Cdc15 and Imp2 contain N-terminal F-BAR domains that also directly bind the membrane (Roberts-Galbraith *et al.*, 2010; McDonald *et al.*, 2015, 2016). We find Spn3 near the membrane, consistent with its assembly into membrane-bound oligomers with additional septin subunits (An *et al.*, 2004). In addition to membrane-binding proteins, the C-terminal tail of the essential contractile ring myosin Myo2 (Kitayama *et al.*, 1997; Palani *et al.*, 2017) is near the membrane, as was observed in cytokinesis precursor nodes (Laporte *et al.*, 2011; Laplante *et al.*, 2016). The N-terminus of the formin Cdc12 is also found near the membrane, in accord with direct binding to the F-BAR domain of Cdc15 (Carnahan and Gould, 2003; Willet, McDonald, Bohnert, *et al.*, 2015). The C-terminus of Cdc12 is found at a similar height, further supporting its localization to a membrane-proximal stratum.

Slightly further from the membrane (80-160 nm) we find the IQGAP Rng2, a scaffolding protein critical for contractile ring formation and constriction (Padmanabhan *et al.*, 2011; Tebbs and Pollard, 2013). Multiple accessory proteins are present in this

layer whose presence is important for ring integrity and which are linked to the underlying layer through direct protein-protein interactions: Cyk3, Spa2, Blt1, paxillin Pxl1, Nod1, and Fic1 (Ge and Balasubramanian, 2007; Pinar *et al.*, 2008; Roberts-Galbraith *et al.*, 2010; Bohnert and Gould, 2012; Pollard *et al.*, 2012; Guzman-Vendrell *et al.*, 2013; Zhu *et al.*, 2013; Ren *et al.*, 2015). Pxl1's localization to an intermediate layer between the membrane and F-actin is comparable to paxillin's position between membrane-embedded integrins and F-actin in focal adhesions (Kanchanawong *et al.*, 2010). At similar intermediate elevations, we find the tail domains of two other myosins: the non-essential myosin-II, Myp2, as well as a myosin-V, Myo51.

Interestingly, we find that the C-termini of three F-BAR proteins (Cdc15, Imp2, and Rga7) extend away from their membrane-bound F-BAR domains into the intermediate layer of the ring (lines, Figure 4-3B). These proteins contain central regions predicted to be unstructured, which may permit the SH3 domains of Cdc15 and Imp2 to extend inward ~100 nm distances and connect with their multiple interactors also found at this layer including Pxl1, Spa2, Fic1, and Cyk3 (Figure 4-3), as well as Rgf3 (Figure 4-6) (Roberts-Galbraith *et al.*, 2009, 2010; Ren *et al.*, 2015).

At the farthest distances from the membrane (160-400 nm), we find F-actin, the head of Myo2, and Fim1, an F-actin crosslinker (Figure 4-3). Since actin is not functional as a fluorescent fusion in *S. pombe* (Wu and Pollard, 2005), we imaged F-actin with two probes: LifeAct-mMaple3 and Phalloidin-Alexa488. Measurements using these two methods were consistent, placing F-actin's  $d_{\text{center}}$  at  $225 \pm 59$  (LifeAct-mMaple3) or  $248 \pm 75$  nm (Phalloidin; Figure 4-4B) from the membrane. The N-terminal head domain of Myo2 is level with F-actin, while its light chain Rlc1 is ~30 nm closer to the



membrane, in accord with its binding to the neck domain of Myo2 that is immediately proximal to the head domain (Naqvi *et al.*, 2000). Two actin crosslinking proteins are present in the contractile ring, fimbrin Fim1 and  $\alpha$ -actinin Ain1 (Wu *et al.*, 2001), with Ain1 being the predominant cytokinetic crosslinker (Wu *et al.*, 2001; Li *et al.*, 2016). We were unable to produce a functional mMaple3-Ain1, but anticipate it would localize in the same region as F-actin, similar to Fim1.

#### *Spatial distribution of signaling contractile ring components*

The contractile ring contains a plethora of signaling proteins that influence the behavior of its structural elements including kinases, phosphatases, GTPase exchange factors (GEFs) and GTPase activating proteins (GAPs). We examined the spatial distribution of 10 such components that are present in fully formed unconstricted rings (Figure 4-6A-B, Figure 4-7). The kinases Orb2/Pak1/Shk1, Sid2, and Pck1 are relatively close to the membrane, on average < 110 nm. In focal adhesions, regulators such as Focal Adhesion Kinase (FAK) are also found at an intermediate layer between the membrane and F-actin (Kanchanawong *et al.*, 2010). In contrast, the N-terminus of the kinase Pom1 was found farther away from the membrane (172 nm) despite the presence of a nearby membrane-binding motif (Hachet *et al.*, 2011). It may be that Pom1 localization to the contractile ring utilizes a different mechanism than when targeted to the cell tip cortex (Hachet *et al.*, 2011); it is noteworthy that Pom1 contains multiple PxxP motifs and may bind the SH3 network established by Cdc15 and Imp2. The RhoGEF Rgf3, a known partner of Cdc15 and Imp2 SH3 domains (Ren *et al.*, 2015), is also present at an intermediate height.

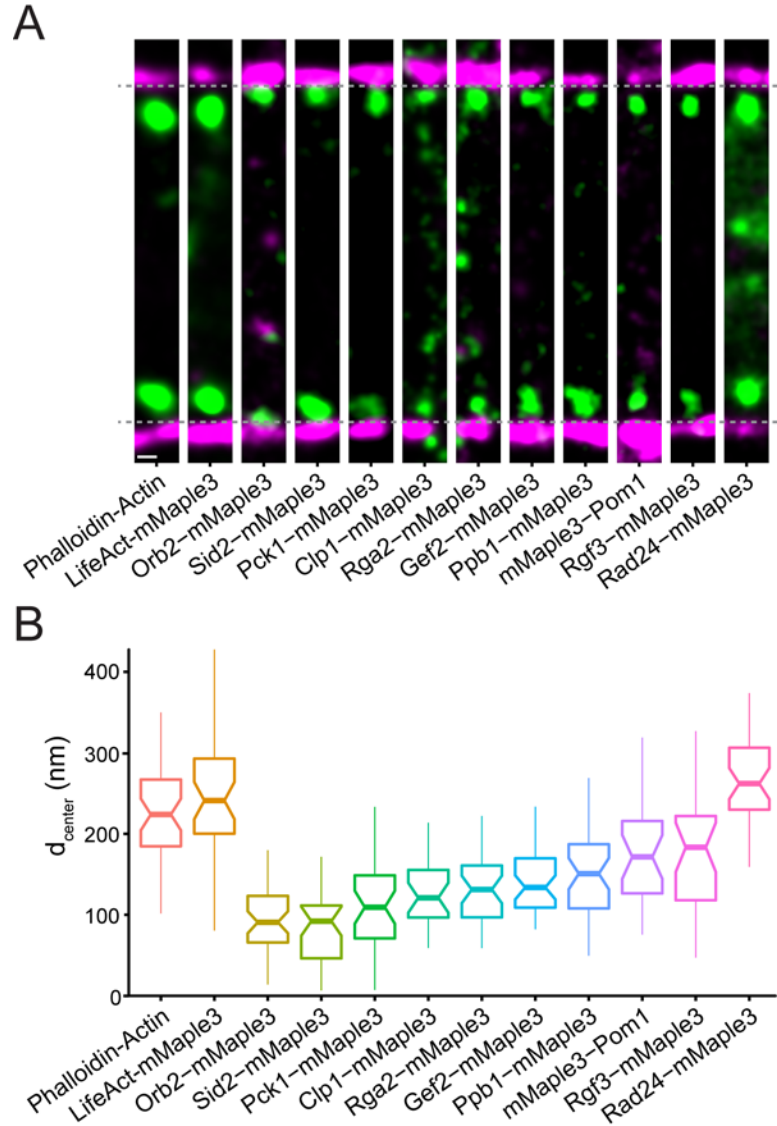
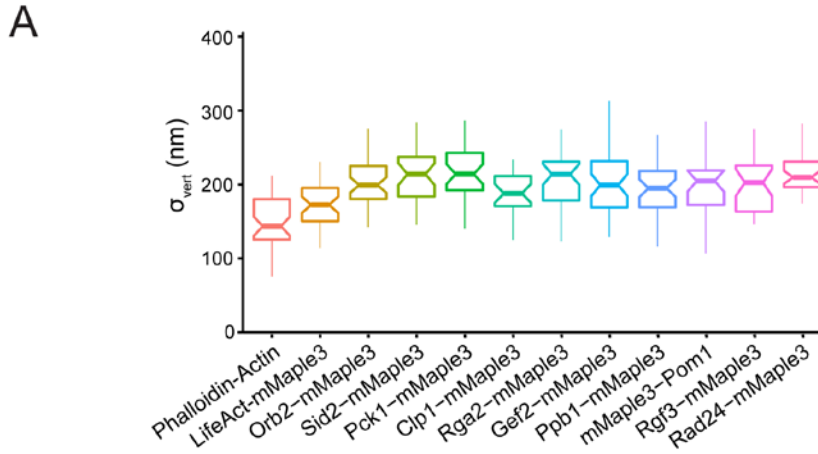


**Figure 4-6. Nanoscale organization of contractile ring signaling components.** A) Representative fPALM images of signaling contractile ring components. Scale, 100 nm. Particles are visualized as normalized Gaussians with standard deviation = localization uncertainty. B) Distance from the plasma membrane ( $d_{\text{center}}$ ) of signaling contractile ring components. Box plots depict 1st and 3rd quartiles and median; Whiskers, minimum and maximum; Notches, 95% confidence intervals.



**B**

Protein	$d_{center} \pm SD$	$\sigma_{vert} \pm SD$	n rings	Total localizations	Avg localizations / ring	Uncertainty $\pm SD$
Phalloidin-Alexa488	248.2 $\pm$ 75.3	172.2 $\pm$ 32.2	41	179411	4376	34.4 $\pm$ 18.5
LifeAct-mMaple3	225.7 $\pm$ 59.0	151.1 $\pm$ 37.3	44	466218	10596	33.2 $\pm$ 8.2
Clp1-mMaple3	136.1 $\pm$ 56.4	190.4 $\pm$ 41.2	25	2052	82	40.2 $\pm$ 10.5
Gef2-mMaple3	139.9 $\pm$ 40.3	203.3 $\pm$ 43.1	42	5866	140	39.5 $\pm$ 8.7
mMaple3-Pom1	174.5 $\pm$ 63.5	198.1 $\pm$ 48.9	27	4566	169	50.2 $\pm$ 21.3
Orb2-mMaple3	93.9 $\pm$ 45.0	201.4 $\pm$ 31.7	45	11320	252	38.3 $\pm$ 7.9
Pck1-mMaple3	110.3 $\pm$ 50.1	216.4 $\pm$ 35.7	36	4391	122	37.8 $\pm$ 7.3
Ppb1-mMaple3	152.2 $\pm$ 52.2	194.7 $\pm$ 40.3	42	11444	272	37.4 $\pm$ 7.1
Rad24-mMaple3	268.6 $\pm$ 55.1	215.8 $\pm$ 29.2	39	41893	1074	29.7 $\pm$ 8.4
Rga2-mMaple3	135.7 $\pm$ 53.7	206.6 $\pm$ 40.4	35	9986	285	37.9 $\pm$ 7.5
Rgf3-mMaple3	167.0 $\pm$ 96.4	201.7 $\pm$ 38.0	29	7064	244	40.0 $\pm$ 18.4
Sid2-mMaple3	88.8 $\pm$ 49.5	210.7 $\pm$ 36.7	33	9649	292	38.1 $\pm$ 7.3

**Figure 4-7. Vertical width parameters ( $\sigma_{vert}$ ) and localization values for strains in Figure 4-6.** A) Vertical width parameters ( $\sigma_{vert}$ ) for signaling contractile ring components in Figure 2. B) Complete particle statistics for proteins in Figure 4-6.

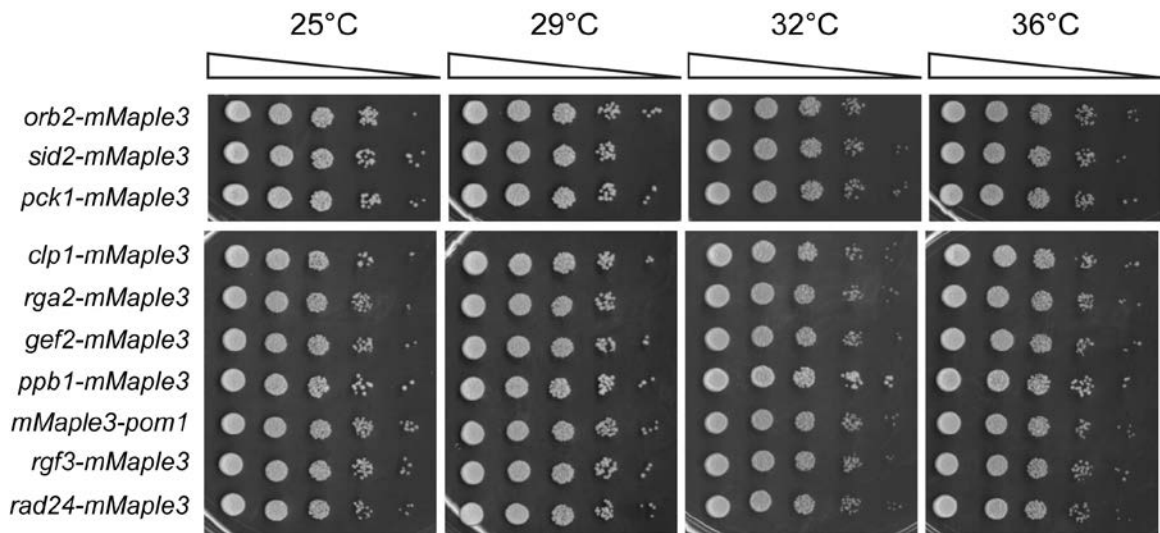


**Figure 4-8. Endogenous mMaple3 tags on signaling components do not perturb normal growth and division.** Serial dilutions of the strains used in Figure 4-6 were grown at the indicated temperatures.

Phosphatases Clp1 (Cdc14-related) and Ppb1 (Calcineurin), RhoGAP Rga2, and RhoGEF Gef2 were also found in an intermediate stratum. Gef2 is in complex with Nod1 (Zhu *et al.*, 2013), and is found at a similar elevation to its binding partner, 140 nm and 156 nm, respectively. Rad24, a 14-3-3 protein, while not technically a signaling molecule, binds to many phosphoproteins to control signaling pathways (Mackintosh, 2004; Aitken, 2006). We find the majority of Rad24 high in elevation, similar to F-actin, though it also localizes throughout the cytoplasm.

#### *Distinct layers around F-BAR protein scaffolds*

The fPALM analysis of Cdc15 and Imp2 F-BAR proteins indicated that their C-termini were positioned in a different stratum of the contractile ring than their N-terminal

membrane-bound F-BAR domains. To verify the existence of distinct layers of F-BAR and SH3 scaffolded components with a different approach, we placed a mCherry fluorophore on either the N-terminus (near the F-BAR domain) or C-terminus (near the SH3 domain) of Cdc15 in combination with GFP- or mNeonGreen (mNG)-conjugated ring components and analyzed each strain by fluorescent resonance energy transfer (FRET) (Figure 4-9A-B).

Supporting the hypothesis that Cdc15 and probably other F-BARs scaffold distinct layers of proteins in the contractile ring, we detected specific FRET signals between mCherry-Cdc15 and membrane bound Acyl-GFP, GFP-Imp2, GFP-Rga7, and both mNG-Cdc12 and Cdc12-mNG (Figure 4-9A). A strong FRET signal between mCherry-Cdc15 and Acyl-GFP is consistent with the binding of Cdc15's F-BAR to anionic phospholipids within the plasma membrane (Roberts-Galbraith *et al.*, 2010; McDonald *et al.*, 2015). Furthermore, the FRET signal of mCherry-Cdc15 with two other F-BAR domains (GFP-Imp2 and GFP-Rga7) indicates that all three cytokinesis F-BARs are packed in close proximity upon the membrane, despite the fact that they do not heterodimerize (Roberts-Galbraith *et al.*, 2009; Martín-García *et al.*, 2014). The FRET signal of mCherry-Cdc15 with both termini of Cdc12 is consistent with the low elevation spatial distribution of both Cdc12 termini observed by fPALM analysis. Importantly, the FRET signals of low elevation ring components with mCherry-Cdc15 were specific, as these particular GFP- and mNG-tagged components did not display significant FRET with Cdc15 tagged at its C-terminus with mCherry (Figure 4-9C-D).

Cdc15-mCherry, on the other hand, showed specific FRET signals with Imp2-GFP, Rga7-GFP, and five known binding partners of its SH3 domain: Fic1-GFP, Pxl1-

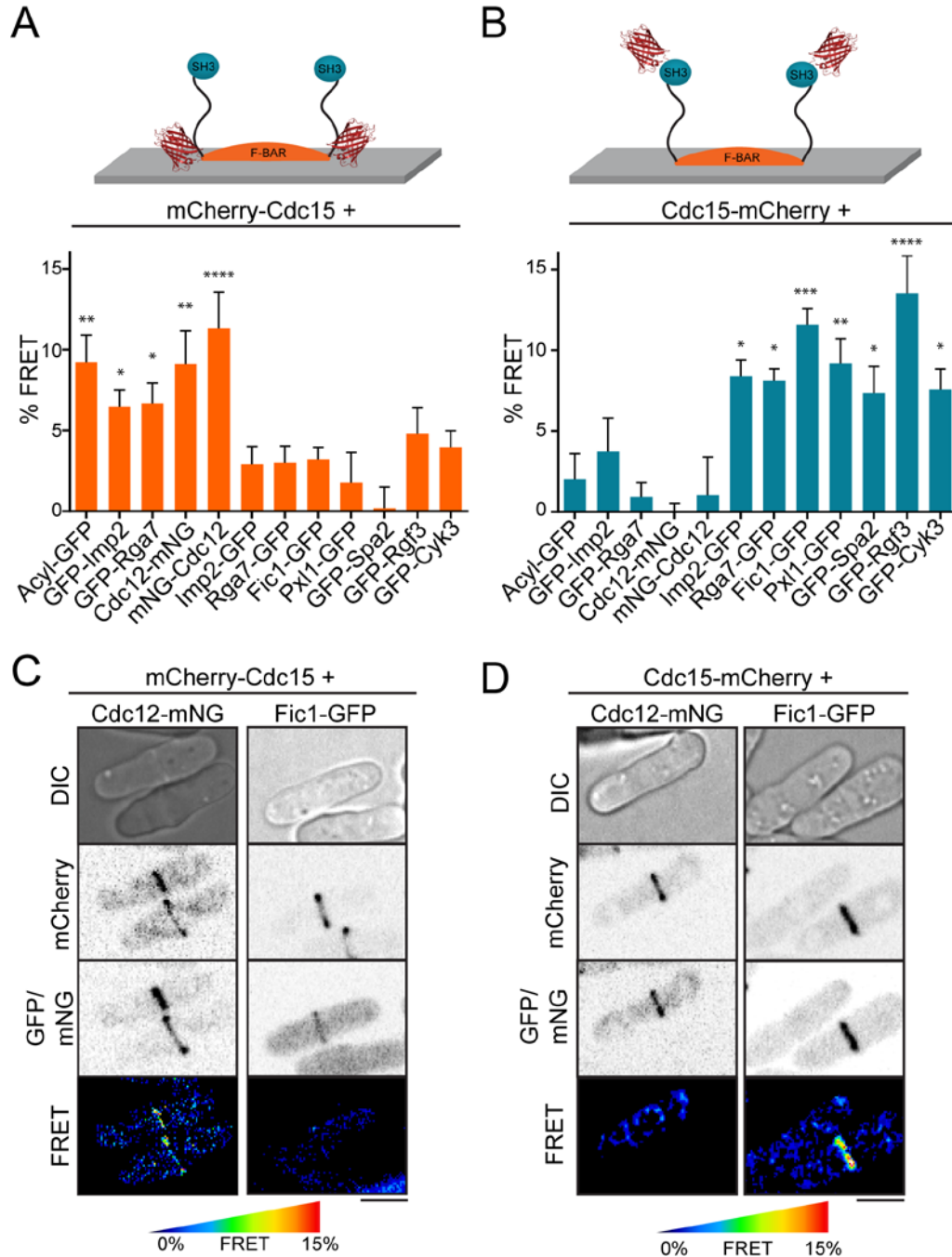
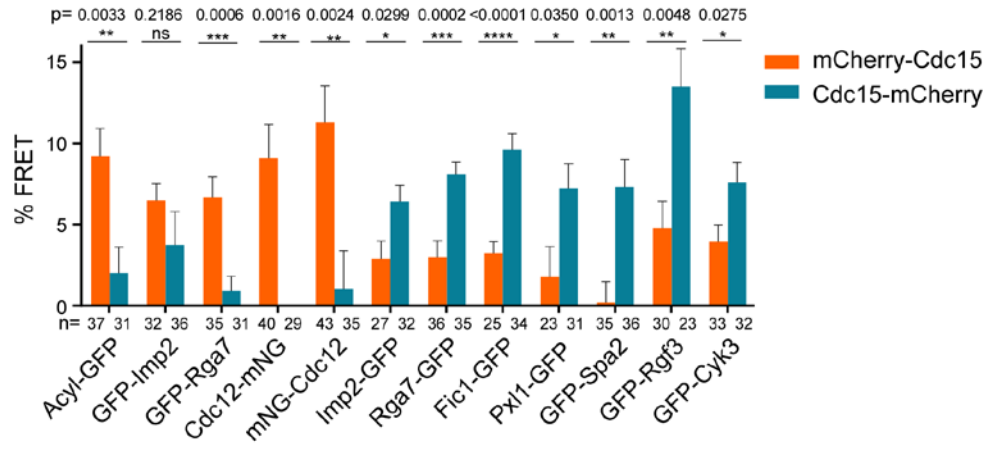


**Figure 4-9. FRET confirms distinct layers around F-BAR proteins in the contractile ring.** A-B) Quantification of FRET between mCherry-Cdc15 (A) or Cdc15-mCherry (B) and GFP- or mNG-conjugated contractile ring components. See also Figure 4 – Supplement 1 for direct mCherry-Cdc15:Cdc15-mCherry comparisons. % FRET is the increase in GFP donor signal following mCherry acceptor photobleaching. One way ANOVA tests were performed for each strain against an Rlc1-GFP negative control. \*,  $p < 0.05$ ; \*\*,  $p < 0.01$ ; \*\*\*,  $p < 0.001$ ; \*\*\*\*,  $p < 0.0001$ . C-D) Cdc12-mNG and Fic1-GFP FRET signals at the contractile ring are specific to mCherry-Cdc15 (C) or Cdc15-mCherry (D). Scale = 4  $\mu\text{m}$ .

A

		mCherry-Cdc15											
p:		0.0012	0.0409	0.0389	0.0011	<0.0001	0.2144	0.6968	0.1764	0.4709	0.3695	0.258	0.4204
n:		37	32	35	40	43	27	36	25	23	35	27	33
		Cdc15-mCherry											
p:		0.9829	0.4628	0.6814	0.0839	0.7066	0.011	0.0127	0.0001	0.0046	0.0281	<0.0001	0.0256
n:		31	36	31	29	35	32	35	34	31	36	33	32
		Acyl-GFP	GFP-Imp2	GFP-Rga7	Cdc12-mNG	mNG-Cdc12	Imp2-GFP	Rga7-GFP	Fic1-GFP	Pxl1-GFP	GFP-Spa2	GFP-Rgf3	GFP-Cyk3

B



C

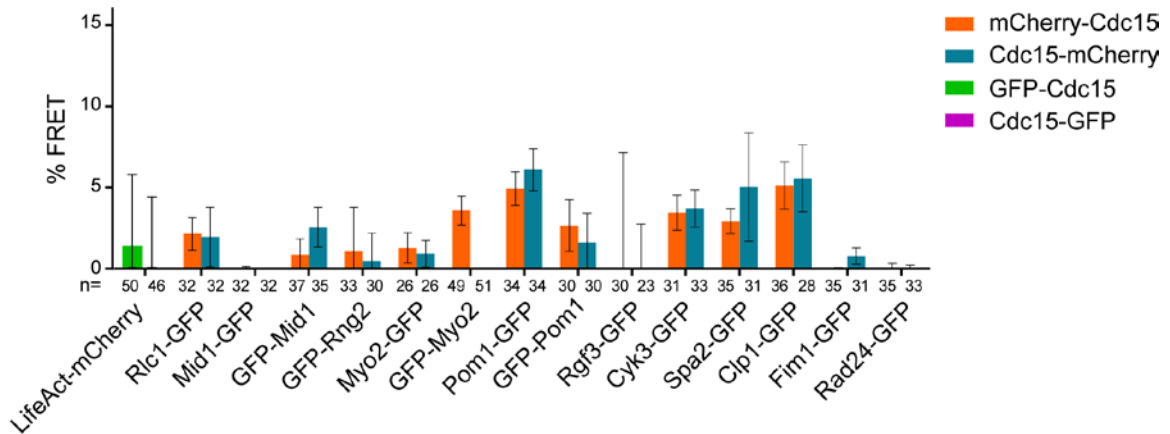


**Figure 4-10. Intermolecular FRET experiments.** A) Statistics for data in Figure 4A-B. A one way ANOVA test was performed between each GFP strain and an Rlc1-GFP negative control and uncorrected p values are reported. B) Comparison of FRET between mCherry-Cdc15 and Cdc15-mCherry combinations. The reported p values are from Fisher's exact tests performed between mCherry-Cdc15 and Cdc15-mCherry conditions. C) mCherry-Cdc15 and Cdc15-mCherry FRET combinations tested without significant FRET signals (ANOVA versus the Rlc1-GFP negative control; all p's >> 0.05).

GFP, GFP-Spa2, GFP-Rgf3, and GFP-Cyk3 (Figure 4-9B) (Roberts-Galbraith *et al.*, 2009, 2010; Ren *et al.*, 2015). The detection of FRET between Cdc15-mCherry and the C-terminal domains of Imp2 and Rga7 supports the spatial distribution of these molecules proposed from our fPALM analysis and indicates these domains, like their F-BAR domains, are positioned close enough together to support FRET. The detection of FRET signals between known Cdc15 SH3-domain binding partners and Cdc15-mCherry was expected; moreover, the specificity of the signal for Cdc15-mCherry over mCherry-Cdc15 (Figure 4-10B) supports the extended orientation of Cdc15 proposed from our fPALM analysis. We detected no significant FRET signal between mCherry labeled Cdc15 and multiple additional contractile ring proteins (Figure 4-10C), again consistent with the CR being composed of distinct strata.

#### *Lateral clustering capability of contractile ring scaffolds*

Our fPALM analysis of the molecular architecture of the contractile ring described above utilized a “side-view”, designed to easily measure distances from the membrane. With this view, information about how protein components organize along the circumferential axis of the ring is missing. Therefore, we performed additional fPALM imaging at the top plane of cells (Figure 4-11A) to capture a lateral view of the contractile ring and assess the organization of a subset of contractile ring components. To quantify the level of clustering, we calculated the Inverse Difference Moment (IDM) of fPALM images along the ring circumferential axis (Haralick *et al.*, 1973). IDM is a measure of local homogeneity; values close to 1 have homogenous local intensities (uniform) and those further from 1 have heterogeneous local intensities (clustered). We



simulated a completely uniform and a clustered distribution for comparison (top, Figure 4-11B).

Surprisingly, we detected multiple distinct patterns of lateral spatial distribution among the subset of contractile ring proteins examined. Some appeared uniform in distribution while others adopted variable clustered organizations; even different domains within a single molecule were distributed differently (Figure 4-11B-D). F-actin, detected by LifeAct-mMaple3, was distributed uniformly along the ring circumference, consistent with electron micrographs of the ring (Kamasaki *et al.*, 2007). The C-terminus of Cdc15 and N-terminus of Myo2 also were uniformly distributed. In contrast, the domains of Cdc15 and Myo2 close to the membrane appeared to form clusters spaced at regular intervals along the circumferential axis with diameters of  $71\pm 17$  and  $104\pm 26$  nm, respectively. Rng2 and Mid1, on the other hand, were present in larger, unevenly spaced clusters  $201\pm 49$  and  $200\pm 44$  nm in diameter, respectively. Cdc15's N-terminal F-BAR forms linear oligomers (McDonald *et al.*, 2015); to test if oligomerization was also responsible for organization of the observed larger scale clusters, we imaged a mMaple3-Cdc15(E30K E152K) oligomerization mutant. Indeed the oligomerization mutant prevented cluster formation. Interestingly, the oligomerization mutation also resulted in a widened mMaple3-Cdc15 ring thickness, suggesting oligomerization also helps concentrate Cdc15 in the ring.

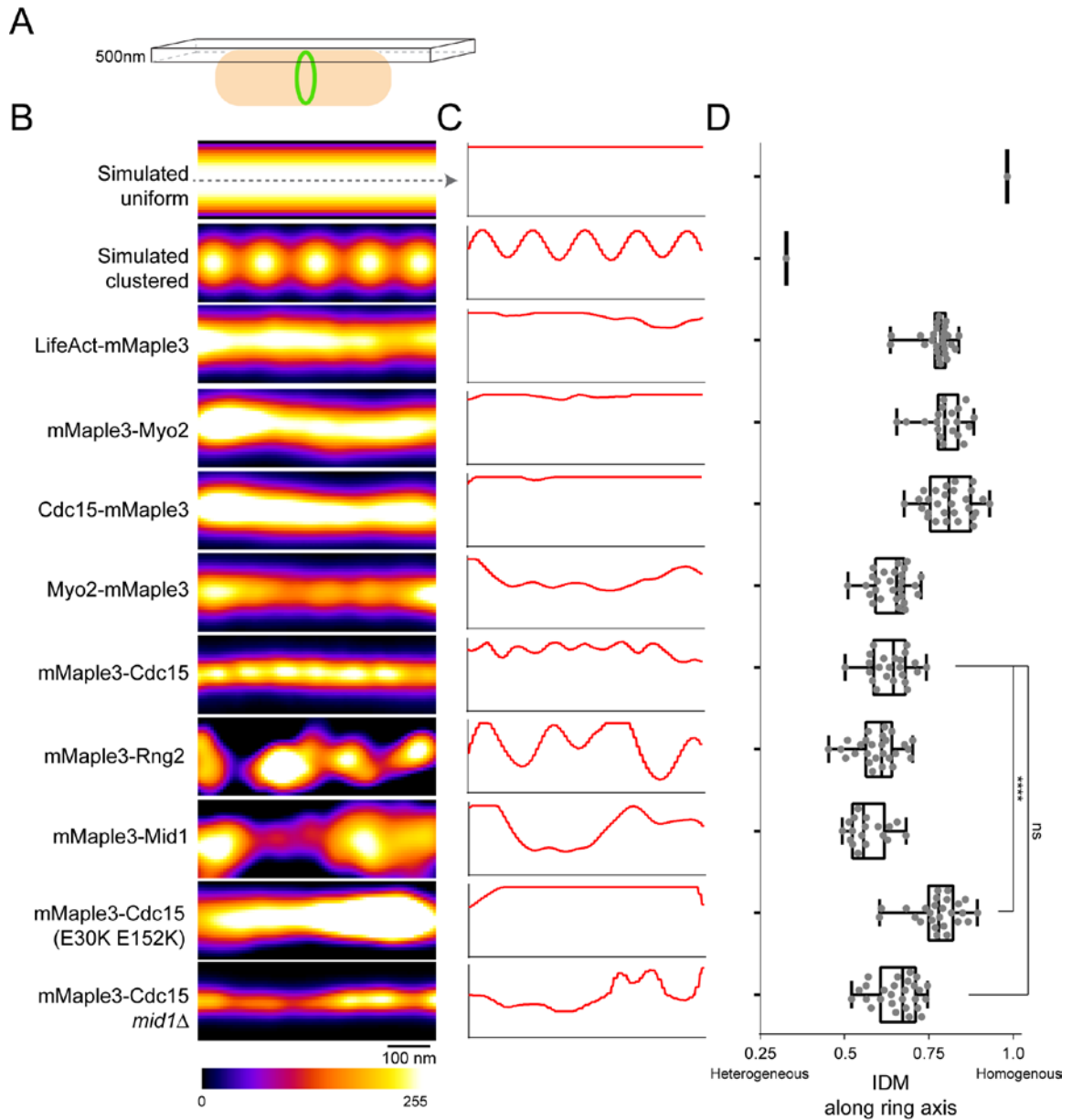


**Figure 4-11. Lateral organization of components in the contractile ring.** A) Schematic of fPALM setup with Z focus at the top of cells. B) Representative fPALM image of the top of contractile rings with the indicated components labeled. Simulated clustered or smooth ring examples are included for comparison. C) Linescans through the center of images in (A). C) Quantification of the Inverse Difference Moment (IDM) of a grey level co-occurrence matrix along the contractile ring's circumferential axis. IDM is a measure of local homogeneity, see Materials and Methods. Lines indicate a one way ANOVA performed against mMaple3-Cdc15; \*\*\*\*,  $p < 0.0001$ .

## Discussion

Using fPALM super-resolution imaging, we have determined the spatial organization of 29 central components of the contractile ring relative to the membrane. We found that these components organize into distinct connected layers rising from the plasma membrane and extending up to 400 nm towards the interior of the cell (Figure 4-12). We also discovered that certain components adopt distinct spatial distributions along the circumference of the contractile ring ranging from uniform to large, irregularly sized and spaced clusters. Our measurements establish a strong foundation for a comprehensive understanding of the molecular architecture and function of a eukaryotic contractile ring.

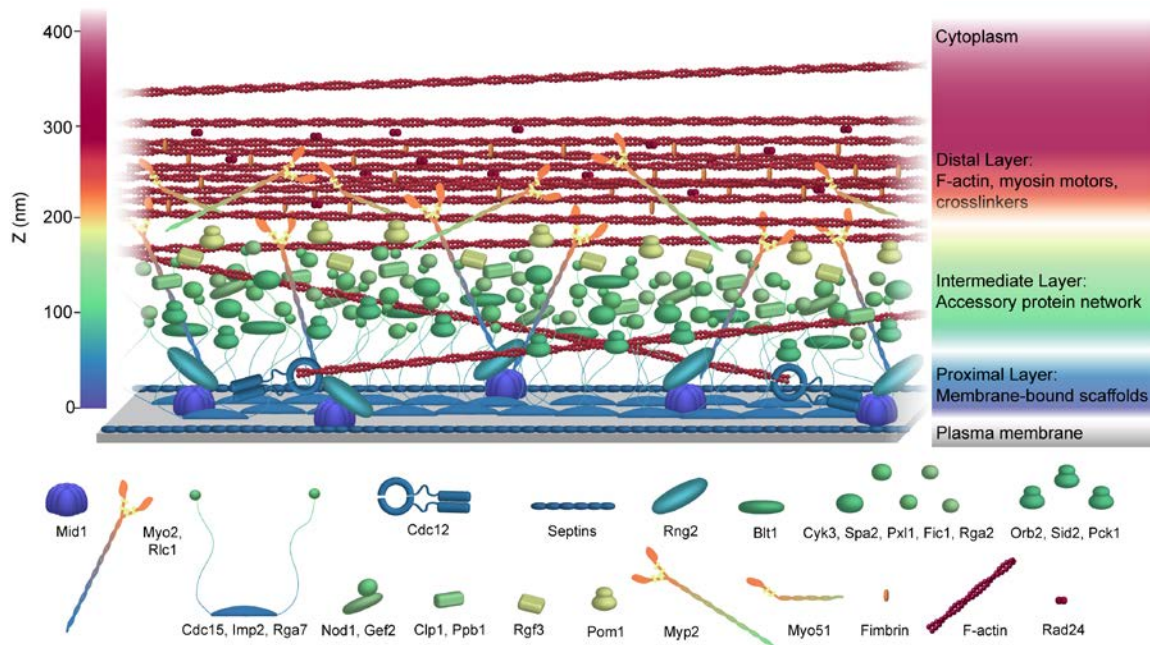


**Figure 4-12. Schematic model of the *S. pombe* contractile ring molecular architecture.** Depicted protein positions were calculated experimentally and are color-coded in the Z dimension. Note that this model does not incorporate stoichiometry.

### *Structural layers within the contractile ring*

Our analysis of 29 components of the contractile ring by fPALM indicates the existence of distinct layers tethering F-actin to the plasma membrane, similar to two previously investigated membrane-tethered F-actin structures, focal adhesions (Kanchanawong *et al.*, 2010) and cadherin junctions (Bertocchi *et al.*, 2017).

Nearest to the membrane (0-80 nm), proteins with membrane binding domains scaffold additional components through a network of protein-protein interactions. The anillin Mid1, tethered to the membrane via its C2 domain, binds the tail of the essential type II myosin, Myo2 (Motegi *et al.*, 2004), as well as extending to bind IQGAP Rng2 (Padmanabhan *et al.*, 2011), which in turn stabilizes the Myo2-Mid1 interaction (Laporte *et al.*, 2011). The F-BAR domain of Cdc15, also bound directly to the membrane, scaffolds the formin Cdc12 (Carnahan and Gould, 2003; Willet, McDonald, Bohnert, *et al.*, 2015). The membrane-binding F-BAR domain of Rga7 may also have a ring binding partner, Rng10 (Liu *et al.*, 2016), suggesting that F-BAR domains may scaffold additional ring components, linking their partners indirectly but closely to the membrane. It is not surprising that the integrity of this proximal layer of the contractile ring is critical for strong attachment to the plasma membrane. In fact, additional time is required to assemble the ring when Mid1 is missing (Wu *et al.*, 2003; Hachet and Simanis, 2008; Y. Huang *et al.*, 2008), while rings can slide and disassemble when Cdc15 abundance is reduced (Arasada and Pollard, 2014; McDonald *et al.*, 2015). It is surprising that the ring remains associated with the plasma membrane in the majority of cells lacking Mid1 or fully functional Cdc15 or both (McDonald *et al.*, 2015), indicating that other ring components important for establishing this tight plasma membrane-contractile ring

linkage must exist, especially during constriction when Mid1 leaves the ring (Wu *et al.*, 2003).

Extending away from the membrane-bound layer (80-160 nm), we find the C-termini of Cdc15 and Imp2 which contain their SH3 domains. These domains are functionally redundant (Ren *et al.*, 2015), but having one or the other is essential for cytokinesis and cell viability (Roberts-Galbraith *et al.*, 2009), demonstrating the importance of an SH3-scaffolded network within the contractile ring. Multiple binding partners of Cdc15 and Imp2's SH3 domains including Pxl1, Fic1, Spa2, Rgf3, and Cyk3 (Roberts-Galbraith *et al.*, 2009, 2010; Ren *et al.*, 2015) concentrate in this intermediate zone. Cyk3 itself contains an SH3 domain, likely further strengthening this interaction network. Cdc15 and Imp2 SH3 domains bind a K/RxLPxΦP motif that is found in a number of additional contractile ring proteins (Ren *et al.*, 2015) that may also be present in this zone. It is interesting to note that the functions of the majority of these proteins remains unclear, and that their functions are not strictly essential. However, given the multiple protein interaction domains present in these components and their spatial organization, we speculate that eliminating pairs or subsets of these elements would undermine the networking of this zone. This may result in weakening the linkage between the strata of the contractile ring ultimately leading to loss of ring integrity and cell viability, irrespective of any mechanistic contribution of these components to ring function. In support of this hypothesis, synthetic lethality has been observed in several cases when null alleles of these genes were combined (Pinar *et al.*, 2008; Roberts-Galbraith *et al.*, 2009; Ren *et al.*, 2015; Chen *et al.*, 2016; Liu *et al.*, 2016). Indeed in the complete absence of Cdc15 and its SH3 interaction network, F-actin rings can still form

but quickly disintegrate (Laporte *et al.*, 2011), underscoring the stabilizing function of the intermediate zone.

Farthest from the membrane (160-400 nm), we find the center of F-actin localization. The elevated localization and ~250 nm thickness of F-actin matches with the limited electron micrographs of *S. pombe* rings that are available (Kamasaki *et al.*, 2007). It is notable that classical electron microscopy studies of animal cells have also measured the contractile ring as 250-500 nm thick vertically from the membrane (Schroeder, 1973). Interestingly, both termini of the formin Cdc12, which nucleates and elongates F-actin in the ring *de novo*, are significantly closer to the membrane. Cdc12 is a 207 kDa protein and its catalytic FH1-FH2 domains may extend a significant distance into the interior of the ring. It is also possible that F-actin is polymerized by Cdc12 close to the membrane, but filaments are pulled upward and incorporated into the main F-actin density by tension from myosin motors and actin crosslinkers. Indeed we found the head domain of Myo2 and the actin crosslinker Fim1 at a high elevation apposed to F-actin. Unlike Myo2, we find the tails of Myp2 and Myo51 at an intermediate layer, but predict their motor domains are also embedded in the higher elevation F-actin. It is likely that other components such as  $\alpha$ -actinin and tropomyosin that depend on F-actin for ring localization will also be present in this most interior layer.

### *Signaling within the contractile ring*

The nanoscale spatial organization of signaling components of the contractile ring has not been studied previously, though we estimate that there are ~10 protein kinases, ~3 phosphatases, and >20 GTPases and associated GAPs and GEFs in the contractile ring.

Though some of these modulators have known binding partners that may help recruit them to the appropriate layer (e.g. the protein kinase Sid2 by Blt1 (Goss *et al.*, 2014), the GTPase exchange factor Gef2 by Nod1 (Zhu *et al.*, 2013), and the Rho1-exchange factor Rgf3 by Cdc15 and Imp2 (Ren *et al.*, 2015)), it is also possible that these enzymes accumulate in distinct zones due to more transient interactions with their substrates. We did find that most localized in the correct areas for modification of their reported substrates. Sid2 is localized at a low elevation (88 nm), properly placed to access its substrates Cdc12 (Bohnert *et al.*, 2013), Spa2 (Gupta *et al.*, 2013), and Clp1 (Chen *et al.*, 2008). The protein kinase Pom1 is in the intermediate layer (175 nm), overlapping with the localization of 3 known substrates: Imp2, Cdc15, and Rga7 (Kettenbach *et al.*, 2015). Furthermore, the Clp1 phosphatase is present at a low-to-intermediate level (136 nm), near its scaffold Mid1 (Clifford *et al.*, 2008) and known and predicted ring substrates Cdc15, Blt1, Rng2, Cyk3, Myp2, and Orb2 (Clifford *et al.*, 2008; Chen *et al.*, 2013).

### *Protein clusters in the contractile ring*

When we examined a lateral view of the ring, we found that components adopted a range of spatial organizations along the circumference. Mid1 and Rng2 form irregularly spaced 200 nm clusters, which resemble the size and shape of cytokinesis precursor nodes (Wu *et al.*, 2006; Laporte *et al.*, 2011). The membrane-proximal termini of Myo2 and Cdc15 form smaller 70-100 nm diameter regularly-spaced clusters along the circumference of the ring. All four of these proteins are present in precursor nodes (Wu *et al.*, 2006), which have recently been suggested to be maintained in the fully developed contractile ring (Laplante *et al.*, 2016). However, the very different diameter and

regularity of Cdc15 and Myo2 clusters from those of Mid1 and Rng2 argues that at the least, node structures change as the ring develops. This is perhaps to be expected since Mid1, responsible for setting up precursor nodes, dissociates from the ring as it constricts (Wu and Pollard, 2005). Additionally, the relative stoichiometry of certain components in the ring change during constriction: Myo2 is concentrated during constriction while Cdc15, Rng2, and Cdc12 remain at a constant concentration (Wu *et al.*, 2003; Wu and Pollard, 2005). Therefore, reorganization of the membrane-proximal level within the ring must occur. Future two-color super-resolution imaging could determine if large clusters contain combinations of components that persist from precursor nodes as well as any additional novel clustering behavior in the fully formed ring.

Interestingly, we found components that are further away from the membrane are uniform in their distribution, even compared to their opposite termini. In particular, the F-actin signal from LifeAct-mMaple3 is uniform, in accord with electron microscopy studies of contractile ring F-actin which show a relatively even distribution in both *S. pombe* and animal cells (Kamasaki *et al.*, 2007; Henson *et al.*, 2017). In contrast to their low elevation termini, the opposite termini of Myo2 and Cdc15 appear quite uniform. A long flexible region between Cdc15's F-BAR and SH3 domains likely acts to eliminate any F-BAR-oligomerization-mediated clustering once the SH3 domain is reached. The even distribution of Myo2's head domain suggests a generally even binding of actin throughout the ring. This distribution is in contrast to myosin-II "stacks" formed in animal cells, where antiparallel myosin units are assembled into large-scale clusters parallel to F-actin filaments (Fenix *et al.*, 2016; Henson *et al.*, 2017).



### *Building the ring bottom up*

Together with prior knowledge of when proteins are recruited to the ring, the spatial architecture of the contractile ring determined here suggests possible mechanics of ring formation. In fact, the different layers seen in our analysis generally correlate with the order of assembly of their components. Of the earliest ring components which are recruited to precursor nodes (Mid1, Rng2, Myo2, Cdc15, and Cdc12) (Wu *et al.*, 2006; Laporte *et al.*, 2011), 4/5 contain termini present within the proximal membrane layer (0-80 nm), and 2/5 contain direct membrane binding domains. The precise order of assembly of Rng2, Myo2, and Cdc12 does not appear to matter for ring formation (Tao *et al.*, 2014), but it seems likely that the initial setup of the ring involves the construction of a membrane anchored scaffold. F-actin is formed *de novo* at nodes and the ring by Cdc12 (Pelham and Chang, 2002) as well as incorporated from longitudinal actin cables (Huang *et al.*, 2012). F-actin, though turning over quickly in the ring (80), may be principally held in its elevated location by the tension from the motor activity of myosins. Circumferential tension due to myosin may produce force on F-actin and other components toward the center of the cell, as in “purse-string” models of ring function (Henson *et al.*, 2017). Once a contiguous ring is formed, many additional components are recruited. Components that join the ring later are generally present within the intermediate layer. Many of these components, therefore, may “fill in” between the membrane-bound proximal layer and F-actin to form a robust structure that withstands the forces of constriction, couples ring constriction with other events of mitosis, and connects the ring to cell wall formation that occurs coincidentally.

## CHAPTER V

### CONCLUSIONS AND FUTURE DIRECTIONS

#### **Chapter summaries**

The protein components and kinetics of cytokinesis in *S. pombe* are well understood, yet how 50+ proteins organize into a functional division apparatus is only beginning to become clear. Here, I presented investigations into the oligomer structures of F-BAR proteins within the contractile ring, as well the spatial organization of 29 ring components relative to the underlying membrane.

In Chapter II, I explored how Cdc15's F-BAR domain oligomerizes. I presented evidence that this F-BAR domain organizes in a tip-to-tip manner to form long filamentous oligomers upon membranes. In the contractile ring, these oligomers were critical for ring stability as well as ring anchoring in the cell middle. This is a novel mechanism of oligomerization by an F-BAR domain and demonstrates that not all F-BAR domains bend membranes when oligomerized. Accordingly, 6 F-BAR domains from human cells also did not bend membranes when oligomerized, though oligomerization was critical for each F-BAR's function when tested. These data suggest our initial understanding that F-BAR domain oligomerization leads only to membrane bending is incomplete. Multiple structural mechanisms of linking together oligomers exist, not all of which lead to membrane bending. Oligomerization appears to instead be a shared feature of all F-BAR domains, and is critical in a variety of cellular contexts.

In Chapter III, I showed that the Imp2 F-BAR domain oligomerizes in a helical manner to result in membrane bending in vitro. Despite bending membranes in vitro,

when Imp2 oligomerization and bending ability was blocked *in vivo*, its function was not compromised. Indeed replacing the Imp2 F-BAR domain with related F-BAR domains that cannot bend membranes completely rescued function. These data suggest that membrane bending by F-BAR domains is not necessarily a critical physiological function. In fact, membrane bending by F-BAR domains may only occur in situations where the domains are present at very high concentrations, such as *in vitro* upon liposomes.

In Chapter IV, I used super-resolution microscopy to map the nanoscale architecture of 29 contractile ring components. These components organized roughly into three layers in relation to the underlying plasma membrane. Proximal to the membrane, membrane binding domains of Cdc15, Imp2, and Mid1 were present along with the formin Cdc12 and the tail of Myo2. At an intermediate distance from the membrane, multiple accessory proteins were present that stabilize and reinforce the structure of the ring, as well as multiple signaling components. Distant from the membrane, I found F-actin, actin crosslinkers, and the motor domains of myosin motors. Different components organized circumferentially within the ring either uniformly or in clusters, though the function of these clusters is not yet clear.

Collectively this work has defined two novel mechanisms for F-BAR organization and function in cytokinesis, as well as the first detailed nanoscale model of a eukaryotic contractile ring. Looking forward, it will be critical to investigate how additional F-BAR domains that do not bend membranes link together and function. Furthermore, though F-BAR proteins have multiple biochemical activities, these activities are transient and often auto-inhibited; future investigation into the regulation of F-BAR activity will deepen our

understanding of F-BAR protein function. In addition, further refining of the contractile ring model presented here will be necessary. An additional 10-15 proteins are known to localize to the ring and can be mapped in the same manner as above. Investigation into later stages of cytokinesis when the ring constricts may also prove fruitful. Moreover, super-resolution microscopy can now be added to the experimental toolkit available for investigating the function of cytokinesis proteins after perturbing their function.

### **F-BAR domain membrane binding and bending**

I have shown here that multiple F-BAR domains are able to bind membranes and oligomerize without bending, in contrast to prevailing models based on *in vitro* studies. These conclusions came out of assays comprehensively measuring F-BAR membrane tubulation *in vitro* upon liposomes or *in vivo* in cultured cells. It could be argued that the perfect condition (such as a specific lipid composition) has not been discovered to support tubulation of these F-BARs. However, cultured cells contain a variety of membranes with different compositions that overexpressed F-BAR domains can access (van Meer *et al.*, 2008), so this seems an unlikely possibility. Also, multiple compositions mimicking physiological membranes have been tested *in vitro*, as well as lipid extracts from tissue. Synthetic membrane conditions with higher concentrations of PIPs or other lipids depart from a realistic cell-like environment. Perhaps most importantly, sufficiently concentrating any protein upon a membrane by adding more binding sites (such as PIPs) is sufficient to induce tubulation through molecular crowding effects (Stachowiak *et al.*, 2012). The simple explanation from the observed lack of tubulation is certain F-BAR domains do not oligomerize in a manner that confers tubulation activity. And indeed, despite not all tubulating membranes, all F-BAR

domains do oligomerize (Cheng *et al.*, 1999; Craig *et al.*, 1999; Roberts-Galbraith *et al.*, 2010; Becalska *et al.*, 2013; McDonald *et al.*, 2015). Membrane tubulation by F-BAR domains, therefore, appears to be one specific consequence of a generally shared ability to oligomerize and simultaneously bind membranes.

Each case of F-BAR oligomerization studied so far has defined a distinct mechanism of dimer-dimer interaction; F-BAR domains therefore have evolved multiple ways to link together. Further investigation will be necessary to determine the full complement of oligomerization mechanisms used by this protein domain. Targeted mutagenesis of prominent charged surface patches on the tips and sides of F-BAR domains (which could mediate dimer-dimer interactions), and subsequent screening for loss of oligomerization is one method to identify new mechanisms.

Oligomerization that does not lead to tubulation nevertheless appears central to F-BAR protein function. Cdc15's linear oligomerization supports a robust avidity (as each repeating F-BAR unit has membrane binding contacts) toward a flat membrane surface. This high avidity membrane binding is critical to accumulate and stabilize Cdc15 at the cell division site (McDonald *et al.*, 2015) where it recruits and scaffolds multiple cytokinesis proteins (Roberts-Galbraith *et al.*, 2009; Ren *et al.*, 2015). Mutations that disrupt F-BAR oligomerization sharply decrease the abundance and increase the turnover of Cdc15 at the division site, which consequently leads to cytokinetic failures (McDonald *et al.*, 2015). Mutations in Fer that block oligomerization compromised its ability to induce lamellipodia formation and enhance cell migration, possibly due to a loss of strong localization to the leading edge membrane (McDonald *et al.*, 2015). Additionally, mutations in the RhoGAP4 F-BAR that disrupt oligomerization compromised

RhoGAP4's ability to inhibit cell migration (McDonald *et al.*, 2015). These examples highlight what may be a generally important characteristic of F-BAR domains - their ability to form oligomers on membrane surfaces for the purpose of scaffolding additional protein elements or forming signaling centers.

Considering the diversity of oligomerization modes and their functional importance, we propose F-BAR domains in general act as membrane binding, oligomerizing modules that serve to concentrate and stabilize F-BAR proteins at sites of action (Figure 5-1). Beyond this generalization, it is likely that different F-BAR domains possess oligomerization interactions that are tailored for distinct functional contexts. When F-BARs are organized by cellular functions, some trends emerge: many endocytic F-BAR domains possess oligomerization interactions that confer binding to or may induce curved membranes (such as FBP17, CIP4, and PACSINs), while F-BARs involved in cytokinesis or cell migration are tuned to bind a relatively "flat" plasma membrane (including Fer, Fes, RhoGAP4, and *S. pombe* Cdc15) (Figure 5-1). It will be critical to test these hypotheses by specifically compromising oligomerization of F-BARs in different contexts.

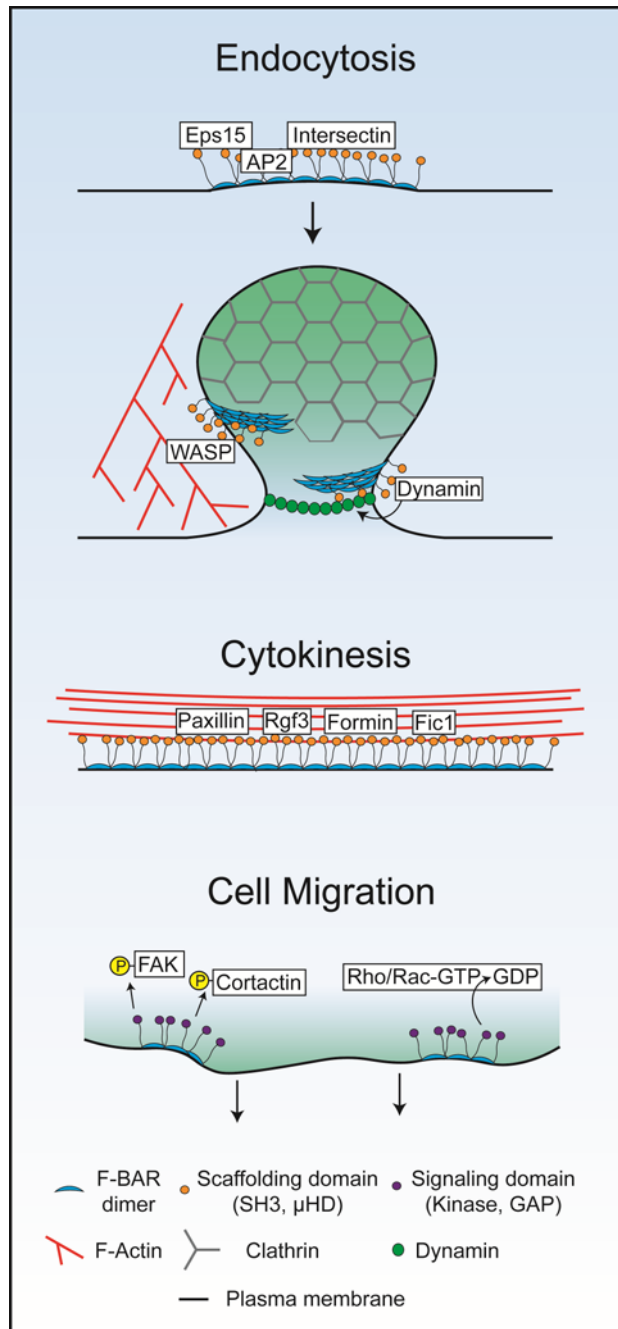


**Figure 5-1. Diverse modes of F-BAR oligomerization in endocytosis, cytokinesis, and cell migration.** Schematics of possible modes of F-BAR protein oligomerization, protein recruitment, and signaling in endocytosis, cytokinesis, and cell migration.

## Regulation of F-BAR protein function

The various activities of F-BAR domains (membrane binding, oligomerization, partner binding, signaling) are not constitutive in cells, but instead are dynamically regulated. In fact, the membrane and partner binding capacity of many F-BAR domain proteins are auto-inhibited and specific activation is required to allow these proteins to carry out their functions (reviewed in (Roberts-Galbraith and Gould, 2010)).

Phosphoregulation is one mechanism that allows for dynamic regulation in line with the short time windows of F-BAR protein activity in dynamic processes. Analyses of phosphoregulation have been carried out for only a few F-BAR proteins such as *S. pombe* Cdc15 (Roberts-Galbraith and Gould, 2010) and *S. cerevisiae* Hof1 (Meitinger *et al.*, 2011, 2013), and thus there is the opportunity to learn more about how F-BAR protein function is integrated in signaling networks, particularly in human cells. In other cases, it is argued that a binding partner pries apart an intramolecular interaction to release the F-BAR domain for membrane binding (Rao *et al.*, 2010; Kelley, Messelaar, *et al.*, 2015). Further investigation is necessary to identify the molecular mechanisms of human F-BAR protein spatial and temporal activation. For Cdc15, preliminary evidence suggests regulation through mechanism involving a phosphorylation-dependent conformational change.

### *Phosphorylation of Cdc15 controls a conformational change*

Previously, Cdc15 has been shown to be phosphorylated in its middle region between F-BAR and SH3 domains (Fankhauser *et al.*, 1995; Roberts-Galbraith *et al.*, 2010). This phosphorylation controls its ability to bind membranes, oligomerize, and bind partners. One possible mechanism of this phosphoregulation suggested from



electron microscopy studies is a conformational change between hyper- and hypo-phosphorylated forms of Cdc15. To directly test if Cdc15 undergoes a change in conformation in vivo, we designed an intramolecular FRET approach. We placed a mCherry fluorophore at Cdc15's N-terminus and a GFP fluorophore at its C-terminus (Figure 5-2A). A FRET signal was measured between these two fluorophores in the cytoplasm; however, at the contractile ring the signal abruptly dropped (Figure 5-2B). The cytoplasmic FRET signal implies the close proximity of Cdc15's N and C termini. The loss of this signal at the contractile ring confirms a conformational change occurs between cytoplasmic and ring localized Cdc15. Using an acceptor photobleaching FRET method, we quantified the level of FRET in the cytoplasm and ring and found a significant decrease in signal at the ring (Figure 5-2C).

Cdc15's conformational change at the contractile ring in cytokinesis correlates with the timing of Cdc15 dephosphorylation (Fankhauser *et al.*, 1995; Roberts-Galbraith *et al.*, 2010). To determine if phosphostatus controls Cdc15's conformation, we performed FRET analysis on a Cdc15(27A) mutation lacking 27 phosphorylation sites previously identified in vivo (Figure 5-3A) (Roberts-Galbraith *et al.*, 2010). Indeed, this phosphomutant had a drastically reduced FRET signal that was unchanged between cytoplasmic and ring localized Cdc15 (Figure 5-3B-C). Therefore, Cdc15 undergoes a conformational change between the cytoplasm and contractile ring that is controlled by phosphorylation.

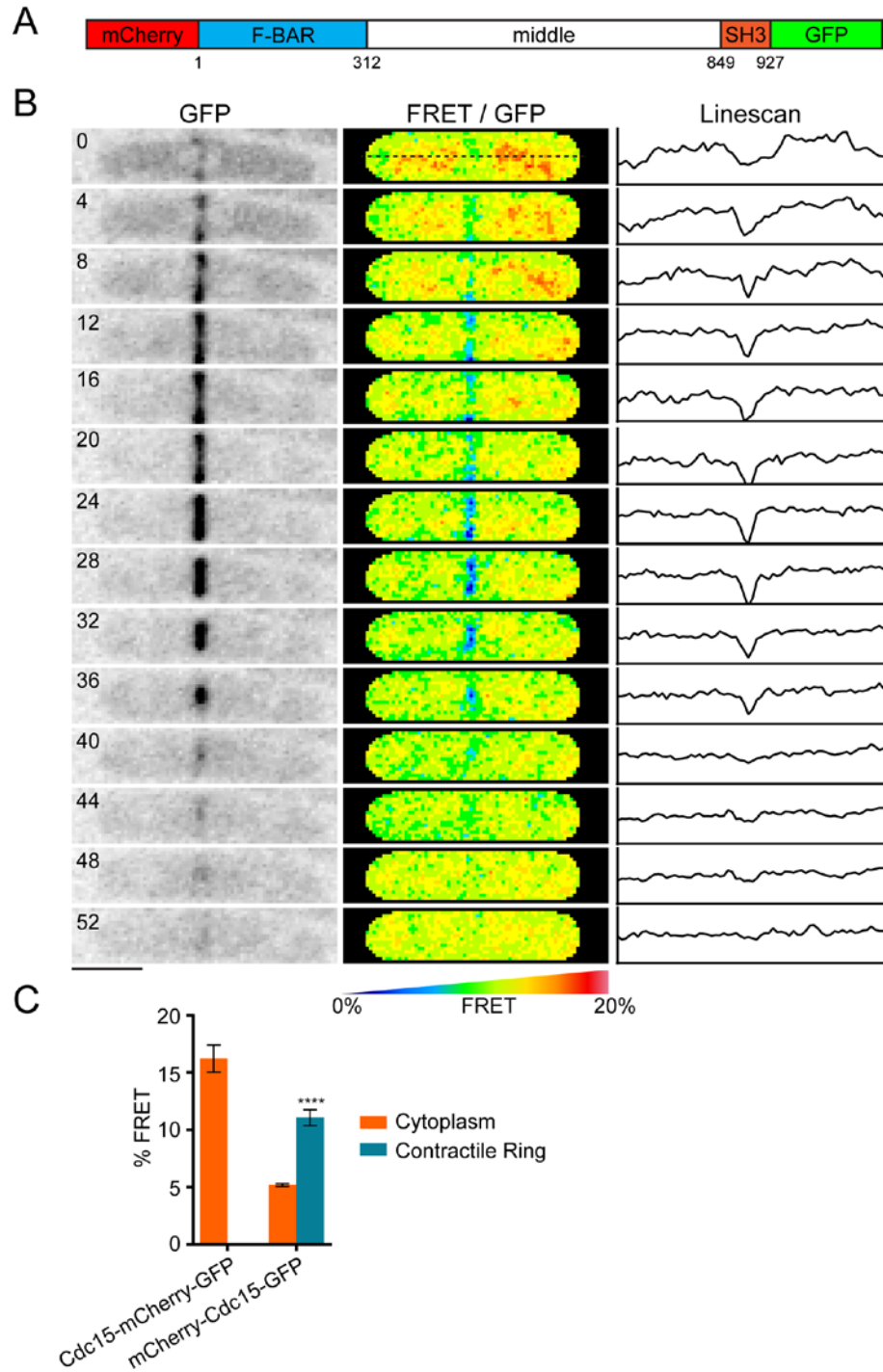


**Figure 5-2. Cdc15 undergoes a spatially and temporally regulated conformational change in cytokinesis.** A) Schematic of the Cdc15 intramolecular FRET construct with fluorophores at opposite termini. B) Live-cell FRET of mCherry-Cdc15-GFP during cytokinesis. C) Acceptor photobleaching quantitative FRET values for cytoplasmic and contractile ring localized Cdc15.

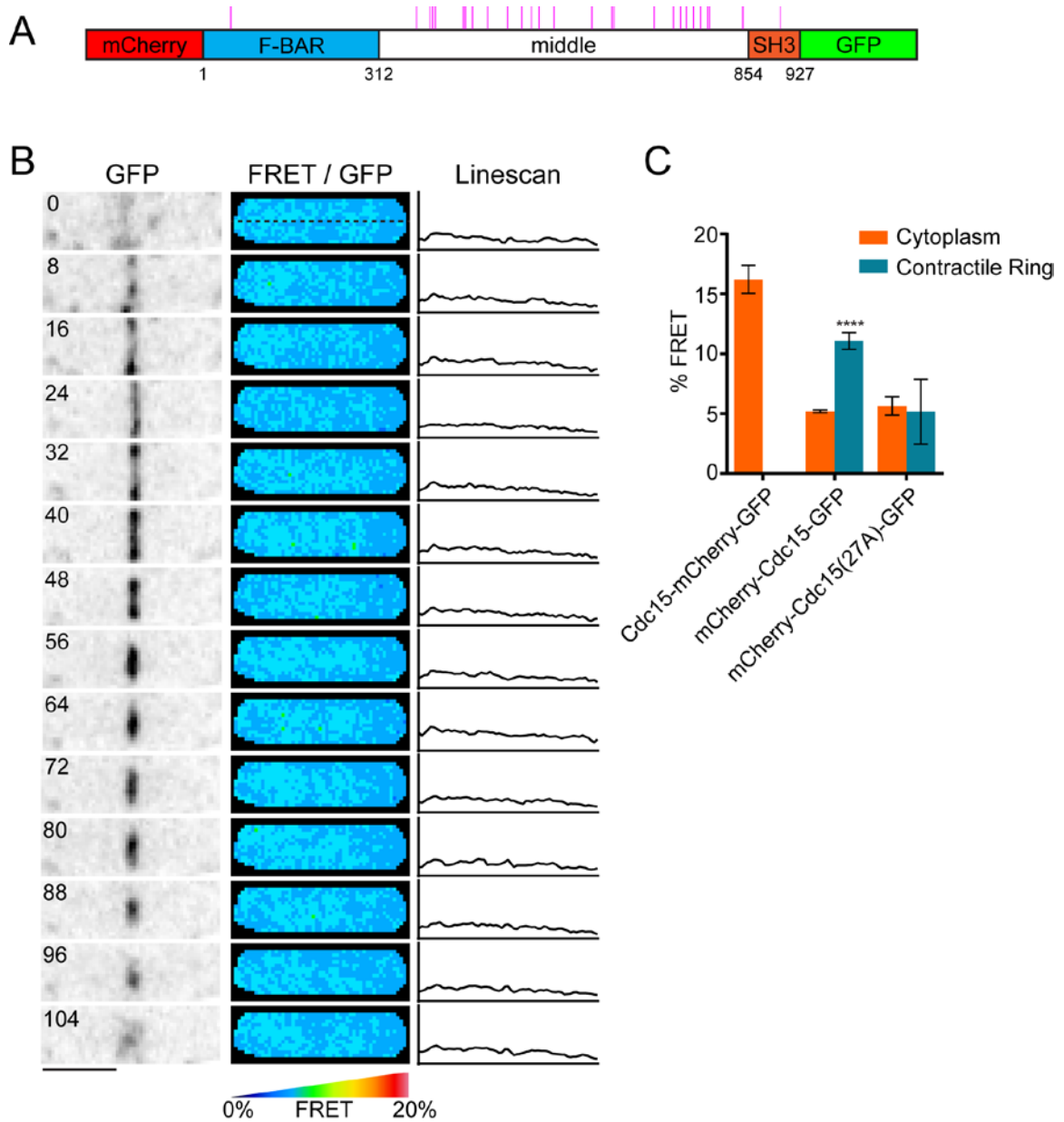


**Figure 5-3. Cdc15's conformational change is regulated by phosphorylation.**  
 A) Schematic of Cdc15 intramolecular FRET construct with phosphosites mutated to alanine in Cdc15(27A) indicated in magenta. B) Live-cell FRET of mCherry-Cdc15(27A)-GFP during cytokinesis. C) Acceptor photobleaching quantitative FRET values for cytoplasmic and contractile ring localized Cdc15.

In the future it will be important to determine mechanistically how this conformational change controls the activity of Cdc15. One possibility is the phosphorylated middle region wraps around the F-BAR and SH3 domains to physically inhibit their activities. Electrostatically, a highly anionic phosphorylated middle region may be an advantageous binding substrate for the positively charged membrane binding face of the F-BAR domain. This mechanism of intramolecular inhibitory interactions would explain how the middle domain exerts influence over the F-BAR and SH3 domains, and how a conformational change is apparent between inhibited (phosphorylated) and active (dephosphorylated) states.

### **Refining the structure of the contractile ring**

The model constructed in Chapter IV is the most comprehensive and highest resolution picture of the contractile ring in *S. pombe* to date, however it remains incomplete. I was able to map the architecture of 29 ring components, but 10-15 remain. Many of these will remain technically challenging to interrogate, as fluorescent tags on their N- or C-terminal sequences compromise protein function (including tropomyosin Cdc8, Cdc4, and small GTPases Rho1/2). Strategies to integrate functional fluorophores within proteins may prove fruitful for the more intractable components.

In addition, the model constructed here is of a pre-constriction contractile ring. As the main function of the ring is to constrict and divide the cell, it will be critical to investigate the architecture of constricting rings as well. Indeed the composition of the ring changes as it constricts, with the additional of more components and loss of others. In the future, these analyses will provide a structural framework for understanding the mechanics of constriction as well as formation of the contractile ring. As additional

biochemical activities and binding interactions of the complete set of contractile ring proteins are revealed, the sum of this information together with the structural template proposed here can be used to develop physical models of the ring to understand its mechanism at a deep level.

### **Conclusions**

In this work I have shown how two F-BAR proteins oligomerize and function in the contractile ring, with broad implications on F-BAR protein function in a variety of cellular processes. I have determined the spatial architecture of the majority of protein components in the contractile ring and proposed a detailed nanoscale model of the ring. I am confident that future investigation along the lines of this work, into the architecture of the contractile ring and biochemical mechanisms of ring components, will achieve a molecular and mechanistic understanding of the contractile ring and cytokinesis.

## APPENDIX A

### MATERIALS AND METHODS

#### Yeast methods

*S. pombe* strains were grown in yeast extract (YE) media with appropriate amino acid supplements, or Edinburgh minimal medium (EMM) lacking thiamine in the case of *nmt* promoter-induced expression (Basi *et al.*, 1993). *S. pombe* transformations were performed with a lithium acetate method (Keeney and Boeke, 1994). Endogenous replacements of essential genes were performed with one of two methods: 1) *cdc15* mutants were constructed by rescuing *cdc15<sup>+</sup>/cdc15::ura4<sup>+</sup>* diploids with pIRT2-*cdc15* constructs containing 5' and 3' flanks. Haploid integrants resistant to 5-fluorouracil (5-FOA) were isolated and verified by PCR. 2) Wildtype cells were transformed with a construct containing a 5' flank, the coding sequence, a KanR cassette, and a 3' flank. G418 resistant transformants were confirmed by PCR. Replacement of nonessential genes was performed by transforming constructs containing a 5' flank, coding sequence, and 3' flank into *ura4<sup>+</sup>* knockout strains of the gene of interest. Integrants resistant to 5-FOA were isolated and verified by PCR. C-terminal epitope tags were created by transforming a pFA6a integration cassette amplified with gene specific primers for insertion at the 3' end of open reading frames (Bähler *et al.*, 1998). Inducible *nmt* promoter constructs were integrated with pJK148 plasmids at the *leu1-32* locus (Keeney and Boeke, 1994).

## Microscopy methods

*S. pombe* cells were imaged live at 25°C or fixed with ice-cold 70% ethanol and stained with Methyl Blue and DAPI before imaging. GUV, *S. pombe*, and COS-7 cell imaging was performed on a Personal DeltaVision microscope system (Applied Precision) that includes an Olympus IX71 microscope, a 60X NA 1.42 planApo objective, and a Photometrics Coolsnap HQ2 camera. Time-lapse imaging was performed on log-phase cells using an ONIX microfluidics perfusion system, flowing YE media at 25°C through the chamber at 5 psi throughout imaging. Image stacks were deconvolved using softWoRx imaging software. COS-7 wound healing images were acquired on an EVOS FL imaging system (ThermoFisher) with a 10X objective. Image projections, intensity measurements, and all other analyses were performed with ImageJ software (<http://imagej.nih.gov/ij/>).

### *Fluorescence resonance energy transfer (FRET)*

Live-cell FRET imaging was performed on a spinning disk system which includes a Zeiss Axiovert200m microscope, Yokogawa CSU-10, 63X NA 1.46 planApochromat objective, Hamamatsu ImageEM-X2 camera, and stringent mCherry FRET emission filters to exclude GFP and laser bleed through. FRET images were calculated with a sensitized emission approach by subtracting GFP and mCh bleed-through and normalizing to total GFP signal.

Quantitative FRET imaging was performed on a Perkin Elmer Ultraview Vox spinning disk system equipped with a Zeiss Axio Observer microscope, 488 and 561 nm solid state lasers with a PhotoKinesis bleaching module, a Yokogawa CSU-X1 spinning

disk, a 63X C-Apochromat objective, and a Hamamatsu ImageEM C9100-13 EMCCD camera. An acceptor photobleaching method was employed for FRET imaging where mCherry-Cdc15 or Cdc15-mCherry was bleached with 100% 561 nm laser power for 20 cycles. 10 frames in the donor GFP channel were acquired pre- and post-bleach. FRET percentages were calculated by first correcting for background and photobleaching over the 10 pre- and post-bleach frames, and subsequently calculating the percentage increase in GFP donor fluorescence at a contractile ring ROI.

#### *Fluorescence recovery after photobleaching (FRAP)*

FRAP experiments were performed on a Zeiss LSM510 META microscope system with a 63X plan-Apochromat objective. COS-7 cell FRAP experiments were performed on a spinning disk system which includes a Zeiss Axiovert200m microscope, Yokogawa CSU-22, 63X NA 1.46 planApochromat objective, Hamamatsu ImageEM-X2 camera, and an Andor Micropoint bleaching system. Bleaching curves were analyzed in ImageJ and Graphpad Prism to determine  $t_{1/2}$  and mobile fraction values.

#### *Fluorescent photoactivation localization microscopy (fPALM)*

fPALM imaging was performed on a Nikon dSTORM 4.0 system which included a Nikon Eclipse Ti microscope, 405, 488, 561, and 647 nm solid state lasers, a Hamamatsu ORCA-Flash4.0 camera, and a 100X CFI HP Apochromat TIRF 1.49NA objective with a 1.5X tubelens (resulting in 110 nm pixels). Imaging was performed at a 0° laser angle (“straight through”). Z drift was minimized using a Nikon Perfect Focus system. The mMaple3 channel was imaged with simultaneous 0.5% 405 nm activation



and 7.5% 561 nm excitation lasers and captured with 30 ms exposures over 10-20k frames. The ATTO647N channel was imaged with simultaneous 0.2% 405 nm activation and 2% 647 nm excitation lasers and captured with 10 ms exposures over 15k frames. The Alexa488 channel for Phalloidin-Alexa488 was imaged with simultaneous 0.2% 405 nm activation and 2% 488 nm excitation lasers and captured with 10 ms exposures over 15k frames. Laser powers and exposure times were optimized for single photoactivated localizations per ring in each frame.

### **Super-resolution analysis**

fPALM images were analyzed using the ImageJ plugin ThunderSTORM (Ovesný *et al.*, 2014). Images were pre-filtered with a wavelet B-spline filter and molecules were approximately localized with the 8-neighborhood local maximum method. Molecules were sub-pixelly localized using the elliptical Gaussian weighted least squares method to identify precise lateral and Z positions. A Z-calibration was performed with 0.1  $\mu\text{m}$  Tetraspek beads (ThermoFisher) for accurate Z positioning. Axial drift, though minimal with this microscope setup, was corrected in post-processing by tracking fiducial gold bead markers as well as cross-correlation analysis. fPALM images are visualized with localizations as normalized Gaussians, where each peak's standard deviation (FWHM) equal to its localization uncertainty (Betzig *et al.*, 2006).

Processed and aligned 2-color images were restricted to a 500 nm plane through the center of the cells. Fully formed, unconstricted rings were identified by a lack of precursor nodes as well as a lack of membrane and septum ingression. The plasma membrane next to each contractile ring was identified as a line in the ATTO647N channel, and the distance of each individual mMaple3 particle in the contractile ring to

this line was calculated. These data were fit with a Gaussian curve and the distance from the membrane ( $d_{\text{center}}$ ) and a vertical width parameter ( $\sigma_{\text{vert}}$  or FWHM) were determined using R, as performed previously in a study of focal adhesion proteins (Kanchanawong *et al.*, 2010).  $d_{\text{center}}$  and  $\sigma_{\text{vert}}$  values from multiple rings were plotted using ggplot2 in R.

Analysis of local homogeneity in Figure 4-11 was performed with 8-bit images using the “Texture Analysis” ImageJ plugin (<https://imagej.nih.gov/ij/plugins/texture.html>). This plugin computes a grey-level co-occurrence matrix for all the pixels in the ROI of a contractile ring  $p(i, j)$ , and calculates multiple of Haralick’s textural features (Haralick *et al.*, 1973) from this matrix. We utilized the Inverse Difference Moment (IDM), a measure of local homogeneity:

$$\sum_{i=1}^{N_g} \sum_{j=1}^{N_g} \frac{1}{1 + (i - j)^2} p(i, j)$$

where  $N_g$  is the maximum grey value and  $p(i, j)$  is the grey level co-occurrence matrix. This analysis was performed specifically in the direction of the ring circumferential axis.

### **Protein purification and crystallization**

Recombinant F-BAR and GFP-F-BAR constructs were produced in *E. coli* Rosetta2 cells (Novagen) grown in TB-broth or T7-crystal express (NEB) in M9-salts supplemented with selenomethionine (SeMet). Protein was purified over His-Bind resin (Novagen), His-select HF resin (Sigma), GST-bind resin (Millipore), or amylose resin (NEB) in the presence of 1% NP-40 and 5 mM BME according to the manufacturer’s protocol. Imp2 F-BAR protein for crystallization was incubated overnight with thrombin to remove the His-tag. Protein was further purified with a cation-exchange chromatography column (GE HiTrap SP) and concentrated with an Amicon Ultra

centrifugal filter (Millipore) to 4-10 mg/mL. Protein crystals were produced by hanging drop vapor diffusion using a Mosquito crystallization robot (TTPLabtech). High quality single crystal grew within 2-3 weeks from a 1:1 mixture of 5.4 mg/mL Imp2:18% PEG 3350, 0.2 M AmFormate.

Native and SeMet-SAD data was collected on the 22-ID beamline of SER-CAT at the Advanced Photon Source at Argonne National Laboratory to 2.35 and 2.7 Å, respectively. Data was processed using HKL2000 (Otwinowski and Minor, 1997). Initial attempts to determine the structure by molecular replacement were not successful. Instead, PHENIX (Adams *et al.*, 2010), employing HYSS (Grosse-Kunstleve and Adams, 2003) and PHASER (McCoy *et al.*, 2007), was used for SeMet SAD phasing. RESOLVE (Terwilliger *et al.*, 2008) was used to extend the resolution to 2.35 Å and generate an initial structural model. The structure was then fully built and refined via iterative model building and refinement using Coot (Emsley *et al.*, 2010) and Refmac5 (Murshudov *et al.*, 1997) or PHENIX (Adams *et al.*, 2010), respectively.

### **Liposome assays**

All lipids were obtained from Avanti Polar Lipids. Liposomes were created from CHCl<sub>3</sub> lipid stocks mixed at the desired ratios and evaporated in a glass tube under N<sub>2</sub> stream, vacuum dried for 1 hour, rehydrated in 20 mM HEPES pH 7.4, 150 mM NaCl buffer before vortexing, 10 cycles of freeze-thawing, and extrusion to various sizes with an Avanti mini-extruder. Liposome co-pelleting assays were performed with 100 uL of 1 mg/mL liposomes mixed with 100 uL of Cdc15 or Imp2 F-BAR for 15 min at room temperature before centrifugation at 150,000 xg in an Optima TL ultracentrifuge for 15 min at 25°C. Supernatant and pellet fractions were separated and run on SDS-PAGE.

Giant Unilamellar Vesicles (GUVs) were formed by drying 10  $\mu$ L of 10 mg/mL  $\text{CHCl}_3$  lipids (69% DOPC, 15% DOPE, 10% DOPS, 5% PI(4)P, 1% Rhodamine-PE) on Indium-Tin-Oxide-coated (ITO) glass coverslips (Sigma-Aldrich) under  $\text{N}_2$  stream followed by vacuum for 1 hour. A 2 mm chamber was assembled between the coverslips and filled with a 20 mM HEPES pH 7.4 and 500 mM sucrose buffer through which a 10 Hz, 2.5 V sinusoidal current was passed for 2 hours. After formation, NaCl was added to 150 mM final concentration. For hypo- and hyper-tonic buffer condition experiments, equal volumes of 20 mM HEPES pH 7.4, 150 mM NaCl or 20 mM HEPES pH 7.4, 150 mM NaCl +100 mM sucrose, respectively, was added to the GUVs before F-BAR addition. Recombinant GFP-F-BAR domain solutions were mixed with GUVs at a final concentration of 10  $\mu$ M (unless otherwise indicated) before imaging in a 0.5 mm chamber.

Cdc15 liposome binding experiments were performed through Bio-Layer Interferometry on an Octet RED96 instrument (ForteBio, Menlo Park, CA) using streptavidin sensor tips (Abdiche *et al.*, 2008). A standard association experiment was performed: streptavidin tips were equilibrated in buffer (20 mM HEPES pH 7.4, 200 mM NaCl) for 120 sec, blocked with 10 mg/mL BSA for 180 sec, 100 nm liposomes (containing 0.1% Biotin-PE and the various compositions indicated in the text) were bound for 300 sec, tips were washed 2x for 180 sec, and 1  $\mu$ M F-BAR association to equilibrium was monitored for 300 sec. Raw data was normalized for unequal liposome loading, and nonspecific binding calculated from a control sensor tip without liposomes was subtracted.

## Cell Culture

COS-7 cells were grown in DMEM media + 10% FBS (Life Technologies). COS-7 cells were plated for transfection and microscopy on glass slides or MatTek glass bottom dishes (MatTek Corporation, Ashland, MA) coated with fibronectin (Sigma-Aldrich). pEGFP F-BAR constructs were transfected into COS-7 cells with Lipofectamine 3000 reagents according to manufacturer's protocols for 24 hours (Life Technologies), co-stained with CellMask Orange plasma membrane dye for 5 minutes at 37°C (Life Technologies), and immediately imaged. A COS-7 wound healing assay was performed as previously described for RhoGAP4 (Vogt *et al.*, 2007). ~80-90% confluent COS-7 cells were transfected with pEGFP RhoGAP4 constructs for 24 hours before a wound was created with a P200 pipet tip. Expression of transfected F-BARs was confirmed by lysing cells in ice-cold RIPA buffer for 30 minutes, SDS-PAGE, and anti-GFP (Roche) immunoblotting.

## Electron microscopy methods

1 µg/mL Cdc15 F-BAR solution diluted 1:1000 into 50 mM NaCl, 20 mM Tris-HCl pH 7.4, or 5 µL of 1:1 1mg/mL liposomes (composed of 70% DOPC / 15% DOPE / 10% DOPS / 5% PI(4)P) : 10 µM F-BAR in 150mM NaCl, 20 mM Tris-HCl pH 7.4, was adsorbed to a glow discharged 200-mesh copper grid covered with carbon-coated collodion film (EMS, Hatfield, PA). For oligomer bound samples, 1 mg/mL Cdc15 F-BAR was mixed with 1 mg/mL liposomes at 200 mM NaCl to allow membrane binding. This sample was diluted to 100 mM NaCl to induce oligomerization before 5 uL was added to an EM grid. Grids were washed in two drops of water to remove unbound sample and stained with two drops of 0.75% uranyl formate (Ohi *et al.*, 2004). Samples

were imaged on a FEI Morgagni electron microscope operated at 100 kV and images were captured at 18,000-36,000X on a 1K x 1K CCD camera (ATM, Woburn, MA).

For preparation of samples in vitrified ice, 2  $\mu$ L of F-BAR-bound liposome sample was applied to a Quantifoil R2/1 holey carbon grid (Quantifoil Micro Tools, Jena, Germany), blotted for 2 seconds, and plunged into liquid ethane using a Vitrobot Mark III (FEI, Hillsboro, OR). Cryo samples were examined at liquid nitrogen temperatures using an FEI Polara at 200 kV equipped with a field emission electron gun.

### **Analytical ultracentrifugation**

F-BAR domains were diluted to a final concentration of 0.5 mg/mL and 50 mM NaCl to induce oligomerization before ultracentrifugation. Sedimentation experiments were run at 42,000 rpm at 4°C on an Optima XLI ultracentrifuge (Beckman-Coulter) with a four-hole An60Ti rotor. 1.2 cm path-length centerpieces with sapphire windows were used to collect 280 and 230 nm scan data. Velocity scans were analyzed with SedFit (version 14.81) using 250 scans collected ~2 min apart (Schuck, 2000). Size distributions were determined for a confidence level of  $p = 0.95$  and resolution of  $n = 200$ .

### **Circular dichroism**

Circular dichroism measurements were performed on a Jasco J-810 spectropolarimeter between 330-250 nm. Scans were acquired at 20 nm/min with 4 sec response times, a 1 nm bandwidth, and 4 accumulations. Ellipticity measurements were converted to molar ellipticity for presentation  $[\theta]$  ( $\text{cm}^2\text{dmol}^{-1}$ ).

## **Structural modeling**

The Cdc15 F-BAR domain structural model was generated using the Protein Homology/analogY Recognition Engine V 2.0 (Phyre<sup>2</sup>) (Kelley and Sternberg, 2009) with the Hof1 F-BAR as a template structure (PDB 4WPE) using the one-to-one threading mode. Fer and RhoGAP4 F-BAR domain models were generated in the standard mode, which identified Fes (PDB: 4DYL) and CIP4 (PDB: 2EFK) F-BAR structures as homologous templates, respectively. Negatively charged surface patches along the sides of the Fer and RhoGAP4 F-BAR models were identified with the use of surface electrostatic potential maps. Graphical representations of the F-BAR model were generated using PyMOL.

## REFERENCES

- Abdiche, Y., Malashock, D., Pinkerton, A. and Pons, J. (2008) Determining kinetics and affinities of protein interactions using a parallel real-time label-free biosensor, the Octet., *Analytical Biochemistry*, 377(2), 209–17.
- Adams, P. D., Afonine, P. V., Bunkóczi, G., Chen, V. B., Davis, I. W., Echols, N., Headd, J. J., Hung, L. W., Kapral, G. J., Grosse-Kunstleve, R. W., McCoy, A. J., Moriarty, N. W., Oeffner, R., Read, R. J., Richardson, D. C., Richardson, J. S., Terwilliger, T. C. and Zwart, P. H. (2010) PHENIX: A comprehensive Python-based system for macromolecular structure solution, *Acta Crystallographica Section D: Biological Crystallography*, 66, 213–221.
- Aitken, A. (2006) 14-3-3 proteins: A historic overview, *Seminars in Cancer Biology*, 16(3), 162–172.
- Albertson, R., Riggs, B. and Sullivan, W. (2005) Membrane traffic: A driving force in cytokinesis, *Trends in Cell Biology*, 15(2), 92–101.
- An, H., Morrel, J. L., Jennings, J. L., Link, A. J. and Kathleen, G. L. (2004) Requirements of Fission Yeast Septins for Complex Formation, Localization, and Function, *Molecular Biology of the Cell*, 15(12), 5551–64.
- Arasada, R. and Pollard, T. D. (2011) Distinct roles for F-BAR proteins Cdc15p and Bzz1p in actin polymerization at sites of endocytosis in fission yeast., *Current Biology*, 21(17), 1450–9.
- Arasada, R. and Pollard, T. D. (2014) Contractile Ring Stability in *S. pombe* Depends on F-BAR Protein Cdc15p and Bgs1p Transport from the Golgi Complex, *Cell Reports*, 8(5), 1533–44.
- Arasada, R. and Pollard, T. D. (2015) A role for F-BAR protein Rga7p during cytokinesis in *S. pombe*, *Journal of Cell Science*, 128(13), 2259–68.
- Aresta, S., de Tand-Heim, M.-F., Beranger, F. and de Gunzburg, J. (2002) A novel Rho GTPase-activating-protein interacts with Gem, a member of the Ras superfamily of GTPases, *Biochemical Journal*, 367, 57–65.
- Bahler, J., Steever, A. B., Wheatley, S., Wang, Y. L., Pringle, J. R., Gould, K. L. and McCollum, D. (1998) Role of Polo kinase and Mid1p in determining the site of cell division in fission yeast, *Journal of Cell Biology*, 143(6), 1603–1616.
- Bähler, J., Wu, J., Longtine, M. S., Shah, N. G., McKenzie III, A., Steever, A. B., Wach, A., Philippsen, P. and Pringle, J. R. (1998) Heterologous Modules for Efficient and Versatile PCR-based Gene Targeting in *Schizosaccharomyces pombe*, *Yeast*, 14, 943–951.
- Bai, X., Meng, G., Luo, M. and Zheng, X. (2012) The rigidity of the wedge loop in



PACSIN 3 is a key factor in dictating the diameters of tubules., *The Journal of Biological Chemistry*, 287(26), 22387–22396.

Balasubramanian, M. K., McCollum, D., Chang, L., Wong, K. C., Naqvi, N. I., He, X., Sazer, S. and Gould, K. L. (1998) Isolation and characterization of new fission yeast cytokinesis mutants., *Genetics*, 149(3), 1265–75.

Basi, G., Schmid, E. and Maundrell, K. (1993) TATA box mutations in the *Schizosaccharomyces pombe* nmt1 promoter affect transcription efficiency but not the transcription start point or thiamine repressibility, *Gene*, 123, 131–136.

Becalska, A. N., Kelley, C. F., Berciu, C., Stanishneva-Konovalova, T. B., Fu, X., Wang, S., Sokolova, O. S., Nicastro, D. and Rodal, A. A. (2013) Formation of membrane ridges and scallops by the F-BAR protein Nervous Wreck., *Molecular Biology of the Cell*, 24(15), 2406–18.

Bertocchi, C., Wang, Y., Ravasio, A., Hara, Y., Wu, Y., Sailov, T., Baird, M. A., Davidson, M. W., Zaidel-Bar, R., Toyama, Y., Ladoux, B., Mege, R.-M. and Kanchanawong, P. (2017) Nanoscale architecture of cadherin-based cell adhesions, *Nature Cell Biology*, 19(1), 28–37.

Betzig, E., Patterson, G. H., Sougrat, R., Lindwasser, O. W., Olenych, S., Bonifacino, J. S., Davidson, M. W., Lippincott-Schwartz, J. and Hess, H. F. (2006) Imaging intracellular fluorescent proteins at nanometer resolution., *Science*, 313(5793), 1642–5.

Bezanilla, M., Gladfelter, A. S., Kovar, D. R. and Lee, W.-L. (2015) Cytoskeletal dynamics: A view from the membrane, *The Journal of Cell Biology*, 209(3), 329–337.

Bohnert, K. A. and Gould, K. L. (2012) Cytokinesis-Based Constraints on Polarized Cell Growth in Fission Yeast, *PLoS Genetics*, 8(10), e1003004.

Bohnert, K. A., Grzegorzewska, A. P., Willet, A. H., Vander Kooi, C. W., Kovar, D. R. and Gould, K. L. (2013) SIN-dependent phosphoinhibition of formin multimerization controls fission yeast cytokinesis., *Genes & development*, 27(19), 2164–2177.

Busch, D. J., Houser, J. R., Hayden, C. C., Sherman, M. B., Lafer, E. M. and Stachowiak, J. C. (2015) Intrinsically disordered proteins drive membrane curvature., *Nature communications*, 6, 7875.

Carlson, B. R., Lloyd, K. E., Kruszewski, A., Kim, I.-H., Rodriguiz, R. M., Heindel, C., Faytell, M., Dudek, S. M., Wetsel, W. C. and Soderling, S. H. (2011) WRP/srGAP3 facilitates the initiation of spine development by an inverse F-BAR domain, and its loss impairs long-term memory., *The Journal of Neuroscience*, 31(7), 2447–60.

Carnahan, R. H. and Gould, K. L. (2003) The PCH family protein, Cdc15p, recruits two F-actin nucleation pathways to coordinate cytokinetic actin ring formation in *Schizosaccharomyces pombe*., *The Journal of Cell Biology*, 162(5), 851–62.

- Casamayor, A. and Snyder, M. (2002) Bud-site selection and cell polarity in budding yeast, *Current Opinion in Microbiology*, 5(2), 179–186.
- Celton-Morizur, S., Bordes, N., Fraissier, V., Tran, P. T. and Paoletti, A. (2004) C-Terminal Anchoring of mid1p to Membranes Stabilizes Cytokinetic Ring Position in Early Mitosis in Fission Yeast, *Molecular and Cellular Biology*, 24(24), 10621–10635.
- Chang, F., Drubin, D. and Nurse, P. (1997) Cdc12p, a Protein Required for Cytokinesis in Fission Yeast, Is a Component of the Cell Division Ring and Interacts With Profilin., *The Journal of Cell Biology*, 137(1), 169–82.
- Chang, F., Woollard, A. and Nurse, P. (1996) Isolation and characterization of fission yeast mutants defective in the assembly and placement of the contractile actin ring., *Journal of Cell Science*, 109, 131–42.
- Charrier, C., Joshi, K., Coutinho-Budd, J., Kim, J.-E., Lambert, N., de Marchena, J., Jin, W.-L., Vanderhaeghen, P., Ghosh, A., Sassa, T. and Polleux, F. (2012) Inhibition of SRGAP2 Function by Its Human-Specific Paralogs Induces Neoteny during Spine Maturation, *Cell*, 149(4), 923–935.
- Cheffings, T. H., Burroughs, N. J. and Balasubramanian, M. K. (2016) Actomyosin Ring Formation and Tension Generation in Eukaryotic Cytokinesis, *Current Biology*, 26(15), R719–R737.
- Chen, C. T., Feoktistova, A., Chen, J. S., Shim, Y. S., Clifford, D. M., Gould, K. L. and McCollum, D. (2008) The SIN Kinase Sid2 Regulates Cytoplasmic Retention of the *S. pombe* Cdc14-like Phosphatase Clp1, *Current Biology*, 18(20), 1594–1599.
- Chen, J.-S., Beckley, J. R., Ren, L., Feoktistova, A., Jensen, M. A., Rhind, N. and Gould, K. L. (2016) Discovery of genes involved in mitosis, cell division, cell wall integrity and chromosome segregation through construction of *Schizosaccharomyces pombe* deletion strains, *Yeast*, 33, 507–517.
- Chen, J.-S., Broadus, M. R., McLean, J. R., Feoktistova, A., Ren, L. and Gould, K. L. (2013) Comprehensive proteomics analysis reveals new substrates and regulators of the fission yeast clp1/cdc14 phosphatase., *Molecular and Cellular Proteomics*, 12(5), 1074–86.
- Cheng, H., Rogers, J. A., Dunham, N. A. and Smithgall, T. E. (1999) Regulation of c-Fes tyrosine kinase and biological activities by N-terminal coiled-coil oligomerization domains., *Molecular and Cellular Biology*, 19(12), 8335–8343.
- Clifford, D. M., Wolfe, B. A., Roberts-Galbraith, R. H., McDonald, W. H., Yates, J. R. and Gould, K. L. (2008) The Clp1/Cdc14 phosphatase contributes to the robustness of cytokinesis by association with anillin-related Mid1., *The Journal of Cell Biology*, 181(1), 79–88.
- Cocucci, E., Aguet, F., Boulant, S. and Kirchhausen, T. (2012) The First Five Seconds in

the Life of a Clathrin-Coated Pit, *Cell*, 150, 495–507.

Cong, F., Spencer, S., Côté, J. F., Wu, Y., Tremblay, M. L., Lasky, L. A. and Goff, S. P. (2000) Cytoskeletal protein PSTPIP1 directs the PEST-type protein tyrosine phosphatase to the c-Abl kinase to mediate Abl dephosphorylation, *Molecular Cell*, 6, 1413–1423.

Cortés, J. C. G., Sato, M., Muñoz, J., Moreno, M. B., Clemente-Ramos, J. A., Ramos, M., Okada, H., Osumi, M., Durán, A. and Ribas, J. C. (2012) Fission yeast Ags1 confers the essential septum strength needed for safe gradual cell abscission., *The Journal of Cell Biology*, 198(4), 637–56.

Côté, J.-F., Chung, P. L., Théberge, J.-F., Hallé, M., Spencer, S., Lasky, L. A. and Tremblay, M. L. (2002) PSTPIP is a substrate of PTP-PEST and serves as a scaffold guiding PTP-PEST toward a specific dephosphorylation of WASP., *The Journal of Biological Chemistry*, 277(4), 2973–86.

Coutinho-Budd, J., Ghukasyan, V., Zylka, M. J. and Polleux, F. (2012) The F-BAR domains from srGAP1, srGAP2 and srGAP3 regulate membrane deformation differently., *Journal of Cell Science*, 125, 3390–401.

Coyle, I. P., Koh, Y.-H., Lee, W.-C. M., Slind, J., Fergestad, T., Littleton, J. T. and Ganetzky, B. (2004) Nervous Wreck, an SH3 Adaptor Protein that Interacts with Wsp, Regulates Synaptic Growth in *Drosophila*, *Neuron*, 41, 521–534.

Craig, A. W. B., Zirngibl, R. and Greer, P. (1999) Disruption of coiled-coil domains in Fer protein-tyrosine kinase abolishes trimerization but not kinase activation, *Journal of Biological Chemistry*, 274(28), 19934–19942.

Daga, R. R. and Chang, F. (2005) Dynamic positioning of the fission yeast cell division plane, *Proceedings of the National Academy of Sciences*, 102(23), 8228.

Daumke, O., Roux, A. and Haucke, V. (2014) BAR Domain Scaffolds in Dynamin-Mediated Membrane Fission, *Cell*, 156(5), 882–892.

Demeter, J. and Sazer, S. (1998) imp2, a New Component of the Actin Ring in the Fission Yeast, *The Journal of Cell Biology*, 143, 415–427.

Dharmalingam, E., Haeckel, A., Pinyol, R., Schwintzer, L., Koch, D., Kessels, M. M. and Qualmann, B. (2009) F-BAR proteins of the syndapin family shape the plasma membrane and are crucial for neuromorphogenesis., *The Journal of Neuroscience*, 29(42), 13315–13327.

Doherty, G. J. and McMahon, H. T. (2009) Mechanisms of endocytosis., *Annual Review of Biochemistry*, 78, 857–902.

Edeling, M. A., Sanker, S., Shima, T., Umasankar, P. K., Höning, S., Kim, H. Y., Davidson, L. A., Watkins, S. C., Tsang, M., Owen, D. J. and Traub, L. M. (2009) Structural requirements for PACSIN/syndapin operation during zebrafish embryonic

notochord development, *PLoS ONE*, 4(12), e8150.

Emsley, P., Lohkamp, B., Scott, W. G. and Cowtan, K. (2010) Features and development of Coot, *Acta Crystallographica Section D: Biological Crystallography*, 66, 486–501.

Fankhauser, C., Reymond, A., Cerutti, L., Utzig, S., Hofmann, K. and Simanis, V. (1995) The *S. pombe* *cdc15* gene is a key element in the reorganization of F-actin at mitosis., *Cell*, 82(3), 435–44.

Fenix, A. M., Taneja, N., Buttler, C. A., Lewis, J., Van Engelenburg, S. B., Ohi, R. and Burnette, D. T. (2016) Expansion and concatenation of nonmuscle myosin IIA filaments drive cellular contractile system formation during interphase and mitosis, *Molecular Biology of the Cell*, 27(9), 1465–1478.

Ferguson, S. M. and De Camilli, P. (2012) Dynamin, a membrane-remodelling GTPase, *Nature Reviews Molecular Cell Biology*, 13, 75–88.

Fricke, R., Gohl, C., Dharmalingam, E., Grevelhörster, A., Zahedi, B., Harden, N., Kessels, M., Qualmann, B. and Bogdan, S. (2009) *Drosophila* Cip4/Toca-1 Integrates Membrane Trafficking and Actin Dynamics through WASP and SCAR/WAVE, *Current Biology*, 19(17), 1429–1437.

Fritz, R. D., Menshykau, D., Martin, K., Reimann, A., Pontelli, V. and Pertz, O. (2015) SrGAP2-Dependent Integration of Membrane Geometry and Slit-Robo-Repulsive Cues Regulates Fibroblast Contact Inhibition of Locomotion, *Developmental Cell*, 35, 78–92.

Frost, A., Perera, R., Roux, A., Spasov, K., Destaing, O., Egelman, E. H., De Camilli, P. and Unger, V. M. (2008) Structural basis of membrane invagination by F-BAR domains., *Cell*, 132(5), 807–17.

Frost, A., Unger, V. M. and De Camilli, P. (2009) The BAR domain superfamily: membrane-molding macromolecules., *Cell*, 137(2), 191–6.

Fujiwara, T., Bandi, M., Nitta, M., Ivanova, E. V, Bronson, R. T. and Pellman, D. (2005) Cytokinesis failure generating tetraploids promotes tumorigenesis in p53-null cells., *Nature*, 437(7061), 1043–7.

G. Cortés, J. C., Pujol, N., Sato, M., Pinar, M., Ramos, M., Moreno, B., Osumi, M., Ribas, J. C. and Pérez, P. (2015) Cooperation between Paxillin-like Protein Pxl1 and Glucan Synthase Bgs1 Is Essential for Actomyosin Ring Stability and Septum Formation in Fission Yeast, *PLoS Genetics*, 11(7), e1005358.

Gallop, J. L., Jao, C. C., Kent, H. M., Butler, P. J. G., Evans, P. R., Langen, R. and McMahon, H. T. (2006) Mechanism of endophilin N-BAR domain-mediated membrane curvature., *EMBO*, 25(12), 2898–910.

Ganem, N. J., Godinho, S. a and Pellman, D. (2009) A mechanism linking extra centrosomes to chromosomal instability., *Nature*, 460(7252), 278–82.

- Ge, W. and Balasubramanian, M. K. (2007) Pxl1p, a Paxillin-related Protein, Stabilizes the Actomyosin Ring during Cytokinesis in Fission Yeast, *Molecular Biology of the Cell*, 19(4), 1680–1692.
- Goss, J. W., Kim, S., Bledsoe, H. and Pollard, T. D. (2014) Characterization of the roles of Blt1p in fission yeast cytokinesis, *Molecular Biology of the Cell*, 25, 1946–1957.
- Goyal, A., Takaine, M., Simanis, V. and Nakano, K. (2011) Dividing the spoils of growth and the cell cycle: The fission yeast as a model for the study of cytokinesis., *Cytoskeleton*, 68(2), 69–88.
- Green, R. A., Paluch, E. and Oegema, K. (2012) Cytokinesis in Animal Cells., *Annual Review of Cell and Developmental Biology*, 28, 29–58.
- Greer, P. (2002) Closing in on the biological functions of Fps/Fes and Fer., *Nature Reviews Molecular Cell Biology*, 3(4), 278–89.
- Grosse-Kunstleve, R. W. and Adams, P. D. (2003) Substructure search procedures for macromolecular structures, *Acta Crystallographica - Section D Biological Crystallography*, 59, 1966–1973.
- Gu, Y., Yam, C. and Oliferenko, S. (2015) Rewiring of Cellular Division Site Selection in Evolution of Fission Yeasts, *Current Biology*, 25(9), 1187–1194.
- Guerrier, S., Coutinho-Budd, J., Sassa, T., Gresset, A., Jordan, N. V., Chen, K., Jin, W.-L., Frost, A. and Polleux, F. (2009) The F-BAR domain of srGAP2 induces membrane protrusions required for neuronal migration and morphogenesis., *Cell*, 138(5), 990–1004.
- Gupta, S., Mana-Capelli, S., McLean, J. R., Chen, C. T., Ray, S., Gould, K. L. and McCollum, D. (2013) Identification of SIN pathway targets reveals mechanisms of crosstalk between NDR kinase pathways, *Current Biology*, 23(4), 333–338.
- Güttinger, S., Laurell, E. and Kutay, U. (2009) Orchestrating nuclear envelope disassembly and reassembly during mitosis, *Nature Reviews Molecular Cell Biology*, 10(3), 178–191.
- Guzman-Vendrell, M., Baldissard, S., Almonacid, M., Mayeux, A., Paoletti, A. and Moseley, J. B. (2013) Blt1 and mid1 provide overlapping membrane anchors to position the division plane in fission yeast., *Molecular and Cellular Biology*, 33(2), 418–28.
- Hachet, O., Berthelot-Grosjean, M., Kokkoris, K., Vincenzetti, V., Moosbrugger, J. and Martin, S. G. (2011) A phosphorylation cycle shapes gradients of the DYRK family kinase Pom1 at the plasma membrane., *Cell*, 145(7), 1116–28.
- Hachet, O. and Simanis, V. (2008) Mid1p/anillin and the septation initiation network orchestrate contractile ring assembly for cytokinesis., *Genes & Development*, 22(22), 3205–16.

- Haeusser, D. P. and Margolin, W. (2016) Splitsville: structural and functional insights into the dynamic bacterial Z ring, *Nature Reviews Microbiology*, 14(5), 305–319.
- Hansen, C. G., Howard, G. and Nichols, B. J. (2011) Pacsin 2 is recruited to caveolae and functions in caveolar biogenesis., *Journal of Cell Science*, 124(16), 2777–2785.
- Haralick, R., Shanmugan, K. and Dinstein, I. (1973) Textural features for image classification, *IEEE Transactions on Systems, Man and Cybernetics*, 610–621.
- Hartig, S. M., Ishikura, S., Hicklen, R. S., Feng, Y., Blanchard, E. G., Voelker, K. a, Pichot, C. S., Grange, R. W., Raphael, R. M., Klip, A. and Corey, S. J. (2009) The F-BAR protein CIP4 promotes GLUT4 endocytosis through bidirectional interactions with N-WASp and Dynamin-2, *Journal of Cell Science*, 122(Pt 13), 2283–91.
- He, J., Zhou, R., Wu, Z., Carrasco, M. A., Kurshan, P. T., Farley, J. E., Simon, D. J., Wang, G., Han, B., Hao, J., Heller, E., Freeman, M. R., Shen, K., Maniatis, T., Tessier-Lavigne, M. and Zhuang, X. (2016) Prevalent presence of periodic actin-spectrin-based membrane skeleton in a broad range of neuronal cell types and animal species., *Proceedings of the National Academy of Sciences*, 113(21), 6029–6034.
- Henne, W. M., Boucrot, E., Meinecke, M., Evergren, E., Vallis, Y., Mittal, R. and McMahon, H. T. (2010) FCHO proteins are nucleators of clathrin-mediated endocytosis, *Science*, 328, 1281–1284.
- Henne, W. M., Kent, H. M., Ford, M. G. J., Hegde, B. G., Daumke, O., Butler, P. J. G., Mittal, R., Langen, R., Evans, P. R. and McMahon, H. T. (2007) Structure and analysis of FCHO2 F-BAR domain: a dimerizing and membrane recruitment module that effects membrane curvature, *Structure*, 15(7), 839–52.
- Henson, J. H., Ditzler, C. E., Germain, A., Irwin, P. M., Vogt, E. T., Yang, S., Wu, X. and Shuster, C. B. (2017) The Ultrastructural Organization of Actin and Myosin II Filaments in the Contractile Ring: New Support for an Old Model of Cytokinesis, *Molecular Biology of the Cell*, 28(5), 613–623.
- Hess, S. T., Girirajan, T. P. K. and Mason, M. D. (2006) Ultra-High Resolution Imaging by Fluorescence Photoactivation Localization Microscopy, *Biophysical Journal*, 91(11), 4258–4272.
- Hollopeter, G., Lange, J. J., Zhang, Y., Vu, T. N., Gu, M., Ailion, M., Lambie, E. J., Slaughter, B. D., Unruh, J. R., Florens, L. and Jorgensen, E. M. (2014) The membrane-associated proteins FCHO and SGIP are allosteric activators of the AP2 clathrin adaptor complex., *eLife*, 3, e03648.
- Holm, L. and Rosenström, P. (2010) Dali server: Conservation mapping in 3D, *Nucleic Acids Research*, 38(May), 545–549.
- Hongtao, Y., Chen, J. K., Feng, S., Dalgarno, D. C., Brauer, A. W. and Schreiber, S. L. (1994) Structural basis for the binding of proline-rich peptides to SH3 domains, *Cell*, 76,

933–945.

Huang, B., Wang, W., Bates, M. and Zhuang, X. (2008) Three-Dimensional Super-Resolution Imaging by Stochastic Optical Reconstruction Microscopy, *Science*, 319(5864), 810–13.

Huang, J., Huang, Y., Yu, H., Subramanian, D., Padmanabhan, A., Thadani, R., Tao, Y., Tang, X., Wedlich-Soldner, R. and Balasubramanian, M. K. (2012) Nonmedially assembled F-actin cables incorporate into the actomyosin ring in fission yeast, *The Journal of Cell Biology*, 199(5), 831–847.

Huang, Y., Chew, T. G., Ge, W. and Balasubramanian, M. K. (2007) Polarity determinants Tea1p, Tea4p, and Pom1p inhibit division-septum assembly at cell ends in fission yeast., *Developmental Cell*, 12(6), 987–96.

Huang, Y., Yan, H. and Balasubramanian, M. K. (2008) Assembly of normal actomyosin rings in the absence of Mid1p and cortical nodes in fission yeast, *The Journal of Cell Biology*, 183(6), 979–988.

Humbel, B. M., Konomi, M., Takagi, T., Kamasawa, N., Ishijima, S. a and Osumi, M. (2001) In situ localization of beta-glucans in the cell wall of *Schizosaccharomyces pombe*., *Yeast*, 18(5), 433–444.

Icking, A., Matt, S., Opitz, N., Wiesenthal, A., Müller-Esterl, W. and Schilling, K. (2005) NOSTRIN functions as a homotrimeric adaptor protein facilitating internalization of eNOS., *Journal of Cell Science*, 118(21), 5059–5069.

Itoh, T., Erdmann, K. S., Roux, A., Habermann, B., Werner, H. and De Camilli, P. (2005) Dynamin and the actin cytoskeleton cooperatively regulate plasma membrane invagination by BAR and F-BAR proteins., *Developmental Cell*, 9(6), 791–804.

Itoh, T., Hasegawa, J., Tsujita, K., Kanaho, Y. and Takenawa, T. (2009) The tyrosine kinase Fer is a downstream target of the PLD-PA pathway that regulates cell migration., *Science Signaling*, 2(87), ra52.

Ju, Y.-T., Chang, A. C. Y., She, B.-R., Tsauro, M.-L., Hwang, H.-M., Chao, C. C.-K., Cohen, S. D. and Lin-Chao, S. (1998) gas 7 : A gene expressed preferentially in growth-arrested fibroblasts and terminally differentiated Purkinje neurons affects neurite formation, *Proceedings of the National Academy of Sciences*, 95, 11423–11428.

Kakimoto, T., Katoh, H. and Negishi, M. (2006) Regulation of neuronal morphology by Toca-1, an F-BAR/EFC protein that induces plasma membrane invagination., *The Journal of Biological Chemistry*, 281(39), 29042–53.

Kamasaki, T., Osumi, M. and Mabuchi, I. (2007) Three-dimensional arrangement of F-actin in the contractile ring of fission yeast., *The Journal of Cell Biology*, 178(5), 765–71.

Kamioka, Y., Fukuhara, S., Sawa, H., Nagashima, K., Masuda, M., Matsuda, M. and

- Mochizuki, N. (2004) A novel dynamin-associating molecule, formin-binding protein 17, induces tubular membrane invaginations and participates in endocytosis., *The Journal of Biological Chemistry*, 279(38), 40091–9.
- Kanchanawong, P., Shtengel, G., Pasapera, A. M., Ramko, E. B., Davidson, M. W., Hess, H. F. and Waterman, C. M. (2010) Nanoscale architecture of integrin-based cell adhesions., *Nature*, 468(7323), 580–4.
- Keeney, J. B. and Boeke, J. D. (1994) Efficient Targeted Integration at leu1-32 and ura4-294 in *Schizosaccharomyces pombe*, *Genetics*, 136, 849–856.
- Kelley, C. F., Becalska, A. N., Berciu, C., Nicastro, D. and Rodal, A. A. (2015) Assembly of actin filaments and microtubules in Nwk F-BAR-induced membrane deformations, *Communicative & Integrative Biology*, 8(2), e1000703.
- Kelley, C. F., Messelaar, E. M., Eskin, T. L., Wang, S., Song, K., Vishnia, K., Becalska, A. N., Shupliakov, O., Hagan, M. F., Danino, D., Sokolova, O. S., Nicastro, D. and Rodal, A. A. (2015) Membrane Charge Directs the Outcome of F-BAR Domain Lipid Binding and Autoregulation, *Cell Reports*, 13, 2597–2609.
- Kelley, L. A. and Sternberg, M. J. E. (2009) Protein structure prediction on the Web: a case study using the Phyre server., *Nature Protocols*, 4(3), 363–371.
- Kettenbach, A. N., Deng, L., Wu, Y., Baldissard, S., Adamo, M. E., Gerber, S. A. and Moseley, J. B. (2015) Quantitative phosphoproteomics reveals pathways for coordination of cell growth and division by the fission yeast DYRK kinase Pom1, *Molecular & Cellular Proteomics*, 14, 1275–1287.
- Kim, L. and Wong, T. W. (1995) The cytoplasmic tyrosine kinase FER is associated with the catenin-like substrate pp120 and is activated by growth factors., *Molecular and Cellular Biology*, 15(8), 4553–4561.
- Kim, L. and Wong, T. W. (1998) Growth factor-dependent phosphorylation of the actin-binding protein cortactin is mediated by the cytoplasmic tyrosine kinase FER, *Journal of Biological Chemistry*, 273(36), 23542–23548.
- Kitayama, C., Sugimoto, A. and Yamamoto, M. (1997) Type II Myosin Heavy Chain Encoded by the myo2 Gene Composes the Contractile Ring during Cytokinesis in *Schizosaccharomyces pombe*, *The Journal of Cell Biology*, 137(6), 1309–1319.
- Kostan, J., Salzer, U., Orlova, A., Törö, I., Hodnik, V., Senju, Y., Zou, J., Schreiner, C., Steiner, J., Meriläinen, J., Nikki, M., Virtanen, I., Carugo, O., Rappsilber, J., Lappalainen, P., Lehto, V., Anderluh, G., Egelman, E. H. and Djinovi, K. (2014) Direct interaction of actin filaments with F-BAR protein pacsin2, *EMBO Reports*, 15(11), 1154–1162.
- de Kreuk, B.-J., Anthony, E. C., Geertss, D. and Hordijk, P. L. (2012) The F-BAR protein PACSIN2 regulates epidermal growth factor receptor internalization, *Journal of*



*Biological Chemistry*, 287(52), 43438–43453.

Laplante, C., Huang, F., Tebbs, I. R., Bewersdorf, J. and Pollard, T. D. (2016) Molecular organization of cytokinesis nodes and contractile rings by super-resolution fluorescence microscopy of live fission yeast., *Proceedings of the National Academy of Sciences*, 113(40), E5876–E5885.

Laporte, D., Coffman, V. C., Lee, I.-J. and Wu, J.-Q. (2011) Assembly and architecture of precursor nodes during fission yeast cytokinesis., *The Journal of Cell Biology*, 192(6), 1005–21.

Leibfried, A., Fricke, R., Morgan, M. J., Bogdan, S. and Bellaiche, Y. (2008) Drosophila Cip4 and WASp Define a Branch of the Cdc42-Par6-aPKC Pathway Regulating E-Cadherin Endocytosis, *Current Biology*, 18(21), 1639–1648.

Lemmon, M. A. (2008) Membrane recognition by phospholipid-binding domains., *Nature Reviews Molecular Cell Biology*, 9, 99–111.

Li, S. S.-C. (2005) Specificity and versatility of SH3 and other proline-recognition domains: structural basis and implications for cellular signal transduction., *The Biochemical Journal*, 390, 641–53.

Li, Y., Christensen, J. R., Homa, K. E., Hocky, G. M., Fok, A., Sees, J. A., Voth, G. A. and Kovar, D. R. (2016) The F-actin bundler  $\alpha$ -actinin Ain1 is tailored for ring assembly and constriction during cytokinesis in fission yeast, *Molecular Biology of the Cell*, 27(11), 1821–1833.

Lippincott, J. and Li, R. (1998) Dual function of Cyk2, a cdc15/PSTPIP family protein, in regulating actomyosin ring dynamics and septin distribution., *The Journal of Cell Biology*, 143(7), 1947–60.

Liu, J., Wang, H. and Balasubramanian, M. K. (2000) A checkpoint that monitors cytokinesis in *Schizosaccharomyces pombe*., *Journal of Cell Science*, 113, 1223–1230.

Liu, J., Wang, H., McCollum, D. and Balasubramanian, M. K. (1999) Drc1p/Cps1p, a 1,3- $\beta$ -glucan synthase subunit, is essential for division septum assembly in *Schizosaccharomyces pombe*, *Genetics*, 153, 1193–1203.

Liu, Y., Lee, I. J., Sun, M., Lower, C. A., Runge, K. W., Ma, J. and Wu, J. Q. (2016) Roles of the novel coiled-coil protein Rng10 in septum formation during fission yeast cytokinesis, *Mol Biol Cell*.

Lutkenhaus, J., Pichoff, S. and Du, S. (2012) Bacterial cytokinesis: From Z ring to divisome, *Cytoskeleton*, 69(10), 778–790.

Mackintosh, C. (2004) Dynamic interactions between 14-3-3 proteins and phosphoproteins regulate diverse cellular processes, *Biochemical Journal*, 342, 329–342.

- Marks, J. and Hyams, J. (1985) Localization of F-actin through the cell division cycle of *Schizosaccharomyces pombe*, *European Journal of Cell Biology*, 39, 27–32.
- Martín-García, R., Coll, P. M. and Pérez, P. (2014) F-BAR domain protein Rga7 collaborates with Cdc15 and Imp2 to ensure proper cytokinesis in fission yeast., *Journal of Cell Science*, 127(Pt 19), 4146–58.
- Masuda, M., Takeda, S., Sone, M., Ohki, T., Mori, H., Kamioka, Y. and Mochizuki, N. (2006) Endophilin BAR domain drives membrane curvature by two newly identified structure-based mechanisms., *EMBO*, 25(12), 2889–97.
- Matsuyama, A., Arai, R., Yashiroda, Y., Shirai, A., Kamata, A., Sekido, S., Kobayashi, Y., Hashimoto, A., Hamamoto, M., Hiraoka, Y., Horinouchi, S. and Yoshida, M. (2006) ORFeome cloning and global analysis of protein localization in the fission yeast *Schizosaccharomyces pombe*, *Nature Biotechnology*, 24(7), 841–847.
- McCoy, A. J., Grosse-Kunstleve, R. W., Adams, P. D., Winn, M. D., Storoni, L. C. and Read, R. J. (2007) Phaser crystallographic software, *Journal of Applied Crystallography*, 40, 658–674.
- McDonald, N. A., Vander Kooi, C. W., Ohi, M. D. and Gould, K. L. (2015) Oligomerization but Not Membrane Bending Underlies the Function of Certain F-BAR Proteins in Cell Motility and Cytokinesis, *Developmental Cell*, 35(6), 725–736.
- McDonald, N. A., Takizawa, Y., Feoktistova, A., Xu, P., Ohi, M. D., Vander Kooi, C. W. and Gould, K. L. (2016) The Tubulation Activity of a Fission Yeast F-BAR Protein Is Dispensable for Its Function in Cytokinesis, *Cell Reports*, 14(3), 534–46.
- van Meer, G., Voelker, D. R. and Feigenson, G. W. (2008) Membrane lipids: where they are and how they behave., *Nature reviews. Molecular cell biology*, 9(2), 112–124.
- Meitinger, F., Boehm, M. E., Hofmann, A., Hub, B., Zentgraf, H., Lehmann, W. D. and Pereira, G. (2011) Phosphorylation-dependent regulation of the F-BAR protein Hof1 during cytokinesis, *Genes & Development*, 25(8), 875–888.
- Meitinger, F., Palani, S., Hub, B. and Pereira, G. (2013) Dual function of the NDR-kinase Dbf2 in the regulation of the F-BAR protein Hof1 during cytokinesis., *Molecular Biology of the Cell*, 24, 1290–304.
- Mennella, V., Keszthelyi, B., McDonald, K. L., Chhun, B., Kan, F., Rogers, G. C., Huang, B. and Agard, D. A. (2012) Subdiffraction-resolution fluorescence microscopy reveals a domain of the centrosome critical for pericentriolar material organization., *Nature Cell Biology*, 14(11), 1159–68.
- Millard, T. H., Bompard, G., Heung, M. Y., Dafforn, T. R., Scott, D. J., Machesky, L. M. and Fütterer, K. (2005) Structural basis of filopodia formation induced by the IRSp53/MIM homology domain of human IRSp53., *EMBO*, 24(2), 240–250.

- Mim, C. and Unger, V. M. (2012) Membrane curvature and its generation by BAR proteins, *Trends in Biochemical Sciences*, 37(12), 526–533.
- Mishra, M., Kashiwazaki, J., Takagi, T., Srinivasan, R., Huang, Y., Balasubramanian, M. K. and Mabuchi, I. (2013) In vitro contraction of cytokinetic ring depends on myosin II but not on actin dynamics, *Nature Cell Biology*, 15, 853–859.
- Mitchison, J. M. and Nurse, P. (1985) Growth in Cell Length in the Fission Yeast *Schizosaccharomyces Pombe*, *Journal of Cell Science*, 75, 357–376.
- Mogilner, A. and Oster, G. (2003) Force generation by actin polymerization II: the elastic ratchet and tethered filaments., *Biophysical Journal*, 84(3), 1591–1605.
- Moravcevic, K., Alvarado, D., Ferguson, K. M., Lemmon, M. A., Moravcevic, K., Alvarado, D., Schmitz, K. R., Kenniston, J. A. and Mendrola, J. M. (2015) Comparison of *Saccharomyces cerevisiae* F-BAR Domain Structures Reveals a Conserved Inositol Phosphate Binding Site, *Structure*, 23(2), 252–63.
- Morrell-Falvey, J. L., Ren, L., Feoktistova, A., Haese, G. Den and Gould, K. L. (2005) Cell wall remodeling at the fission yeast cell division site requires the Rho-GEF Rgf3p., *Journal of Cell Science*, 118, 5563–5573.
- Motegi, F., Mishra, M., Balasubramanian, M. K. and Mabuchi, I. (2004) Myosin-II reorganization during mitosis is controlled temporally by its dephosphorylation spatially by Mid1 in fission yeast, *Journal of Cell Biology*, 165(5), 685–695.
- Muñoz, J., Cortés, J. C. G., Sipiczki, M., Ramos, M., Clemente-Ramos, J. A., Moreno, M. B., Martins, I. M., Pérez, P. and Ribas, J. C. (2013) Extracellular cell wall  $\beta(1,3)$ glucan is required to couple septation to actomyosin ring contraction., *The Journal of Cell Biology*, 203(2), 265–82.
- Murshudov, G. N., Vagin, A. A. and Dodson, E. J. (1997) Refinement of macromolecular structures by the maximum-likelihood method, *Acta Crystallographica Section D: Biological Crystallography*, 53, 240–255.
- Myagmar, B.-E., Umikawa, M., Asato, T., Taira, K., Oshiro, M., Hino, A., Takei, K., Uezato, H. and Kariya, K.-I. (2005) PARG1, a protein-tyrosine phosphatase-associated RhoGAP, as a putative Rap2 effector, *Biochemical and Biophysical Research Communications*, 329(3), 1046–1052.
- Naba, A., Reverdy, C., Louvard, D. and Arpin, M. (2008) Spatial recruitment and activation of the Fes kinase by ezrin promotes HGF-induced cell scattering., *The EMBO Journal*, 27(1), 38–50.
- Naqvi, N. I., Wong, K. C., Tang, X. and Balasubramanian, M. K. (2000) Type II myosin regulatory light chain relieves auto-inhibition of myosin-heavy-chain function., *Nature Cell Biology*, 2(11), 855–858.

- Nishihama, R., Schreiter, J. H., Onishi, M., Vallen, E. A., Hanna, J., Moravcevic, K., Lippincott, M. F., Han, H., Lemmon, M. A., Pringle, J. R. and Bi, E. (2009) Role of Inn1 and its interactions with Hof1 and Cyk3 in promoting cleavage furrow and septum formation in *S. cerevisiae*., *The Journal of Cell Biology*, 185(6), 995–1012.
- Nurse, P., Thuriaux, P. and Nasmyth, K. (1976) Genetic control of the cell division cycle in the fission yeast *Schizosaccharomyces pombe*, *Molecular & General Genetics*, 146(2), 167–178.
- O'Connor-Giles, K. M., Ho, L. L. and Ganetzky, B. (2008) Nervous Wreck Interacts with Thickveins and the Endocytic Machinery to Attenuate Retrograde BMP Signaling during Synaptic Growth, *Neuron*, 58, 507–518.
- Oh, M. A., Choi, S., Lee, M. J., Choi, M.-C., Lee, S.-A., Ko, W., Cance, W. G., Oh, E. S., Buday, L., Kim, S.-H. and Lee, J. W. (2009) Specific tyrosine phosphorylation of focal adhesion kinase mediated by Fer tyrosine kinase in suspended hepatocytes, *Biochimica et Biophysica Acta*, 1793(5), 781–791.
- Oh, Y., Schreiter, J., Nishihama, R., Wloka, C. and Bi, E. (2013) Targeting and functional mechanisms of the cytokinesis-related F-BAR protein Hof1 during the cell cycle., *Molecular Biology of the Cell*, 24, 1305–20.
- Ohi, M., Li, Y., Cheng, Y. and Walz, T. (2004) Negative Staining and Image Classification - Powerful Tools in Modern Electron Microscopy., *Biological Procedures Online*, 6(1), 23–34.
- Ojkic, N., Wu, J.-Q. and Vavylonis, D. (2011) Model of myosin node aggregation into a contractile ring: the effect of local alignment., *Journal of Physics: Condensed Matter*, 23(37), 374103.
- Otwinowski, Z. and Minor, W. (1997) Processing of X-ray Diffraction Data Collected in Oscillation Mode, *Methods in Enzymology*, 276, 307–326.
- Ovesný, M., Křížek, P., Borkovec, J., Švindrych, Z. and Hagen, G. M. (2014) ThunderSTORM: A comprehensive ImageJ plug-in for PALM and STORM data analysis and super-resolution imaging, *Bioinformatics*, 30(16), 2389–2390.
- Padmanabhan, A., Bakka, K., Sevugan, M., Naqvi, N. I., D'Souza, V., Tang, X., Mishra, M. and Balasubramanian, M. K. (2011) IQGAP-related Rng2p organizes cortical nodes and ensures position of cell division in fission yeast, *Current Biology*, 21(6), 467–472.
- Palani, S., Chew, T. G., Ramanujam, S., Kamnev, A., Harne, S., Chapa-y-Lazo, B., Hogg, R., Sevugan, M., Mishra, M., Gayathri, P. and Balasubramanian, M. K. (2017) Motor Activity Dependent and Independent Functions of Myosin II Contribute to Actomyosin Ring Assembly and Contraction in *Schizosaccharomyces pombe*, *Current Biology*, 27(5), 751–757.
- Pang, X., Fan, J., Zhang, Y., Zhang, K., Gao, B., Ma, J., Li, J., Deng, Y., Zhou, Q.,

- Egelman, E. H., Hsu, V. W. and Sun, F. (2014) A PH domain in ACAP1 possesses key features of the BAR domain in promoting membrane curvature., *Developmental Cell*, 31(1), 73–86.
- Paoletti, A. and Chang, F. (2000) Analysis of mid1p, a protein required for placement of the cell division site, reveals a link between the nucleus and the cell surface in fission yeast., *Molecular Biology of the Cell*, 11(8), 2757–2773.
- Di Paolo, G. and De Camilli, P. (2006) Phosphoinositides in cell regulation and membrane dynamics, *Nature*, 443, 651–657.
- Pardo, M. and Nurse, P. (2003) Equatorial retention of the contractile actin ring by microtubules during cytokinesis., *Science*, 300(5625), 1569–1574.
- Pelham, R. and Chang, F. (2002) Actin dynamics in the contractile ring during cytokinesis in fission yeast, *Nature*, 419, 82–86.
- Peter, B. J., Kent, H. M., Mills, I. G., Vallis, Y., Butler, P. J. G., Evans, P. R. and McMahon, H. T. (2004) BAR domains as sensors of membrane curvature: the amphiphysin BAR structure., *Science*, 303(5657), 495–9.
- Pichot, C. S., Arvanitis, C., Hartig, S. M., Jensen, S. A., Bechill, J., Marzouk, S., Yu, J., Frost, J. A. and Corey, S. J. (2010) Cdc42-interacting protein 4 promotes breast cancer cell invasion and formation of invadopodia through activation of N-WASp, *Cancer Research*, 70(21), 8347–8356.
- Pinar, M., Coll, P. M., Rincon, S. A. and Pérez, P. (2008) Schizosaccharomyces pombe Pxl1 Is a Paxillin Homologue That Modulates Rho1 Activity and Participates in Cytokinesis, *Molecular Biology of the Cell*, 19(April), 308–317.
- Pollard, L. W., Onishi, M., Pringle, J. R. and Lord, M. (2012) Fission yeast Cyk3p is a transglutaminase-like protein that participates in cytokinesis and cell morphogenesis, *Molecular Biology of the Cell*, 23(13), 2433–2444.
- Pollard, T. and Wu, J.-Q. (2010) Understanding cytokinesis: lessons from fission yeast, *Nature Reviews Molecular Cell Biology*, 11, 149–155.
- Posor, Y., Eichhorn-Grunig, M. and Haucke, V. (2015) Phosphoinositides in endocytosis, *Biochimica et Biophysica Acta*, 1851, 794–804.
- Proctor, S. A., Minc, N., Boudaoud, A. and Chang, F. (2012) Contributions of Turgor Pressure, the Contractile Ring, and Septum Assembly to Forces in Cytokinesis in Fission Yeast., *Current Biology*, 22, 1–8.
- Qualmann, B., Koch, D. and Kessels, M. M. (2011) Let's go bananas: revisiting the endocytic BAR code., *EMBO*, 30(17), 3501–15.
- Rao, Y., Ma, Q., Vahedi-Faridi, A., Sundborger, A., Pechstein, A., Puchkov, D., Luo, L.,

- Shupliakov, O., Saenger, W. and Haucke, V. (2010) Molecular basis for SH3 domain regulation of F-BAR-mediated membrane deformation., *Proceedings of the National Academy of Sciences*, 107(18), 8213–8.
- Reider, A., Barker, S. L., Mishra, S. K., Im, Y. J., Maldonado-Báez, L., Hurley, J. H., Traub, L. M. and Wendland, B. (2009) Syp1 is a conserved endocytic adaptor that contains domains involved in cargo selection and membrane tubulation., *The EMBO Journal*, 28(20), 3103–3116.
- Ren, L., Willet, A. H., Roberts-Galbraith, R. H., McDonald, N. A., Feoktistova, A., Chen, J.-S., Huang, H., Guillen, R., Boone, C., Sidhu, S. S., Beckley, J. R. and Gould, K. L. (2015) The Cdc15 and Imp2 SH3 domains cooperatively scaffold a network of proteins that redundantly ensure efficient cell division in fission yeast, *Molecular Biology of the Cell*, 26(2), 256–269.
- Revelo, N. H., Kamin, D., Truckenbrodt, S., Wong, A. B., Reuter-Jessen, K., Reisinger, E., Moser, T. and Rizzoli, S. O. (2014) A new probe for super-resolution imaging of membranes elucidates trafficking pathways., *The Journal of Cell Biology*, 205(4), 591–606.
- Rincon, S. A. and Paoletti, A. (2012) Mid1/anillin and the spatial regulation of cytokinesis in fission yeast, *Cytoskeleton*, 69(10), 764–777.
- Rincon, S. A. and Paoletti, A. (2016) Molecular control of fission yeast cytokinesis, *Seminars in Cell & Developmental Biology*, 53, 28–38.
- Roberts-Galbraith, R. H., Chen, J.-S., Wang, J. and Gould, K. L. (2009) The SH3 domains of two PCH family members cooperate in assembly of the schizosaccharomyces pombe contractile ring, *Journal of Cell Biology*, 184(1), 113–127.
- Roberts-Galbraith, R. H. and Gould, K. L. (2010) Setting the F-BAR: Functions and regulation of the F-BAR protein family, *Cell Cycle*, 9(20), 4091–4097.
- Roberts-Galbraith, R. H., Ohi, M. D., Ballif, B. A., Chen, J. S., McLeod, I., McDonald, W. H., Gygi, S. P., Yates, J. R. and Gould, K. L. (2010) Dephosphorylation of F-BAR Protein Cdc15 Modulates Its Conformation and Stimulates Its Scaffolding Activity at the Cell Division Site, *Molecular Cell*, 39(1), 86–99.
- Rodal, A. A., Blunk, A. D., Akbergenova, Y., Jorquera, R. A., Buhl, L. K. and Littleton, J. T. (2011) A presynaptic endosomal trafficking pathway controls synaptic growth signaling, *Journal of Cell Biology*, 193(1), 201–217.
- Rodal, A. A., Motola-Barnes, R. N. and Littleton, J. T. (2008) Nervous wreck and Cdc42 cooperate to regulate endocytic actin assembly during synaptic growth., *The Journal of Neuroscience*, 28(33), 8316–8325.
- Rust, M. J., Bates, M. and Zhuang, X. W. (2006) Sub-diffraction-limit imaging by stochastic optical reconstruction microscopy (STORM), *Nature Methods*, 3(10), 793–

795.

Saarikangas, J., Zhao, H., Pykäläinen, A., Laurinmäki, P., Mattila, P. K., Kinnunen, P. K. J., Butcher, S. J. and Lappalainen, P. (2009) Molecular mechanisms of membrane deformation by I-BAR domain proteins., *Current Biology*, 19(2), 95–107.

Saengsawang, W., Mitok, K., Viesselmann, C., Pietila, L., Lombard, D. C., Corey, S. J. and Dent, E. W. (2012) The F-BAR Protein CIP4 Inhibits Neurite Formation by Producing Lamellipodial Protrusions., *Current Biology*, 22(6), 494–501.

Saengsawang, W., Taylor, K. L., Lombard, D. C., Mitok, K., Price, A., Pietila, L., Gomez, T. M. and Dent, E. W. (2013) CIP4 coordinates with phospholipids and actin-associated proteins to localize to the protruding edge and produce actin ribs and veils., *Journal of Cell Science*, 126(Pt 11), 2411–23.

Saras, J., Franzén, P., Aspenström, P., Hellman, U., Gonez, L. J. and Heldin, C. H. (1997) A novel GTPase-activating protein for Rho interacts with a PDZ domain of the protein-tyrosine phosphatase PTPL1, *Journal of Biological Chemistry*, 272(39), 24333–24338.

Schneider, K., Seemann, E., Liebmann, L., Ahuja, R., Koch, D., Westermann, M., Hübner, C. A., Kessels, M. M. and Qualmann, B. (2014) ProSAP1 and membrane nanodomain-associated syndapin I promote postsynapse formation and function, *Journal of Cell Biology*, 205(2), 197–215.

Schroeder, T. E. (1973) Actin in dividing cells: contractile ring filaments bind heavy meromyosin., *Proceedings of the National Academy of Sciences*, 70(6), 1688–92.

Schuck, P. (2000) Size-distribution analysis of macromolecules by sedimentation velocity ultracentrifugation and lamm equation modeling., *Biophysical Journal*, 78(3), 1606–19.

Senju, Y., Itoh, Y., Takano, K., Hamada, S. and Suetsugu, S. (2011) Essential role of PACSIN2/syndapin-II in caveolae membrane sculpting., *Journal of Cell Science*, 124(12), 2032–2040.

Shimada, A., Niwa, H., Tsujita, K., Suetsugu, S., Nitta, K., Hanawa-Suetsugu, K., Akasaka, R., Nishino, Y., Toyama, M., Chen, L., Liu, Z.-J., Wang, B.-C., Yamamoto, M., Terada, T., Miyazawa, A., Tanaka, A., Sugano, S., Shirouzu, M., Nagayama, K., *et al.* (2007) Curved EFC/F-BAR-domain dimers are joined end to end into a filament for membrane invagination in endocytosis., *Cell*, 129(4), 761–72.

Shimada, A., Takano, K., Shirouzu, M., Hanawa-Suetsugu, K., Terada, T., Toyooka, K., Umehara, T., Yamamoto, M., Yokoyama, S. and Suetsugu, S. (2010) Mapping of the basic amino-acid residues responsible for tubulation and cellular protrusion by the EFC/F-BAR domain of pacsin2/Syndapin II., *FEBS letters*, 584(6), 1111–8.

Shoham, N. G., Centola, M., Mansfield, E., Hull, K. M., Wood, G., Wise, C. A. and Kastner, D. L. (2003) Pryn binds the PSTPIP1/CD2BP1 protein, defining familial

- Mediterranean fever and PAPA syndrome as disorders in the same pathway., *Proceedings of the National Academy of Sciences*, 100(23), 13501–13506.
- Smith, L. G. (2001) Plant cell division: building walls in the right places, *Nature Reviews Molecular Cell Biology*, 2(1), 33–39.
- Sohrmann, M., Fankhauser, C., Brodbeck, C. and Simanis, V. (1996) The *dmf1/mid1* gene is essential for correct positioning of the division septum in fission yeast, *Genes & Development*, 10(21), 2707–2719.
- Stachowiak, J. C., Brodsky, F. M. and Miller, E. A. (2013) A cost–benefit analysis of the physical mechanisms of membrane curvature, *Nature Cell Biology*, 15(9), 1019–1027.
- Stachowiak, J. C., Schmid, E. M., Ryan, C. J., Ann, H. S., Sasaki, D. Y., Sherman, M. B., Geissler, P. L., Fletcher, D. A. and Hayden, C. C. (2012) Membrane bending by protein-protein crowding., *Nature Cell Biology*, 14(9), 944–949.
- Stachowiak, M. R., Laplante, C., Chin, H. F., Guirao, B., Karatekin, E., Pollard, T. D. and O’Shaughnessy, B. (2014) Mechanism of cytokinetic contractile ring constriction in fission yeast., *Developmental Cell*, 29(5), 547–61.
- Stimpson, H. E. M., Toret, C. P., Cheng, A. T., Pauly, B. S. and Drubin, D. G. (2009) Early-Arriving Syp1p and Ede1p Function in Endocytic Site Placement and Formation in Budding Yeast, *Molecular Biology of the Cell*, 20, 4640–4651.
- Suetsugu, S., Toyooka, K. and Senju, Y. (2010) Subcellular membrane curvature mediated by the BAR domain superfamily proteins, *Seminars in Cell & Developmental Biology*, 21(4), 340–349.
- Sun, L., Guan, R., Lee, I. J., Liu, Y., Chen, M., Wang, J., Wu, J. Q. and Chen, Z. (2015) Mechanistic Insights into the Anchorage of the Contractile Ring by Anillin and Mid1, *Developmental Cell*, 33(4), 413–426.
- Sydor, A. M., Czymmek, K. J., Puchner, E. M. and Mennella, V. (2015) Super-Resolution Microscopy: From Single Molecules to Supramolecular Assemblies, *Trends in Cell Biology*, 25(12), 730–748.
- Szwedziak, P., Wang, Q., Bharat, T. A. M., Tsim, M. and Lowe, J. (2014) Architecture of the ring formed by the tubulin homologue FtsZ in bacterial cell division, *eLife*, 3, e04601.
- Tajadura, V., García, B., García, I., García, P. and Sánchez, Y. (2004) *Schizosaccharomyces pombe* Rgf3p is a specific Rho1 GEF that regulates cell wall beta-glucan biosynthesis through the GTPase Rho1p, *Journal of Cell Science*, 117, 6163–6174.
- Tao, E. Y., Calvert, M. and Balasubramanian, M. K. (2014) Rewiring Mid1p-Independent Medial Division in Fission Yeast., *Current Biology*, 24(18), 2181–2188.



- Taylor, M. J., Perrais, D. and Merrifield, C. J. (2011) A high precision survey of the molecular dynamics of mammalian clathrin-mediated endocytosis., *PLoS Biology*, 9(3), e1000604.
- Tebbs, I. R. and Pollard, T. D. (2013) Separate roles of IQGAP Rng2p in forming and constricting the *S. pombe* cytokinetic contractile ring., *Molecular Biology of the Cell*, 24(12), 1904–1917.
- Terwilliger, T. C., Grosse-Kunstleve, R. W., Afonine, P. V., Moriarty, N. W., Adams, P. D., Read, R. J., Zwart, P. H. and Hung, L. W. (2008) Iterative-build OMIT maps: Map improvement by iterative model building and refinement without model bias, *Acta Crystallographica Section D: Biological Crystallography*, 64, 515–524.
- Tsujita, K., Suetsugu, S., Sasaki, N., Furutani, M., Oikawa, T. and Takenawa, T. (2006) Coordination between the actin cytoskeleton and membrane deformation by a novel membrane tubulation domain of PCH proteins is involved in endocytosis, *The Journal of Cell Biology*, 172(2), 269–79.
- Umasankar, P. K., Ma, L., Thieman, J. R., Jha, A., Doray, B., Watkins, S. C. and Traub, L. M. (2014) A clathrin coat assembly role for the muniscin protein central linker revealed by TALEN-mediated gene editing., *eLife*, 3, 1–33.
- Ungewickell, E. J. and Hinrichsen, L. (2007) Endocytosis: clathrin-mediated membrane budding, *Current Opinion in Cell Biology*, 19(4), 417–425.
- Vavylonis, D., Wu, J.-Q., Hao, S., O’Shaughnessy, B. and Pollard, T. D. (2008) Assembly mechanism of the contractile ring for cytokinesis by fission yeast., *Science*, 319(5859), 97–100.
- Vogt, D. L., Gray, C. D., Young, W. S., Orellana, S. A. and Malouf, A. T. (2007) ARHGAP4 is a novel RhoGAP that mediates inhibition of cell motility and axon outgrowth., *Molecular and Cellular Neurosciences*, 36(3), 332–42.
- Wachtler, V., Huang, Y., Karagiannis, J. and Balasubramanian, M. K. (2006) Cell Cycle-dependent Roles for the FCH-Domain Protein Cdc15p in Formation of the Actomyosin Ring in *Schizosaccharomyces pombe*, *Molecular Biology of the Cell*, 17(July), 3254–3266.
- Wagner, E. and Glotzer, M. (2016) Local RhoA activation induces cytokinetic furrows independent of spindle position and cell cycle stage, *Journal of Cell Biology*, 213(6), 641–649.
- Wang, Q., Navarro, M. V. A. S., Peng, G., Molinelli, E., Goh, S. L., Judson, B. L., Rajashankar, K. R. and Sondermann, H. (2009) Molecular mechanism of membrane constriction and tubulation mediated by the F-BAR protein Pacsin/Syndapin., *Proceedings of the National Academy of Sciences*, 106(31), 12700–5.
- Wang, S., Moffitt, J. R., Dempsey, G. T., Xie, X. S. and Zhuang, X. (2014)

- Characterization and development of photoactivatable fluorescent proteins for single-molecule-based superresolution imaging., *Proceedings of the National Academy of Sciences*, 111(23), 8452–7.
- Willet, A. H., McDonald, N. A., Bohnert, K. A., Baird, M. A., Allen, J. R., Davidson, M. W. and Gould, K. L. (2015) The F-BAR Cdc15 promotes contractile ring formation through the direct recruitment of the formin Cdc12, *The Journal of Cell Biology*, 208(4), 391–399.
- Willet, A. H., McDonald, N. A. and Gould, K. L. (2015) Regulation of contractile ring formation and septation in *Schizosaccharomyces pombe*, *Current Opinion in Microbiology*, 28, 46–52.
- Wong, K., Ren, X. R., Huang, Y. Z., Xie, Y., Liu, G., Saito, H., Tang, H., Wen, L., Brady-Kalnay, S. M., Mei, L., Wu, J. Y., Xiong, W. C. and Rao, Y. (2001) Signal transduction in neuronal migration: Roles of GTPase activating proteins and the small GTPase Cdc42 in the Slit-Robo pathway, *Cell*, 107(2), 209–221.
- Wood, V., Harris, M. A., McDowall, M. D., Rutherford, K., Vaughan, B. W., Staines, D. M., Aslett, M., Lock, A., Bähler, J., Kersey, P. J. and Oliver, S. G. (2012) PomBase: A comprehensive online resource for fission yeast, *Nucleic Acids Research*, 40(D1), 695–699.
- Wu, J.-Q., Kuhn, J. R., Kovar, D. R. and Pollard, T. D. (2003) Spatial and temporal pathway for assembly and constriction of the contractile ring in fission yeast cytokinesis., *Developmental Cell*, 5(5), 723–34.
- Wu, J.-Q. and Pollard, T. D. (2005) Counting cytokinesis proteins globally and locally in fission yeast., *Science*, 310(5746), 310–4.
- Wu, J.-Q., Sirotkin, V., Kovar, D. R., Lord, M., Beltzner, C. C., Kuhn, J. R. and Pollard, T. D. (2006) Assembly of the cytokinetic contractile ring from a broad band of nodes in fission yeast., *The Journal of Cell Biology*, 174(3), 391–402.
- Wu, J. Q., Bähler, J. and Pringle, J. R. (2001) Roles of a fimbrin and an alpha-actinin-like protein in fission yeast cell polarization and cytokinesis., *Molecular Biology of the Cell*, 12(4), 1061–1077.
- Wu, Y., Spencer, S. D. and Lasky, L. A. (1998) Tyrosine Phosphorylation Regulates the SH3-mediated Binding of the Wiskott-Aldrich Syndrome Protein to PSTPIP , a Cytoskeletal-associated Protein, *The Journal of Biological Chemistry*, 273(10), 5765–5770.
- Xu, K., Zhong, G. and Zhuang, X. (2013) Actin, spectrin, and associated proteins form a periodic cytoskeletal structure in axons., *Science*, 339(6118), 452–6.
- You, J.-J. and Lin-Chao, S. (2010) Gas7 functions with N-WASP to regulate the neurite outgrowth of hippocampal neurons, *The Journal of Biological Chemistry*, 285(15),

11652–66.

Yu, H. and Schulten, K. (2013) Membrane sculpting by F-BAR domains studied by molecular dynamics simulations, *PLoS Computational Biology*, 9(1), e1002892.

Yu, J. W., Fernandes-Alnemri, T., Datta, P., Wu, J., Juliana, C., Solorzano, L., McCormick, M., Zhang, Z. and Alnemri, E. S. (2007) Pyrin Activates the ASC Pyroptosome in Response to Engagement by Autoinflammatory PSTPIP1 Mutants, *Molecular Cell*, 28(2), 214–227.

Zhang, M., Chang, H., Zhang, Y., Yu, J., Wu, L., Ji, W., Chen, J., Liu, B., Lu, J., Liu, Y., Zhang, J., Xu, P. and Xu, T. (2012) Rational design of true monomeric and bright photoactivatable fluorescent proteins, *Nature Methods*, 9(7), 727–9.

Zhao, H., Michelot, A., Koskela, E. V., Tkach, V., Stamou, D., Drubin, D. G. and Lappalainen, P. (2013) Membrane-Sculpting BAR Domains Generate Stable Lipid Microdomains, *Cell Reports*, 4, 1213–1223.

Zhu, Y.-H., Ye, Y., Wu, Z. and Wu, J.-Q. (2013) Cooperation between Rho-GEF Gef2 and its binding partner Nod1 in the regulation of fission yeast cytokinesis, *Molecular Biology of the Cell*, 24(20), 3187–204.

Zimmermann, K., Opitz, N., Dedio, J., Renne, C., Muller-Esterl, W. and Oess, S. (2002) NOSTRIN: a protein modulating nitric oxide release and subcellular distribution of endothelial nitric oxide synthase, *Proceedings of the National Academy of Sciences*, 99(26), 17167–72.